HIGH CAPACITY MEMBRANE DESIGN FOR SIZE EXCLUSION BASED VIRUS REMOVAL

Von der Naturwissenschaftlichen Fakultät
der Gottfried Wilhelm Leibniz Universität Hannover

zur Erlangung des Grades
Doktor der Naturwissenschaften
Dr. rer. nat.

genehmigte Dissertation
von

M.Sc. Louis Villain
geboren am 11.11.1980 in Laxou (Frankreich)

2010

Referent/in: Prof. Dr. Thomas Scheper

Korreferent/in: Prof. Dr. Bernd Hitzmann

Tag der Promotion: 3.06.2010

Erklärung

Ich versichere, dass ich diese Dissertation selbstständig und nur unter Verwendung der angegebenen Hilfsmittel und Quellen durchgeführt habe. Diese Arbeit wurde nicht als Diplomarbeit oder ähnliche Prüfungsarbeit verwendet.

Hannover, im März 2010

Acknowledgments

I am grateful to my supervisor Prof. Dr. Thomas Scheper for giving me the chance to perform my thesis on a highly interesting topic, for his guidance and critical advices.

I thank Prof. Dr. Bernd Hitzmann for being the co-advisor of this thesis.

I am thankful to Prof. Dr. Jürgen Caro for accepting to be a member of the final examination committee.

I am also really Grateful to Volkmar Thom, Isabelle Masselin for the excellent supervision and support during my PhD at Sartorius-Stedim Biotech.

I am so grateful to my dear trainee students Carsten Siebenhaar, Claire Roulin, my three angels Veronica Rico Perez, Claire Schacher and Nadiia Kondratiuk for their fruitful contribution to this work.

Thx to Claire Roulin for the careful reading and correction of this work! Je te dois toujours un coup a boire.

Un grand merci a ces amis exceptionnels que sont Pierre Moretti, Stephan Barbe et Edouard Herbillon pour leur soutien pendant les périodes difficiles.

Enfin, un grand merci a mes chers parents et a ma chère soeur pour leur soutien pendant mes si lonnnngues études.

Abstract

Size exclusion based virus filtration is a robust virus clearance technology for biotech- and plasma derived therapeutics. The filters are especially effective in the removal of small non-enveloped viruses of about 20 nm diameter, that are resistant to heat and solvent or detergent based inactivation methods. However, the fine porous membrane structure, required for high resolution protein/virus separation, makes the method highly sensitive to impurities and solute/membrane interactions. This is especially true for demanding streams like plasma derived therapeutics for intravenous administration, containing pooled immunoglobulin G (IgG) of over thousands of blood donors, whose filtration is often observed to be throughput limited.

In a first part, the mechanisms governing virus retention were characterized. Using a bacteriophage based evaluation method, the impact of various structural factors such as membrane heterogeneity, asymmetry, orientation and protein concentration on virus retention was demonstrated. According to these results, the optimal membrane structure and evaluation conditions were determined in order to ensure effective virus clearance under a large variety of operating conditions.

In a second part, the main mechanisms involved in membrane fouling were elucidated. Zeta potential measurements of the membrane material together with isoelectric focusing of the pooled IgG containing solution revealed strong electrostatic interactions that impact filterability, depending on the protonation state of proteins. However, at near neutral pH-values, corresponding to the standard stabilization conditions for the majority of plasma-derived therapeutics, unspecific adsorption is mainly driven by hydrophobic interactions. The data suggested that a small subset of hydrophobic monomeric IgG can dramatically impact the filterability of the whole pooled IgG mixture.

In a last part, strategies to overcome these limitations were tested. Innovative automated high throughput methods for performance testing were developed to allow the parallel characterization of a large variety of materials generated by electron-beam initiated graft modification. Finally, a high capacity membrane, exhibiting high viral clearance efficiency and fouling resistant properties due to efficient shielding of the hydrophobic surface, was developed.

Keywords: virus filtration, membrane modification, hydrophobic interactions, immunoglobulin.

Kurzfassung

Die auf Größenausschluß basierende Virenfiltration ist eine sehr effektive Virenabreicherungstechnologie für biotechnologisch hergestellte oder vom Plasma isolierte therapeutische Moleküle. Die dafür verwendeten Membranfilter sind besonders effizient gegen 20 nm große nicht-umhüllte Viren, die durch thermische und chemische Behandlungen nicht deaktiviert werden können. Aufgrund der feinen porösen Struktur, die für hochauflösende Virus/Protein Auftrennung erforderlich ist, weisen solche Membranen eine hohe Empfindlichkeit gegenüber Verunreinigungen und Protein/Membran Wechselwirkungen auf. Dies wird besonders beim gepoolten Immunoglobulin G aus dem Plasma von tausenden Blutspendern beobachtet. Die Filtrationsleistung bei derartigen Lösungen ist oft niedrig.

In dem ersten Teil dieser Arbeit wurden die Mechanismen identifiziert, die für die Virenrückhaltung relevant sind. Dank einer auf Bakteriophagen basierten Charakterisierungsmethode, konnte der Einfluss wichtiger struktureller Parameter wie Membran Heterogenität, Asymmetrie, Ausrichtung und Proteinkonzentration auf die Virenrückhaltung evaluiert werden. Dadurch konnten die optimale Membranstruktur sowie Testbedingungen bestimmt werden, um die Abreicherung von Viren unter zahlreichen Betriebsbedingungen zu sichern.

In einem zweiten Teil, wurden die Hauptverblockungsmechanismen aufgeklärt. Die Messung des Zeta-Potentials an der Membranoberfläche sowie die Isoelektrische Fokussierung der in der Lösung enthaltenden Immunoglobulin machten den Einfluss von elektrostatische Wechselwirkungen sowie die Abhängigkeit von Protonierungszustand der Proteinen in der Lösung deutlich. Bei neutralen pH-Werten allerdings, die typischerweise für die Formulierung und Stabilisierung der meisten Plasma Produkte verwendet werden, konnte gezeigt werden, dass die Verblockung der Membran hauptsächlich durch hydrophobe Wechselwirkungen verursacht wird. Die Ergebnisse zeigten außerdem, dass eine kleine Teilmenge von hydrophoben Immunoglobulin-Monomeren die Filtrierbarkeit der gesamten Proteinlösung dramatisch beeinflussen kann.

In dem letzten Teil der Arbeit wurden Strategien zur Minderung der oben genannten Leistungslimitierung vorgeschlagen. Hochdursatz-Charakterisierungsmethoden zur Leistungsbewertung wurden entwickelt. Diese erlaubten die parallele Charakterisierung von verschiedenen Materialien, die durch Elektronstrahlen initiierte Graft-Modifizierung hergestellt wurden. Durch die effiziente Beschichtung der hydrophoben Oberfläche wurde eine hoch kapazitive Membran entwickelt, welche außerdem ein hohes Virenabreicherungspotenzial aufweist.

Schlagwörter: Virenfiltration, Membranmodifizierung, hydrophobe Wechselwirkungen, Immunoglobulin

Table of contents

ACKNOWLEDGMENTS ..... **IV**

ABSTRACT ..... **V**

KURZFASSUNG ..... **VI**

TABLE OF CONTENTS **1**

1 INTRODUCTION **4**

2 SIZE EXCLUSION BASED VIRUS REMOVAL **6**

2.1 Virus clearance in the pharmaceutical Industry **6**

2.1.1 Regulatory aspects and state-of-the-art in virus clearance. 6

2.1.2 Virus detection methods 9

2.1.3 Performance aspects of virus filtration 11

2.2 Production of virus retentive polymer membranes **13**

2.2.1 Membrane preparation by immersion precipitation 13

2.2.2 Graft surface modification of polymeric membranes 15

3 CHARACTERIZATION OF DOMINANT MECHANISMS GOVERNING VIRUS RETENTION **18**

3.1 Retention assessment with PP7-bacteriophages **18**

3.2 Membrane orientation **21**

3.3 Effect of flow decay on retention **26**

3.4 Prediction model for precise retention targeting **30**

3.4.1 Influence of membrane heterogeneity 31

3.4.2 Influence of membrane layer configuration 37

3.5 Conclusion **41**

4 CHARACTERIZATION OF DOMINANT MECHANISMS GOVERNING MEMBRANE FOULING 43

4.1 Electrostatic solute-membrane interactions 44

4.1.1 Isoelectric point distribution of pooled Immunoglobulins 44

4.1.2 Electrical properties of membrane surface 45

4.1.3 pH-dependent protein adsorption 47

4.2 Hydrophobic solute-membrane interactions 52

4.2.1 Fractionation by Hydrophobic Interaction Chromatography (HIC) 52

4.2.2 Correlation between hydrophobicity and unspecific protein adsorption 54

4.2.3 Filterability of immunoglobulin fractions 55

4.2.4 Molecular size of Immunoglobulin fractions 56

4.3 Adsorptive aspects of protein aggregation 57

4.4 Conclusion 61

5 HIGH CAPACITY VIRUS RETENTIVE MEMBRANE 62

5.1 High throughput automated characterization of filtration capacity 63

5.2 Electron-beam initiated graft modification 65

5.2.1 Screening of promising combination of mono and bifunctional vinyl compounds . 65

5.2.2 Optimum crosslinker/monomer ratio in regard to unspecific adsorption 69

5.2.3 Impact of modification conditions on membrane filtration performance 70

5.2.4 Structure and swelling properties of new developed porous material 72

5.3 Trade-off between filtration capacity and retention 75

5.4 Applicability of the development 78

5.5 Conclusion 81

6 GENERAL CONCLUSION AND OUTLOOK 83

7 REFERENCES 87

8 APPENDICES 96

8.1 List of abbreviation 96

8.2 Materials 97

8.2.1 Equipments 97

8.2.2 Membranes 98

8.2.3 Chemicals & culture media 98

8.2.4 Bacteriophage and bacterial strains 99

8.3 Characterization of membrane surface properties 99

8.3.1 Measurement of unspecific protein adsorption 99

8.3.2 Measurement of zeta-potential 100

8.4 Characterization of membrane structure properties 100

8.4.1 Air and liquid permeability 100

8.4.2 Electron microscopy 102

8.4.3 BET surface area 102

8.5 Determination of the filtration performance: 103

8.5.1 Determination of virus retention with bacteriophage PP7 103

8.5.2 Filtration capacity 104

8.6 Physico-chemical properties of therapeutic protein solutions 105

8.6.1 Protein fractionation by hydrophobic interaction chromatography (HIC) 105

8.6.2 Size exclusion chromatography (SEC) 105

8.6.3 2D-gelelectrophoresis 105

8.6.4 SDS-PAGE 106

8.7 Electron beam initiated surface modification 106

8.7.1 Graft modification with vinyl monomers 106

8.7.2 Degree of grafting 107

8.7.3 Membrane swelling 108

8.8 CV 109

8.9 List of publications 111

1 Introduction

The increasing need for plasma derived therapeutics is a constant challenge for the pharmaceutical industry. New advances in all production steps are needed to attain both high purity and recovery at minimal costs: from the capturing of the targeted therapeutical molecule to its purification and formulation. However, besides qualitative and economic considerations, the product safety, especially in regards to virus contaminants, remains the most challenging issue in many manufacturing processes. In the past, contamination of source plasma by enveloped viruses (HIV, HCV) has led to the contamination of plasma derived therapeutics and, at last, to patient infection. In response, several viral safety strategies were adopted by the industry to significantly minimize the risk of viral contamination. These strategies typically include source plasma control, donor screening and integration of multiple orthogonal clearance steps within the product manufacturing. State-of-the-art clearance of large enveloped viruses is ensured by heat or chemical/detergent treatments, exposure to low pH, adsorption to chromatographic media or size exclusion based techniques. Currently, product safety concerns are principally focused on the clearance of smaller non-enveloped viruses that are resistant to existing thermal and chemical inactivation methods.

Virus filtration is a robust, size exclusion based virus clearance technology. The membranes used allow the passage of molecules up to 8-12 nm while retaining virus particles with a diameter of at least 20 nm. Therefore, this clearance strategy is especially effective in the removal of small non-enveloped viruses like e.g. parvoviruses. Furthermore, the tight membranes used are inert and do not damage the targeted product and consequently high product recovery is achieved in most applications.

One major issue governing virus filtration is membrane fouling, causing a marked decrease of the permeate flux during the filtration process. This phenomenon is especially observed with feed streams containing pooled immunoglobulin G (IgG) of thousands of blood donors. For this particular application, commercially available virus filters do not always meet the performance specifications required by the industry, which are: high filtration capacity, to reduce the membrane surface area required for this cost intensive step, and high viral safety, since these products are typically injected intravenously to people with reduced immune capabilities.

The main object of the present work was the development of a membrane exhibiting high virus retention and filtration capacity for high plugging plasma derivatives. This work comprised the three following objectives:

Description of the mechanisms governing virus retention. In this part a bacteriophage-based model parvovirus was developed to assess the virus retention capacity of porous materials. This model was used to determine the impact of various factors like membrane heterogeneity, orientation and morphology on virus retention, the optimum product configuration and, finally, to define the required membrane specifications regarding virus retention and facilitate up-scaling.

Elucidation of the dominant mechanisms involved in membrane fouling. In this part, the influence of the operating conditions, solute-to-membrane interactions and solute size distribution on membrane fouling was investigated. The dominant parameters affecting the filtration performance of pooled IgGs were identified and strategies to overcome these limitations are discussed.

Development of a high capacity virus retentive membrane. In this last part, different materials with various structure and surface properties, generated by electron-beam initiated surface graft modification, were tested in respect of filtration capacity and virus retention. A high throughput screening characterization system was developed to enhance the screening and performance testing of membrane modified under various conditions. Finally a complete product concept, comprising a low binding porous material operated at determined optimum conditions is proposed.

2 Size exclusion based virus removal

2.1 Virus clearance in the pharmaceutical Industry

2.1.1 Regulatory aspects and state-of-the-art in virus clearance.

Virus contamination poses a threat to the safety of biopharmaceuticals [1-4]. This is especially true for therapeutics that are sourced from mammalian fluids like plasma derived coagulation factors or immunoglobulins. In order to address the risk of contamination, regulatory mandates were designed to reduce the risk of virus transmission in the plasma pool used in the manufacturing process [5]. These mandates typically include donor selection, testing of donations and plasma pools for specific relevant viruses (HBV, HCV, HIV and HTLV) [1, 5-8] and have contributed significantly to the increased safety of plasma derivatives in the last two decades. However, in spite of these measures, viruses still have been detected in plasma pools and plasma derived coagulation factors (factors VIII and IX) have been responsible for transmission of HIV, hepatitis viruses, and parvoviruses [9-15]. For this reason, additional clearance steps are necessary to ensure product safety and minimize the risk of contamination.

Depending on their mode of clearance, these additional virus clearance methods are classified as virus removal strategies, which aim at (mechanical) reduction of viral numbers, or virus inactivation methods where the objective is irreversible loss of viral infectivity [5]. Virus inactivation methods typically include heat, UV and chemical/detergent treatments or low pH. In contrast, virus removal strategies are mostly based on adsorptive mechanisms using chromatography techniques or molecular sieving in the case of virus filtration [3, 6, 8, 16-19]. The choice of a definite technique or method combination is not only guided by clearance efficiency but also by the characteristics and stability of the target molecule under the conditions inherent to the method. Methods like heat or chemical treatment can, for instance, lead to changes in the conformation or even denaturation of the therapeutic molecule of interest [20, 21] and could have a dramatic impact on its biological activity. Furthermore, an ideal clearance method should be robust or, in other terms, efficient under a large variety of operating or solution related conditions. It should also have a broad spectrum of clearance (either through inactivation or removal) of viruses [5].

Besides the strategies specifically designed for virus clearance, virus removal or inactivation can also be achieved as a consequence of routine processing and purification operations.

Many unit operations that are part of the manufacturing process co-incidentally provide virus clearance. Operations that are typically incorporated in the purification process e.g. clarification, centrifugation, extraction, precipitation or chromatography techniques, may physically remove viruses from the solution due to size exclusion, charge related or adsorptive mechanisms. Furthermore, virus inactivation can also be a consequence of pH or solvent change during processing. This is especially true in the case of immunoglobulin G (IgG) that are isolated from human plasma by performing the well-established cold ethanol fractionation, which also provides very effective viral inactivation [22]. The use of low pH-buffer for elution of target molecules from chromatography columns is another typical example of an inactivation operation that is not specifically dedicated to virus clearance [23].

The clearance efficiency is evaluated in terms of $\log_{10}$ reduction value (LRV), which is the ratio of viral concentration per unit volume in the pre-treatment suspension to concentration per unit volume in the post-treatment suspension.

For every manufacturing process, the minimum level of viral clearance to be attained is evaluated by a risk assessment. The major factors influencing the viral safety of biotherapeutics and that are considered in the risk calculation are the following [24]:

- The species of origin of the starting material since non-human viruses are less susceptible to infect humans.
- The degree of source variability of starting material, since products derived from pooled human plasma pose a higher risk compared to products derived from well-characterized cell banks.
- The different operation and purification units and their potential for virus reduction.
- The existence of specific viral clearance steps implemented in the process.

From the determined risk calculations will result the amount of virus clearance efficiency that is required for a given manufacturing process. As an additional safety margin, regulatory agencies encourage manufacturers to validate processes, able to remove or inactivate $>6 \log_{10}$ more virus than is estimated to be present in the starting material.

The targeted viral clearance efficiency for therapeutics derived from human plasma typically exceeds 20 orders of magnitude. Since such degree of clearance cannot be achieved by a single unit operation, multiple orthogonal clearance methods operating in concert are needed. The term orthogonal means and can be here replaced by “based on different separation or

inactivation principles". Since each viral clearance method, individually, may have limitations, their use in an integrated manner provides overlapping and complementary levels of protection [5]. Besides the implementation of a multiple orthogonal clearance strategy into the purification process, regulatory agencies also emphasize the presence of at least one clearance method effective against small non-enveloped viruses [25], which are not eliminated substantially by the large majority of existing thermal and chemical inactivation methods [26]. Table 2.1 gives an overview of clearance methods used in the manufacture of biotherapeutics.

Table 2.1: Overview of clearance methods used in the manufacture of biotherapeutics and their respective efficiency against enveloped and non-enveloped viruses.

	Technology	Efficient against non-enveloped viruses	Efficient against enveloped viruses
Virus removal	chromatography		√
	Virus filtration	√	√
Virus inactivation	Heat inactivation		√
	S&D		√
	Low pH		√
	UV-C	√	√

S&D: solvent and detergent

UV-C: shortwave UV (100-280 nm)

As already mentioned in the introduction, product safety concerns are currently focused on the clearance of small non enveloped parvoviruses. Parvoviruses are small (18-26 nm) non-enveloped icosahedral structures containing a single-stranded DNA molecule. In contrast to enveloped viruses, parvoviruses have no lipid bilayer envelope around the viral protein capsid and consequently exhibit high resistance against solvent and detergent, but also against heat and dessication. One particular challenging virus that belongs to the *parvoviradae* family is the human parvovirus B19. B19 virus is a common human pathogen associated with a wide variety of diseases [27] and also a frequent contaminant of blood donations and plasma derived therapeutics [28]. Since B19 virus also exhibits high resistance to many inactivation methods, virus filtration remains the most effective technology to ensure the absence of such contaminants in the final product [16, 18, 19, 29-31].

In order to ensure that the total viral clearance targeted is achieved, the potential of virus clearance for each of the manufacturing unit operations has to be evaluated. Typically, virus

clearance evaluation studies are conducted at scale down conditions due to logistic and economic limitations. However, the scale down must be a true representation of what occurs in the manufacturing process. For this reason, the impact of critical operating parameters on viral clearance, such as volume, flow rate, contact time, product load and, in some cases, device design or geometry has first to be evaluated to determine if they have to be conserved at small scale. Finally, Evaluation should be performed under conditions that constitute a "worst-case" scenario in order to demonstrate the minimum clearance efficiency an operation unit can provide. As an example, worst-case conditions for S&D treatment are provided at low detergent concentrations combined with short exposure times.

2.1.2 Virus detection methods

Evaluation of the viral clearance efficiency necessitates methods to detect and quantify the virus particles remaining in the post-treatment solution. There are several available detection methods: infectivity assays, molecular probes, biochemical assays, morphological assays, and antibody production tests (in animals). The particular viral detection will depend on the objective of the test, what is being tested and other issues. For example, the effectiveness of a virus clearance unit operation is commonly assessed using infectivity tests, though PCR-based assays are being increasingly used. To estimate the non-infectious retroviral burden, assays of choice include morphological (electron microscopy) or biochemical assays.

Infectivity assays are standard assays for validation studies [32]. They involve the inoculation of susceptible cell lines with the specific virus, followed by observation of cytopathic effects, for example, formation of plaques, focus forming units or induction of abnormal cellular morphology, as a consequence of the infection [5]. The main type of in vitro infectivity assay commonly used to estimate virus titer is the plaque-forming assay. In a first step, the process solution is spiked with a concentrated virus stock solution and used as a feed solution for the unit operation, whose clearance efficiency has to be assessed. Several dilutions of the post-treatment solution are used to infect cells, which are kept stable in an overlay of agarose to limit virus spreading. When each infected cell produces virus and eventually lyses, only the immediately adjacent cells become infected. Each group of infected cells is referred to as a plaque. Uninfected cells surround the plaques. After several infection cycles, the infected cells in the center of the plaques begin to lyse and the peripheral infected cells remain surrounded by uninfected cells. This phenomenon causes the light passing through the infected cells to

refract differently than the surrounding uninfected cells, and the counting of plaque forming units (pfu/mL) can be performed either by the naked eye or by light microscopy

The plaque-forming assay offers extreme sensitivity and is especially useful when the virus is present at extremely low titers. However, the requirement for a different assay system for each virus (due to the cell culture-specific infectivity) makes biological assays cumbersome. For this reason, bacterial viruses, also referred to as bacteriophages, are commonly used by filter manufacturers to evaluate the size exclusion properties of their virus removal filters and by some end users for preliminary evaluation of size-based filtration under process conditions [33-35]. Bacteriophages are not pathogen for humans, are available at different sizes and are consequently adequate for development phases. Furthermore, the cultivation of the corresponding bacterial host cell does not necessitate expensive culture media and the result of the plaque-forming assay can already be obtained 12 hours after inoculation.

Molecular probes, such as hybridization or RT-PCR assays [32, 36], are being increasingly used because of their specificity and the rapidity of results. These methods, in general, detect the presence of specific nucleic acid sequences (DNA and RNA) but cannot differentiate between infectious or non-infectious particles. Additionally, the method is applicable only when the genomic sequence of the virus is known and stable in regards to mutation [36]. Furthermore, quantitative PCR is especially relevant if the viral agent cannot be grown in vitro. It should also be mentioned, that a negative PCR result does not prove unequivocally the absence of viruses (infectious or not), due to limitations in assay sensitivity.

Finally, biochemical assays such as reverse transcriptase assays, radiolabel incorporation into nucleic acids, radioimmunoassay, immunofluorescence and Western blot are also used for virus detection. However these tests are semi-quantitative. These assays also detect enzymes with optimal activity under the test conditions and their interpretation may be difficult due to the presence of cellular enzymes or other background material [5].

2.1.3 Performance aspects of virus filtration

Virus filtration is a robust, size exclusion based virus clearance technology [1]. This clearance strategy is especially effective in the removal of small non-enveloped viruses that are resistant to heat and solvent or detergent based inactivation methods [19, 31]. The membranes used, allow the passage of molecules up to 8-12 nm while retaining viruses with a diameter of at least 20 nm and may at present be the only method allowing both virus reduction and recovery of 90-95 % protein activity [1].

Since the presence of only a small number of abnormally large pores will permit excessive virus leakage, virus filters must be manufactured so as to eliminate all macro defects [37]. Ideally they should exhibit a homogeneous pore structure and a narrow pore size distribution. Typically, commercial virus filters have a complex multilayer structure to ensure the absence of defect paths [18]. They are available both as flat sheet or hollow fiber (HF) modules. Table 2.2 gives an overview of commercially available virus filters used for the removal of small non-enveloped viruses.

Table 2.2: Overview of commercially virus filters against small non-enveloped viruses and their characteristics

Virus filter name	Type	Material	Structure	Claimed LRV
Millipore NFP	Flat sheet	Hydrophilic PVDF	Strong asymmetric (composite)	>4 $\log_{10}$
Pall DV20	Flat sheet	Hydrophilic PVDF	Symmetric	>3 $\log_{10}$
Sartorius Virosart CPV	Flat sheet	Hydrophilic PES	Slightly asymmetric	>4 $\log_{10}$
Asahi Planova 20N	HF	Regenerated cellulose	Slightly asymmetric	>4 $\log_{10}$

Virus filter were originally designed for use in tangential flow filtration (TFF) with the fluid adjacent to the membrane. However the simplicity and lower capital cost of normal flow filtration (NFF), also referred to as dead-end filtration, has led to the widespread use of virus filters specifically designed for NFF [37]. In contrast to TFF, where the membrane surface is continuously swept by the tangential flux, NFF is significantly more sensitive to phenomena such as concentration polarization and fouling. Membrane fouling is characterized by a marked decrease of permeability as a function of permeated solution volume per membrane area and can have dramatic economic consequences. This is especially true in the case of virus filtration since the used membrane filters are single-use products and thus discarded after processing. Furthermore, the fine porous membrane structure, required to permit high resolution protein/virus separation, makes the method highly sensitive to impurities. The

complex multilayer structure of the virus filtration membranes features selective pores that are only slightly larger than the size of the proteins [18]. The presence of protein aggregates or high molecular weight molecules in the product stream can lead to pore plugging, resulting in throughput limitation [29, 37].

To prevent this issue, virus filtration is usually performed near the end of the purification process, where the product contains a low level of contaminants [18] or following a prefiltration step. Recently, Bolton et al. [29] reported the use of a diatomaceous earth based depth filter situated upstream to the virus filter. The prefilter provided a dramatic increase of filtration capacity for solution containing human IgG by removing the species responsible for fouling. However, the dominant foulant of most virus filters is the protein product [18] and throughput limitations remain difficult to overcome for many applications. Syedain et al. [18] demonstrated the importance of the membrane structure and orientation in fouling phenomena using a composite membrane. This membrane consisted of a thick skin layer that was supported on a more open membrane substructure and was consequently exhibiting a strong asymmetric structure (see also section 2.2.1). Higher filtration capacity was obtained with the more open side facing the feed solution, allowing protein aggregates or large foulants to be captured within the macroporous substructure and protecting the fouling sensitive skin layer [18, 20, 37].

Beside the fact that membrane fouling can be associated with additional cost and product loss, membrane fouling also may have an impact on virus safety. Many articles reported that the virus reduction capability of some virus removal filters sometimes decreases with increasing flow decay [16, 38]. Bolton et al. [16] proposed an explanation to this phenomenon based on pore selectivity. Considering that the membrane also contains a small amount of pores that are somewhat larger than viruses, The gradual plugging of small pores will result in an increase of the relative proportion of solution that pass through the larger pores, leading to virus breakthrough. Additionally, strong flow decay can also complicate the collection of sample when the sample volume necessary for testing is not achievable [39]. In both cases, this can lead to product failure during expensive validation studies.

As already mentioned in the introductive part, pooled IgG purified from human plasma are therapeutic solutions, whose filtration is often observed to be throughput limited. Large filtration surface area is required to process such solutions. In contrast to the production of

recombinant proteins or monoclonal antibodies (Mab), purification processes in the plasma fractionation industry are old, well-established processes and the produced IgG containing therapeutics are products with low added value. Consequently, filtration capacity is one of the most important factors for the selection of a virus filter in such applications.

2.2 Production of virus retentive polymer membranes

2.2.1 Membrane preparation by immersion precipitation

The large majority of commercial flat sheet virus filter are phase inversion membranes obtained by immersion precipitation. Phase inversion membranes can be prepared from a large variety of polymers. The only requirement is that the polymer must be soluble in a solvent or solvent mixture [40] and must be film forming. Typical polymers used for the fabrication of virus retentive membranes are polyethersulfone (PES) and polyvinyldifluoride (PVDF). The preparation of flat membranes on a semi-technical or technical scale is shown schematically in Figure 2.1.

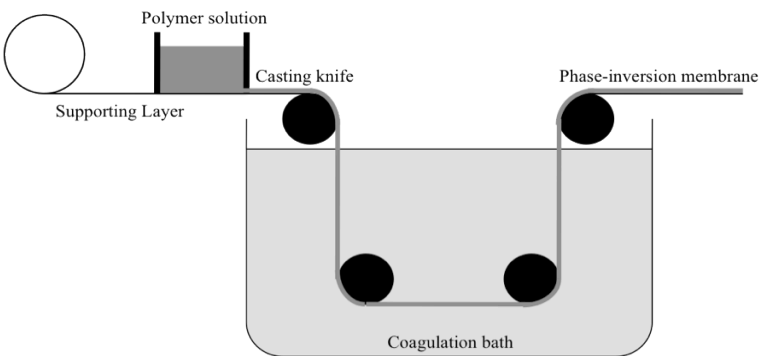

Figure 2.1: Schematic drawing depicting the preparation of flat membrane by immersion precipitation

The polymer solution also referred to as the casting solution or dope is cast directly upon a supporting layer by means of a casting knife. The casting thickness can vary between 30 and 300 μm. The cast film is then immersed in a non-solvent bath where exchange between the solvent and non-solvent occurs. The non-solvent begins to diffuse into the polymer solution and the solvent begins to diffuse into the coagulation bath due to their concentration gradient, bringing the composition of the polymer solution into the miscibility gap of the ternary phase diagram. Hence the polymer solution decomposes into 2 phases: a polymer-rich phase and a polymer-poor phase. The former results in a rigid, structural form of the membrane, while the latter gives a porous substructure of the membrane. Liquid-liquid phase separation (also

referred to as liquid-liquid demixing) continues to form the final membrane structure until the polymer-rich phase is solidified by gellation and/or crystallization of the polymer (also called solid-liquid demixing) [40, 41].

Since the performance and selectivity of the membrane strongly depends on its morphology, it is of great importance to identify and control the parameters that will provide the membrane with adequate final structure properties.

The basic principle of controlling membrane structures from a crystallizable polymer is the competition between the liquid-liquid demixing process and the solid-liquid demixing or crystallization process [42]. In general, the liquid-liquid demixing process engenders cellular pores whereas the crystallization forms interlinked crystalline particles [43]. Typical factors influencing the performance and structural properties of phase inversion membrane are:

- choice of polymer, solvent and non-solvent
- composition of casting solution, of coagulation bath
- crystallization behavior of the polymer
- temperature of casting solution and coagulation bath
- exposure time with the gas phase.

Wang et al. examined the effect of the polymer dissolving temperature on the morphology and crystallization of PVDF membranes. The study pointed out that high dissolution temperatures generate membrane structure with larger cell size observed by electron microscopy in the cross section. Many researchers also demonstrated that the addition of inorganic salt in the casting solution could affect the final structure and the permeability and selectivity characteristics of produced phase inversion membranes [44-46].

Another factor that impacts the morphology of membrane prepared by immersion precipitation is the composition change in the polymer solution prior to immersion into the coagulation bath [42, 47]. Young et al. obtained more symmetric membrane structures while increasing the exposure time of the cast film with the gas phase [42]. Buennomena et al. demonstrated that absorption of humidity from the air brings the cast film closer to demixing conditions when hygroscopic solvents are used. It reduces the gradient of the water concentration in the nascent membrane film upon contact with the coagulation bath and thus promotes a more homogeneous nucleation and symmetric morphology [43].

Asymmetric membranes prepared by phase inversion techniques typically exhibit a very thin selective layer (skin) supported by a more open porous structure. These membranes generally present great advantages regarding permeability. For a given selectivity, asymmetric membranes generally may exhibit higher flow permeation rates compared to symmetric membranes due to decreased flow resistance. As already mentioned in section 2.1.3, some commercial virus retentive membranes are asymmetric composite membranes. Such particular membrane also consists of a thin dense skin layer that is supported by a porous sublayer. However, in this case the two layers originate from different polymeric materials. The advantage of composite membrane is that each layer can be optimized independently to obtain optimal membrane performance with respect to selectivity, permeability and chemical or thermal stability [40].

2.2.2 Graft surface modification of polymeric membranes

The large majority of membranes prepared by phase-inversion are made of rather hydrophobic polymers and the produced porous material typically exhibits low surface energies [48-50]. This presents several disadvantages regarding wettability as well as adsorption of solutes. For some membrane related processes such as virus filtration, protein adsorption can lead to dramatic performance decreases and consequently, additional costs due to larger required filtration surface area and decreased product recovery may occur.

Therefore, the aim of surface modification often is to minimize undesired interaction occurring between the porous material and the solute in order to increase the filtration performance. Two alternative approaches can be distinguished. “Grafting to” is performed by coupling polymers to surfaces, while during the “Grafting from” approach, monomers are polymerized using an initiation at the surface. The former has the potential advantage that the structure of the polymer to be grafted is well characterized. However the grafting densities which may be achieved are limited and the coupling reactions require special efforts [48]. In the case of grafting from, considerably higher grafting density can be attained since the method involves the initiation of a polymerization reaction at the membrane surface. However the modification process often is more difficult to control and various chain length and grafting densities can be obtained.

Chemical reaction onto the membrane surface can be realized either via derivatization of intrinsic functional groups onto the membrane polymer or by degradation of the membrane material for the activation of reactions. However most of the established polymer used in membrane production like e.g. PES or PVDF are inert and lack convenient end groups for heterogeneous functionalization [51]. In contrast, activation of chemical reactions by controlled degradation of polymers can be easily realized by high-energy radiation (γ- or electron-beam), plasma or UV irradiation.

Excitation with high energy irradiation has a low selectivity and bond scissions in the volume of the membrane material cannot be avoided [48]. However, initiating sites are rapidly created directly upon irradiation, which obviates the need for chemical initiators. E-beam can operate at high dose rates and the depth of penetration can be controlled by the E-beam energy [52]. The radiation process is employed at room temperature. It is also free from contamination as no catalyst or additives are required [53].

Excitation with UV irradiation also presents some advantages compared to other technologies. It can be performed at mild reaction conditions and low temperature, high selectivity is possible by choosing the excitation wavelength [54, 55] and similarly to electron-beam irradiation, it can be integrated into continuous manufacturing processes simply and cost-efficiently [48]. However photo-initiated processes remain surface selective and grafting reaction onto the pore inner surface cannot be achieved efficiently with this technology and is then more appropriate for membrane used in tangential flow mode (TFF).

Reported “grafting to” reactions were mostly performed on UF and MF membranes. Hydrophilic polymers such as PEG [56] or PVP [57] were used in order to minimize protein adsorption.

In the case of grafting from reactions, functional monomers such as acrylates, acrylamides derivates and other vinyl monomers have been used almost exclusively until now [58-62]. “Grafting from” reaction proceeds in 3 different ways: pre-irradiation, mutual irradiation technique and peroxidation [63]. In the pre-irradiation technique, the membrane or polymer backbone is first irradiated in vacuum or in the presence of an inert gas to generate stable free radicals. The membrane is then impregnated with the monomer solution. In the mutual irradiation technique, the polymeric membrane and the monomer are irradiated

simultaneously. The main disadvantage of this technique is the probable formation of homopolymers, which does not occur using the pre-irradiation approach. At last in the peroxidation grafting method, the membrane is subjected to radiation in the presence of oxygen to form hydroperoxides. The stable peroxy products are then treated with the monomer at high temperature and decompose to radicals, which can initiate the polymerization. The reaction of acrylate derivatives with free radicals is proposed in Figure 2.2

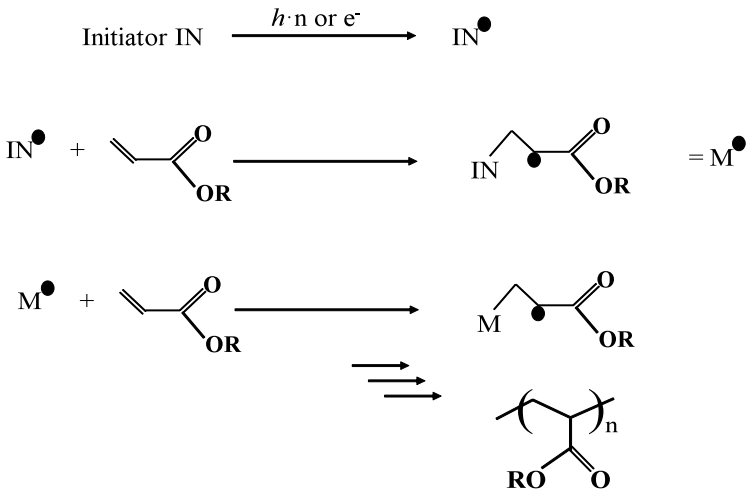

Figure 2.2: Electron beam or photoinitiated polymerization reaction of acrylate derivatives.

Free radicals are generated by UV-irradiation or by electron beam irradiation. The created free radicals react at the β-position of the α,β unsaturated carbonyle compounds to form a new free radical, stabilized by mesomerie, which can couple with another monomeric molecule. The reaction propagates until termination to form polymer chains that can be stabilized using a crosslinker agent if needed. Typically it consists of a bi- or polyfunctional acrylate derivative [64] and allows the formation of stable networks. These networks are sometimes referred to as to hydrogels, due to their ability to swell upon contact with water. Recently, Susanto et al. demonstrated the fouling resistant properties of thin-layer hydrogel composite membranes that have been prepared by photograft polymerization of hydrophilic monomers (poly(ethylene glycol) methacrylate PEGMA and N,N-methylene bisacrylamide MBAA) onto PES UF-membranes [61].

3 Characterization of dominant mechanisms governing virus retention

3.1 Retention assessment with PP7-bacteriophages

The logarithmic reduction value (LRV) gives access to the retention efficiency. The LRV value corresponds to the ratio between virus concentration in the post-treatment solution and virus concentration in the pre-treated/filtered solution.

As already mentioned in section 2.1.2, virus logarithmic reduction values can be precisely determined using a plaque-forming assay. However, this particular detection method is a time and resource consuming process that involves at least 6-7 days of cultivation. The method is routinely used for validation studies, where the virus retention efficiency of a process operation unit has to be assessed accurately with a definite type of virus. However, it remains inadequate for development and screening phases where various materials and operating conditions have to be characterized rapidly.

At the present time, no indirect methods, based for example on measurements of the membrane pore size or flow characteristics, have shown consistent correlation with LRV. The use of the bacteriophage *PP7*, a small 25 nm, non-enveloped ss-RNA Pseudomonas phage from the Leviviridae family as a conceivable model virus for retention testing has been already described in the literature [38] and presents many advantages. First it has a size similar to the porcine parvovirus (PPV), commonly used as a B19 virus model for validation studies and is also not a human pathogen. Furthermore, its use does not require special virology equipment or laboratories and the final LRV result is already available the day following the infection. Last but not least, the high concentrated bacteriophage stock solution (10^7 particle/mL) necessary to assess high LRV values is economically more attractive than the corresponding virus containing stock solutions, due to the high cost and resources involved in their purification and concentration.

The set up of a typical spiking study with bacteriophages PP7 at Sartorius-Stedim Biotech (SSB) is shown in Figure 3.1.

Figure 3.1: Experimental set-up used for spiking study with the bacteriophage PP7 and evaluation of the retention efficiency of virus retentive membrane material. The system allows for 16 filtration experiments in parallel.

As already mentioned, the process solution is spiked with a high concentrated PP7-stock solution. The method allows precise LRV evaluation of at least 7 $\log_{PP7}$ since the minimum initial concentration of the bacteriophage containing solution is $1 \cdot 10^7$ pfu/mL. Therefore this value also corresponds to the detection limit of the method. Several dilutions of the obtained filtrate solution are mixed with a diluted bacterial preculture of *Pseudomonas aeruginosa*, mixed with nutrient broth agar and finally overlaid on the surface of a solid nutrient agar plate. After overnight incubation, the formed plaques on the plate surface are counted. Figure 3.2 gives an example of plaques formed on the surface of an agar plate.

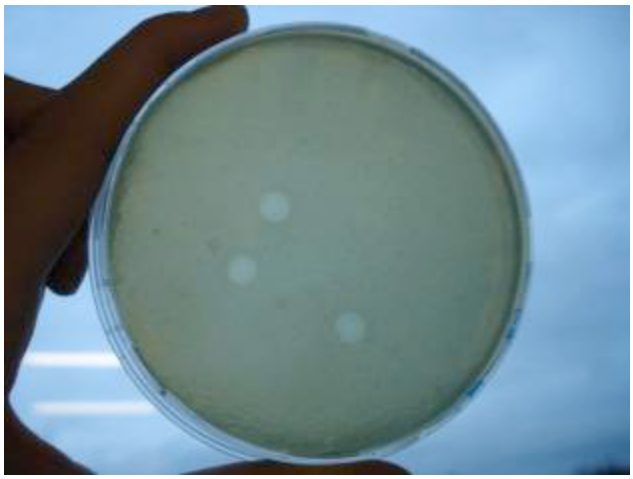

Figure 3.2: Plaques formed on the surface of an agar plate, after infection of *Pseudomonas aeruginosa* with the bacteriophage PP7.

The plaque assay described above is routinely used at SSB for quality controls regarding the release of Virosart® CPV, the commercially available virus filter at SSB. This filter product is validated for at least 4 log removal of bacteriophage PP7 and consists of 2 superposed layers of a polyethersulfone (PES) based flat sheet membrane. In order to achieve a high packing density, which is synonym of large surface area, the membrane material is pleated before sealing into the filter device. Small-scale devices, referred to as Minisart capsules and having a surface area of 5 cm^2, are also available at SSB and are typically used as well for validation studies as for product release (see also Figure 3.3). In both cases, the obtained LRV results are of great importance to determine if the product meets (or not) the required specifications.

Figure 3.3: a small scale filter device at SSB, also referred to as a Minisart module. Membrane surface area: 5 cm^2

Such studies are however mostly performed on filters in the final product configuration and do not consider parameters that may affect virus retention independently, e.g. the membrane orientation, impact of membrane pleating and protein-virus interactions. Furthermore, due to multilayer configurations, the retention efficiency of such devices cannot be assessed accurately when the LRV exceeds the limit of detection. Then, useful information regarding the membrane heterogeneity and its retentive properties may be overlooked, despite of their importance for up-scaling predictions.

The aim of this part is to elucidate how far the membrane orientation, the pore size distribution, the membrane structure and the presence of proteins in the solution can impact virus retention. Answering these questions will provide new insights into the mechanisms governing virus retention. This will also be useful for fixing the membrane structure requirements and to determine the optimum evaluation conditions, which should represent a “worst case” scenario for the membrane. Finally, the gained knowledge will contribute to the

development of prediction tools for up-scaling in order to prevent product failure at manufacturing scale.

3.2 Membrane orientation

Very often, membranes prepared by immersion precipitation exhibit an asymmetrical structure. This structure can be more or less pronounced depending on various physical parameters along the casting process. It depends, amongst other things, on the solvent/nonsolvent composition of the gaseous phase and can be controlled by changing the evaporation time of the solvent from the cast film before immersion. The definitive membrane morphology is permanently fixed in the coagulation bath. In general, membranes exhibiting a strong asymmetry are obtained when the cast film is abruptly immersed into the coagulation bath. The resulting structure consists then of a coarse layer with open pores on one side and a fine skin structure with tighter pores on the other side. In contrast, longer exposure to the gaseous phase before immersion will provide membranes having a more symmetric structure (see also section 2.2.1).

In contrast to ultrafiltration (UF) that is conventionally operated in tangential flow mode (TFF), virus filtration is typically performed by normal flow filtration (NFF). Operation in the NFF mode offers several advantages over TFF, including higher flow rates, easier integration into a production environment and lower capital expenditure [65]. For all of these reasons, virus filtration by NFF is preferred by a large majority of manufacturers.

In the case of ultrafiltration, the membrane side with tighter pores or skin side is typically placed towards the feed solution. The deposited molecules are then sheared from the membrane surface by the tangential flowing stream. This orientation presents the advantage that the solutes are rarely entrapped in the membrane structure, resulting in increased operating time. However, in the case of NFF and especially of virus filtration, viral particles accumulate as a cake on top of or within the filter porous medium and it remains unclear which membrane orientation or/and which degree of asymmetry provides higher retention.

In order to illustrate the impact of membrane morphology on retention properties, 2 PES-based membranes with distinctive structure properties were tested. Both material structures

were analyzed by scanning electron microscopy. Figure 3.4 reveals that the membrane on the right presents a strong asymmetric structure with pores of 500 nm on one side and tighter pores of approximately 50 nm on the other side, also referred to as "skin side". In contrast, the slight asymmetric morphology of the second membrane exhibits pore sizes varying from 200 nm to 50 nm. For this last structure the retentive layer with the smaller pores (approx. 50 nm) is located 10 µm below the represented "skin side", which exhibits here pores larger than 100 nm.

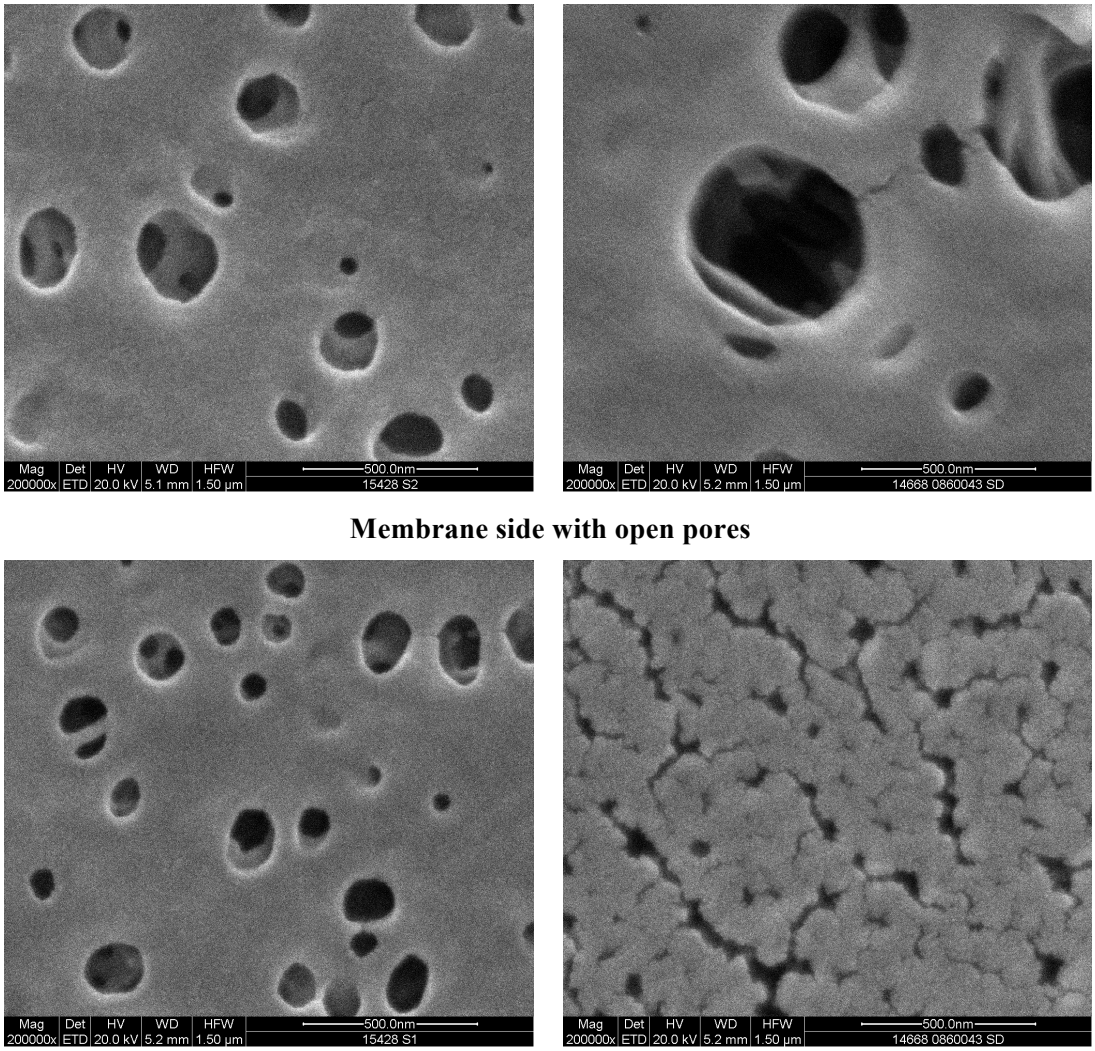

Figure 3.4: Scanning electron microscopy of 2 different PES membranes. Magnification: 200000x. Left: membrane with a slight asymmetric. Right: structure membrane with a strong asymmetric structure. Approx. membrane thickness: 100-110 µm.

Filtration experiments were performed using the two different membrane structures described above. For each membrane morphology, both orientations "skin-up" and "skin-down" were tested. As already mentioned, the term skin refers to the membrane side with the tighter pores.

Consequently, in the skin-up configuration, the skin side of the membrane is placed towards the feed solution.

Small scale devices with the designated configuration were prepared. Filtration of 50 mL of a 10^7pfu/mL PP7-bacteriophage solution was then carried out at constant operating pressure. All solutions were previously prefiltered using membranes having a nominal pore size of 0.1µm to remove small aggregates or impurities that may be present in the solution. This prefiltration was performed throughout this work before all filtration experiments. The increase of the filtrate volume as a function of time was assessed by weighing the collected filtrate. The virus titer in the filtrate was then determined as described in section 8.5.1

The obtained filtration curves for both membrane types as well as the corresponding flow rate as a function of time are shown in Figure 3.5 and Figure 3.6 respectively.

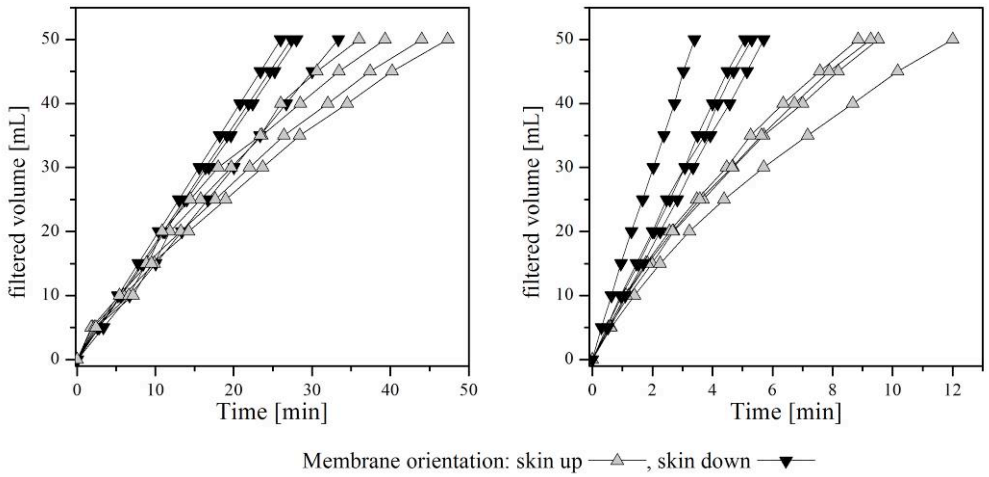

Figure 3.5: Filtration of a 50 mM Phosphate buffer solution spiked with 10^7 PP7-Phage/mL. Two different membrane structures: slight asymmetric (on the left) and strong asymmetric (on the right) and two different membrane orientations: skin up and skin down were tested. Constant operating transmembrane pressure (TMP): 2 bars.

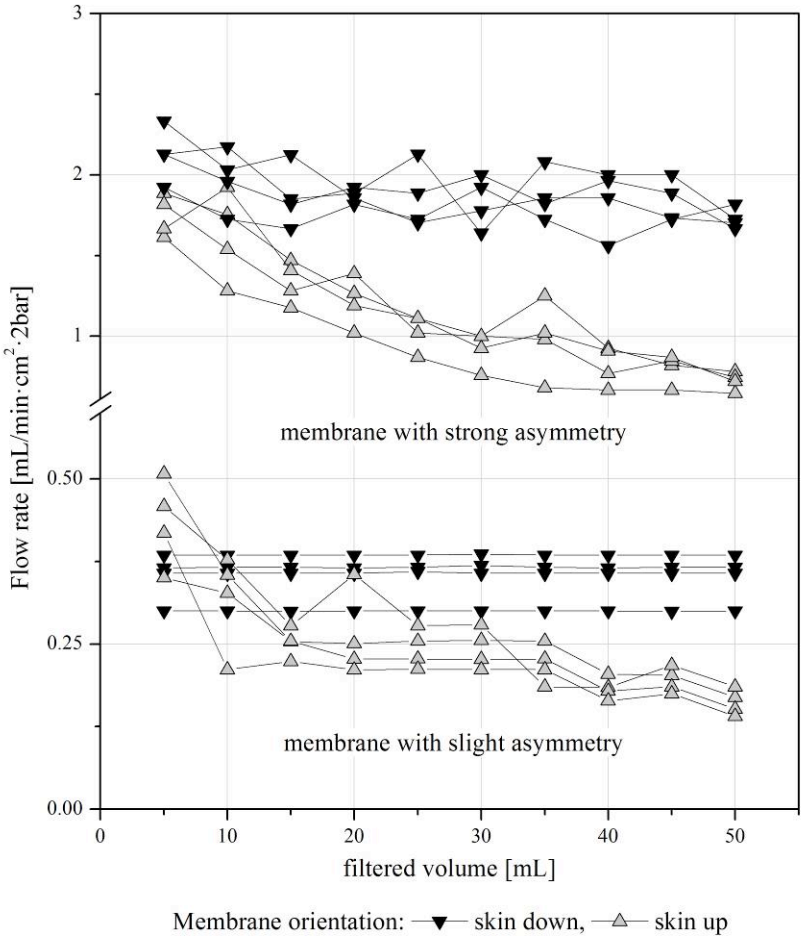

Figure 3.6: Orientation dependent decrease of the permeate flux measured on two membranes exhibiting a different degree of asymmetry**.**

Retention properties of the different membranes or/and filter configuration are illustrated in Figure 3.7. For each membrane type and configuration, membrane materials that originated from two different casting batches and exhibiting different flow characteristics were used.

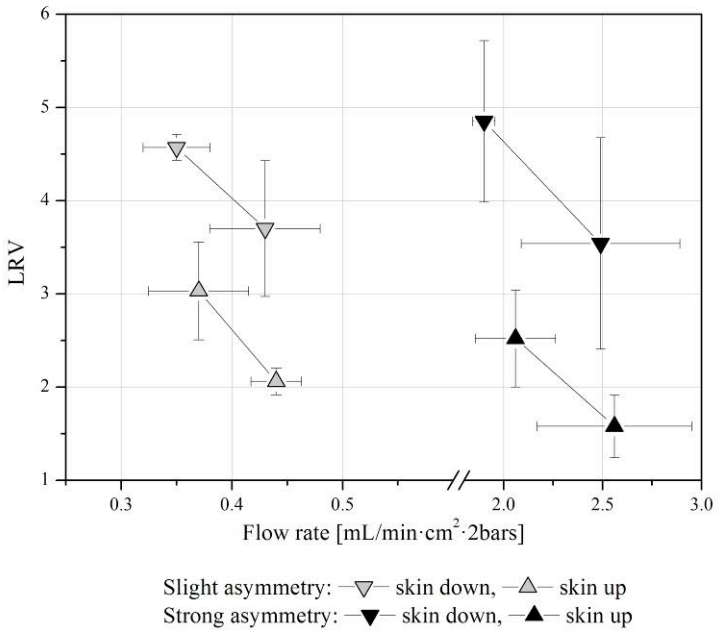

Figure 3.7: Impact of membrane orientation and asymmetry on PP7-bacteriophage retention.

The overall higher flow rate measured on strong asymmetric membranes illustrates the impact of the membrane structure on its flow characteristics. Typically, asymmetric membrane structures provide larger permeability since flow resistance principally occurs in the tight skin layer of the membrane. In the case of membranes with a low degree of asymmetry, flow resistance occurs along the whole membrane thickness, resulting in decreased flow rates.

The data presented in Figure 3.6 demonstrate that the skin-up orientation leads to a marked decrease of the permeate flow rate during the filtration process. In contrast, no decrease of the flow rate was observed for the skin-down configuration. Similar differences between the two filter configurations were observed in regards to PP7-retention. For both tested membrane structures, higher LRV were achieved when the membrane side with larger pores was facing the feed solution. Furthermore, the LRV and flow rates differences between both filter configurations appear to be more pronounced in the case of membrane exhibiting strong asymmetric structures.

The marked decrease of the permeate flux observed for skin-up orientations can be explained through the blockage of pores with bacteriophage particles. When the skin side is facing the feed solution, PP7 retention is mainly ensured on the surface of the thin membrane skin, where pore plugging dramatically affects the measured permeate flux. One can assume that the retentive skin layer possesses a distribution of pore sizes and that a fraction of pores are

somewhat larger than viruses. As the filtration progresses, the small pores become gradually plugged by bacteriophage particles. The proportion of the flow through larger pores progressively increases, resulting in PP7-breakthrough. A similar hypothesis was proposed by Bolton et al. [16] to explain the mechanisms of LRV decline in virus filtration studies.

In contrast, the skin-down orientation may be less affected by mechanisms based on pore size selectivity. Here the coarse structure layer placed towards the feed stream may act as a depth filter. Such filters are well known for retaining large masses of particles before becoming plugged [66]. Particles are retained throughout the filter media rather than just on the surface. Decrease of permeate flux is practically not observed, since the pore flow distribution is less affected on the skin side, where flow resistance principally takes place. Finally, the entrapment of PP7 particles in the tortuous porous medium may occur due either to adsorptive or size exclusion based mechanisms.

On the basis of data obtained in this study, it appears that skin down configurations provide both higher LRV and permeate flux over the entire filtration process than skin-up configurations. At equal retention, strong asymmetric membranes exhibit a 4 times higher permeability than membranes with a rather symmetric structure. Next steps will aim to clarify if the apparent suitability of strong asymmetric structure for virus retention is also ensured in the presence of high plugging product streams like pooled IgG.

3.3 Effect of flow decay on retention

Previous experiments have shown that the retentive efficiency of virus filter may be reduced when a decrease of permeate flux is observed. Virus filtration is typically performed on process solutions that may contain high concentrations of protein, or protein with high fouling tendency. For such applications, decrease of the permeate flux is also a common issue, that may also enhance pore size selectivity, modify flow distribution in the pores, and finally impact retention efficiency. Furthermore, conceivable interactions between bacteriophage-particles and proteins could also have an influence on LRV and have to be examined. The understanding of such mechanisms is essential to determine the optimum experimental conditions for the evaluation of LRV of future materials.

In order to see the influence of protein presence on LRV, different IgG-containing solution were spiked with PP7-bacteriophage at $1 \cdot 10^7$ pfu/mL. The IgG concentration of the three tested solutions was 0 g/L, 1 g/L and 2 g/L. Filtration experiments were carried out using 3 membranes with different structure properties: two of them exhibited a similar slight asymmetric morphology but different permeability and retentive properties. The third membrane had a strong asymmetric structure and a LRV comparable to the more retentive slightly asymmetric membrane. Table 3.1 summarizes the structures properties and performance characteristics of these membranes.

Table 3.1: Structure properties and performance characteristics of used membranes

	Membrane asymmetry	Permeability with water [$L \cdot min^{-1} \cdot cm^{-2}$] at 2 bar	LRV after filtration of 50 mL of 50 mM KPi-buffer spiked with 10^7 Pfu/mL PP7
Membrane A	Slight	0,52 ± 0,01	2,0 ± 0,5
Membrane B	Slight	0,40 ± 0,01	5,0 ± 0,9
Membrane C	strong	1,9 ± 0,05	4,8 ± 0,8

For all tested membranes and spiked IgG solutions, filtrate fractions were collected during the filtration process. The bacteriophage titer at collecting time was determined in each fraction in order to monitor the LRV progression over the entire filtration process. In parallel, the decrease of permeability as a function of time was measured by weighing the collected filtrate quantity. All filtration experiments were performed with the skin-down orientation, which provide higher LRV and lower flow rate variability than skin-up orientation. The influence of the membrane morphology and IgG-concentration on the decrease of permeate flux is illustrated in Figure 3.8. The determined LRV in the collected fractions are shown for all tested membranes and IgG concentrations in Figure 3.9.

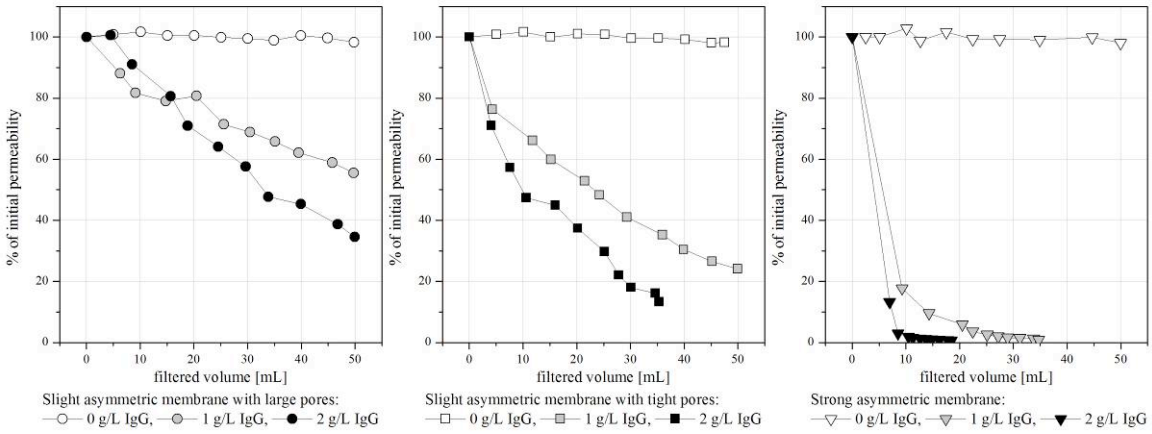

Figure 3.8: Influence of the membrane structure and of the IgG-concentration on decrease of permeate flux during PP7-removal. Tested solutions: 0 g/L, 1 g/L and 2 g/L IgG in 50 mM KPi-buffer spiked with PP7-phages at 10^7 pfu/mL.

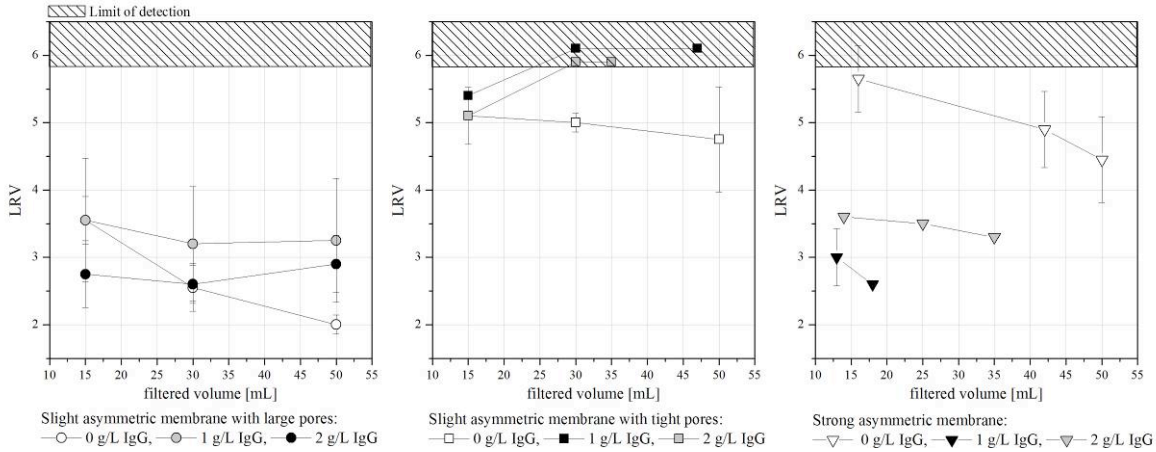

Figure 3.9: Phage clearance of different IgG-containing solutions with 3 membrane filters exhibiting distinctive structure properties. The 3 different solutions with IgG concentrations of 0 g/L, 1 g/L and 2 g/L were spiked with PP7-bacteriophages at 10^7 pfu/mL.

For all membrane types, stronger flow decay was observed with increasing IgG-concentrations. This suggests that the membrane pores become gradually fouled by proteins during the whole filtration process, probably due to size exclusion or adsorptive mechanisms. Figure 3.8 also reveals the trade-off relationship between LRV and filtration capacity. The two membranes with similar morphologies but different retention efficiencies exhibited dissimilar filtration behaviors. Higher resistance to fouling and higher protein passage was achieved by the membrane with lower retention.

Considering the two membranes with equal retentive properties but different morphologies, it appears that strong asymmetric structures are particularly sensitive to fouling. Despite of the considerably higher water permeability typically featured by asymmetric membranes,

dramatic flow decreases were observed in the presence of proteins. Complete plugging of the membrane was even achieved after filtration of only 10 mL of a 2 g/L IgG-solution.

In the absence of proteins, no variation of permeability was observed over the entire filtration process with the 3 tested membranes. However, measurement of the PP7-titer in each collected filtrate fraction pointed out that LRV declines with increasing filtrate volume, reinforcing the theory of pore selectivity described in section 2.1.3 As the filtration progresses, smaller pores become progressively plugged by phage particles, leading to the alteration of the flow distribution. After a certain processing time, a point is reached at which permeate flow through large pores represents a relatively high proportion of the overall liquid flow and bacteriophage breakthrough can occur. This phenomenon explains the decline of LRV without protein that was observed with all tested membrane structures.

Figure 3.9 also suggests that the presence of IgG in the spiked challenge solution does not only impact the permeate flux, but also the retentive properties of all tested membranes. This is especially true for strong asymmetric membranes, whose retention capabilities are dramatically reduced at increased IgG-concentrations. This shows that flow decay due to membrane fouling also affects LRV. The thin retentive skin layer, characteristic of such asymmetric structure, appears to be particularly sensitive to membrane fouling and become plugged early, even with moderate amounts of IgG-containing solution. Additionally, the presence of proteins in the feed medium enhances the selective plugging of pores with smaller size and induces LRV decline.

However, in the case of membrane exhibiting a more symmetric morphology, higher retention is achieved with spiked IgG-solutions than in the absence of protein. Here the flow-decay-versus-LRV relationship observed on asymmetric structures is not applicable anymore and additional, more complex, mechanisms are involved. As described in the previous section, the more symmetric porous structure of membrane A and B may act as a depth filter and retain particles throughout the filter media rather than just in a thin skin layer. This may minimize membrane fouling phenomena but also prevent alteration of the flow distribution. Phage retention appears to be dominated by other mechanisms like pore constriction due to adsorption of protein to the specific surface area or bacteriophage-IgG interactions. Both hypothesis may explain the higher retention attained with IgG-containing solutions.

In conclusion, the LRV progression for this particular membrane structure may result from two separated mechanisms occurring at different stages. During the first stage of the filtration, LRV decline due to pore selectivity may be the dominating mechanism, whose effects may vary depending on the protein concentration and pore size distribution. In a second stage, as a certain amount of feed solution has passed through the membrane filter, pore constriction may overlap pore selectivity mechanisms and lead to an overall higher retention capacity.

According to the results obtained in this part, it appears that membranes with slight asymmetric structure present the best compromise between retention and filtration capacity. Retention evaluation must be conducted with viral spikes that represent a "worst case" challenge. For that reason, retention testing on membrane exhibiting similar structure properties should be further performed without protein.

3.4 Prediction model for precise retention targeting

Section 2.1.2 reported the suitability of bacteriophages as model parvoviruses for virus retention testing. It is known that virus retention is strongly depending on the membrane pore size distribution. Furthermore, a noticeable variability in the retention was observed within filtration experiments performed in the previous sections. These tests were performed using small filter devices. This variability is probably due to the membrane heterogeneity and may be less pronounced for bigger devices containing larger surface area. On the one hand, testing using small filter devices is convenient for development purposes due to lower buffers and solutions requirements. On the other hand, in a set of satisfying small filter devices, a defective test device, exhibiting a low or even no retention, does not weight statistically or can even be considered as an outliner. However, a similar defect can have dramatic consequences for larger filter devices and lead to virus breakthrough. Thus there is a need for a predicting tool able to evaluate how far the variability in the retention can impact the retention characteristics of an upscaled filtration device. Such a tool is essential to define the specifications (average LRV and allowed variability) that have to be met at small scale in order to target assigned retention efficiency with high scale filter devices.

The main goal of the following study was to develop a mathematical model that is able to predict the LRV of an upscaled filter device, based on the average retention, the retention

variability obtained with small devices and the chosen filter configuration like e.g. the number of membrane layers.

3.4.1 Influence of membrane heterogeneity

In a first part, the impact of membrane heterogeneity on bacteriophage retention was investigated. A representative number of filter devices containing one membrane disc with a surface area of 5 cm^2 were built and their retention characteristics were assessed using the bacteriophage based determination method described in section 3.1. Each membrane disc that was sealed into the device originated from the same membrane casting batch. The average targeted retention during the membrane casting process was about 4 $logs_{PP7}$ in order to minimize the probability for a filter sample to exceed the detection limit of 7 $logs_{PP7}$ inherent to the method.

The LRV was determined for each filter device after filtration of 50 mL of a solution with a bacteriophage concentration > 10^7 phages/mL. The average filtration flow rate was also determined for each device as described in section 8.4.1. At the same time, large-scale filtration cartridges (approx. surface area: 0.2 m^2) were built using the same material to allow comparison between results obtained using the prediction tool and the ones determined experimentally. The membrane material was comprised between two layers of protecting fleece material and then pleated. (see Figure 3.10). The pleats were achieved by back-and-forth folding of the flat membrane upon itself and allow for an increased packing density.

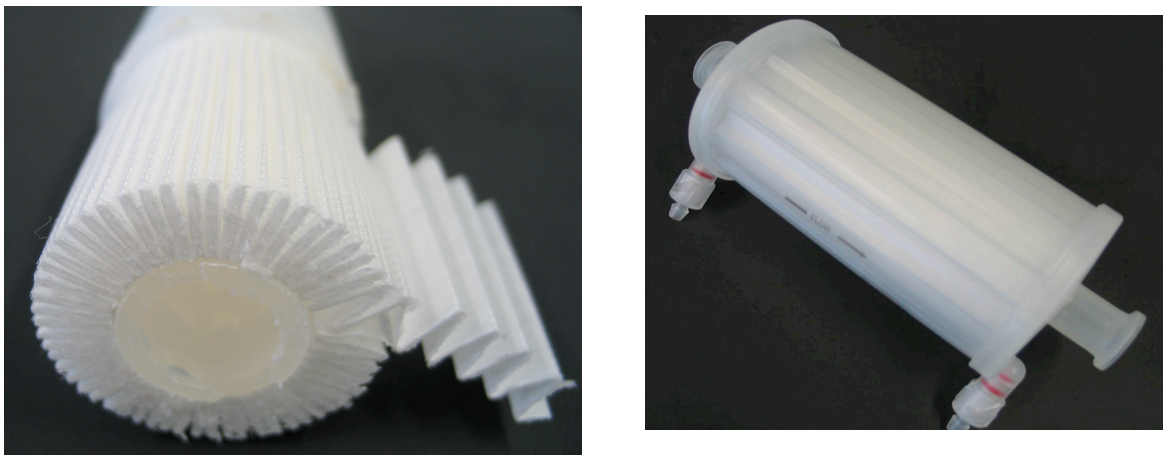

Figure 3.10: Assembly of a large scale filtration device containing a membrane surface area of 0,2 m^2. The membrane is comprised between 2 layers of protecting fleece material, pleated (left) and sealed into a filtration cartridge (right).

The same solution volume-to-surface area-ratio as used in small scale devices was considered. The data obtained on small scale devices was grouped within LRV-classes as follows:]m;m+1] when m<n≤m+1, with n = measured LRV and the corresponding probability P(n) was calculated using the following equation:

$$P(n) = \frac{\text{number of devices with } n \in]m;m+1]}{\text{total number of devices}} \qquad \text{(Eq. 3.1)}$$

The experimental data were then fitted using a normal Gaussian distribution (see Figure 3.11). The obtained parameters were respectively an average LRV μ of 4.5 and a standard deviation σ of 0.91.

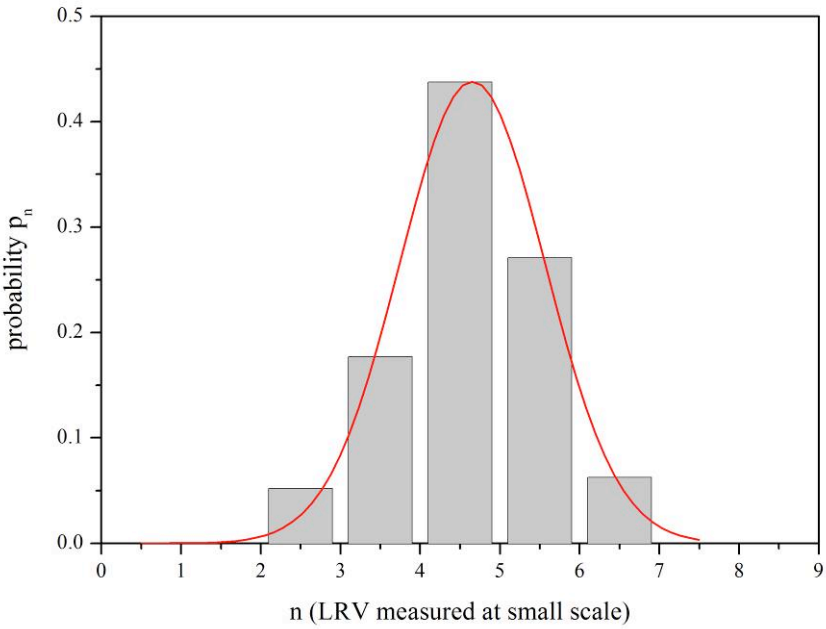

Figure 3.11: Probability density function of LRV using small scale filter devices. The membranes sealed into the filter devices all originate from the same membrane casting batch. The effective filtration surface area was 5 cm^2. The experimental data (n=96) was grouped in LRV intervals and fitted using a normal Gaussian distribution. The obtained parameters are: μ=4,5; σ=0,91.

According to the obtained regression coefficient of 0,993, the heterogeneity of the produced membrane in regard to Phage-retention can be described by a normal Gaussian distribution (see Eq. 3.2).

$$P(n) = \frac{1}{\sigma\sqrt{2\pi}} \cdot e^{-\frac{(n-\mu)^2}{2\cdot\sigma^2}} \qquad \text{(Eq. 3.2)}$$

The logarithmic reduction value measured on a small scale filter device, hereafter referred to as n is defined by:

$$LRV = n = \log\frac{N_{Si}}{N_{Sf}} \Leftrightarrow N_{Sf}(n) = \frac{N_{Si}}{10^n} \qquad \text{(Eq. 3.3)}$$

Where N_{Si} and N_{Sf} are the number of viruses contained initially in the feed solution and in the filtrate respectively.

Small scale devices may be considered as finite surface areas building the discretization scheme of a larger filter device. The expected logarithmic reduction value LRV_B of such a device is described by:

$$LRV_B = \log\frac{N_{Bi}}{N_{Bf}} \qquad \text{(Eq. 3.4)}$$

and $N_{Bi} = N_{Si} \cdot X$ (Eq. 3.5)

where X refers to the number of finite surface elements comprised in the larger filter device. N_{Bf} is the number of bacteriophages collected downstream to the large filter and also corresponds to the sum of particles that have passed through each small scale filter devices.

$$N_{Bf} = \int X \cdot P(n) \cdot N_{Sf}(n) \cdot dn \qquad \text{(Eq. 3.6)}$$

Substituting Eq. 4.3 for N_{Sf}, Eq. 4.6 can be rewritten as

$$\Leftrightarrow N_{Bf} = X\int P(n) \cdot \frac{N_{Si}}{10^n} \cdot dn = X\int P(n) \cdot \frac{N_{Bi}}{X \cdot 10^n} \cdot dn = N_{Bi}\int \frac{P(n)}{10^n} \cdot dn \qquad \text{(Eq. 3.7)}$$

$$LRV_B = \log\left(\frac{1}{\int \frac{P(n)}{10^n} \cdot dn}\right) \qquad \text{(Eq. 3.8)}$$

Since $P(n)=f(n;\mu,\sigma)$, the expression above shows that the average retention μ and the associated standard deviation σ, measured on small scale devices are determining for the retention efficiency of larger filtration devices.

However, it should be pointed out that Eq. 3.8 does not consider flow rate differences between the tested small scale devices. The flow rate in each small scale device, referred to as $J_S(n)$, was measured within these experiments. Figure 3.12 clearly shows that higher flow rates are observed on filters exhibiting lower retention. This suggests the existence of an inhomogeneous flow distribution within the large scale filter and shows that particle passage

predominantly occurs through membrane domains with higher flow rate. Furthermore, these results also pointed out that small flow rates differences can have dramatic consequences on the phage retention efficiency.

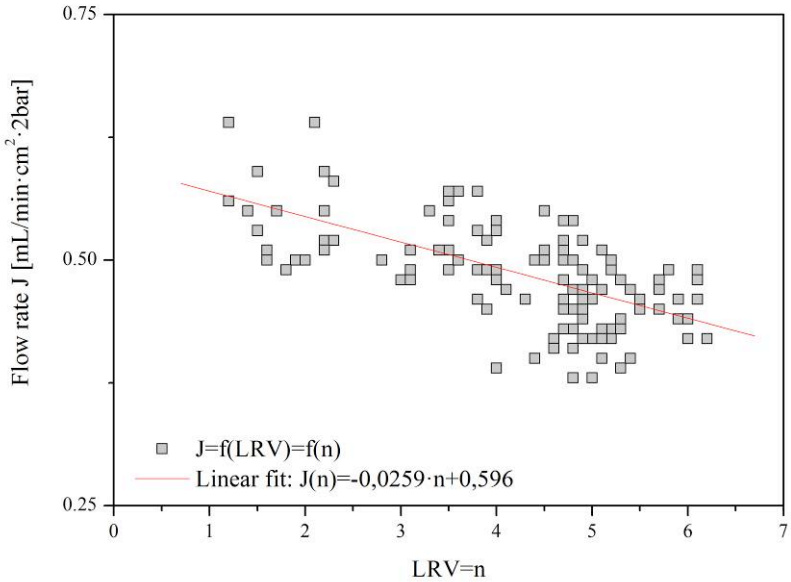

Figure 3.12: linear correlation between LRV and filtration flow J(n) rate measured on small scale filter devices. The filtration experiments were performed at constant pressure P=2bars

One can assume that differences in the $J_S(n)$ values will impact the number of phages retained by each finite surface element. As a consequence, the number of phage N_{Bi} that is processed by each surface element becomes a function of n. Nevertheless, the total number of phages initially contained in the feed solution N_{Bi} and passing through the large scale device at a flow rate J_B remains unchanged.

$$J_B = \int J_S(n) \cdot dn \qquad \text{(Eq. 3.9)}$$

$$N_{Si}(n) = N_{Bi} \cdot \frac{J_S(n)}{J_B} = N_{Bi} \cdot \frac{J_S(n)}{X \cdot \bar{J}_S} \qquad \text{(Eq. 3.10)}$$

Where $\bar{J}_S$ is the mean flow rate across a finite surface element.

$$N_{Bf} = \int X \cdot P(n) \cdot N_{Sf}(n) \cdot dn = X \int P(n) \cdot \frac{N_{Si}(n)}{10^n} \cdot dn = X \int P(n) \cdot \frac{N_{Bi}}{10^n} \cdot \frac{J_S(n)}{X \cdot \bar{J}_S} \cdot dn \qquad \text{(Eq. 3.11)}$$

$$N_{Bf} = N_{Bi} \int \frac{P(n)}{10^n} \cdot \frac{J_S(n)}{\bar{J}_S} \cdot dn \qquad \text{(Eq. 3.12)}$$

After substitution of N_{Bi} with Eq. 3.4, the expected LRV of a large scale filter device is expressed by Eq. 3.13

$$LRV_B = \log\left(\frac{1}{\int \frac{P(n)}{10^n} \cdot \frac{J_S(n)}{\bar{J}_S} \cdot dn}\right) \qquad \text{(Eq. 3.13)}$$

Finally, the expected LRV of the up-scaled filter device was determined theoretically as a function of μ and σ using the following expression:

$$LRV_B = \log\left(\frac{1}{\sum_{n=1}^{n=b} \frac{P(n;\mu,\sigma)}{10^n} \cdot \frac{J_S(n)}{\bar{J}_S} \cdot \Delta n}\right) \qquad \text{(Eq. 3.14)}$$

Where b is the upper boundary. The interval length Δn was chosen according to the following expression:

$$\Delta n = \frac{b}{100} \qquad \text{(Eq. 3.15)}$$

Using this predicting tool, the logarithmic reduction value expected in a large scale filtration device can be evaluated according to the statistical parameters μ and σ, determined using a set of small scale filter devices. These parameters describe respectively the average retention efficiency and the heterogeneity of the membrane material used for the fabrication of such devices. Figure 3.13 illustrates the strong impact of the membrane heterogeneity on bacteriophage retention. Theoretical LRV-values were predicted by varying σ and μ. The model shows, as expected, that up-scaling issues are not observed with ideal membrane materials exhibiting a narrow pore size distribution and having a σ value close to zero. On the contrary, a high σ value indicates a large pore size distribution that strongly affects the retention efficiency of the filter device.

In order to rate the reliability of the prediction tool, the LRV_B obtained theoretically using the parameters μ and σ from Figure 3.11 were then compared to the logarithmic reduction value measured experimentally on large scale filter devices containing the same monolayer membrane material.

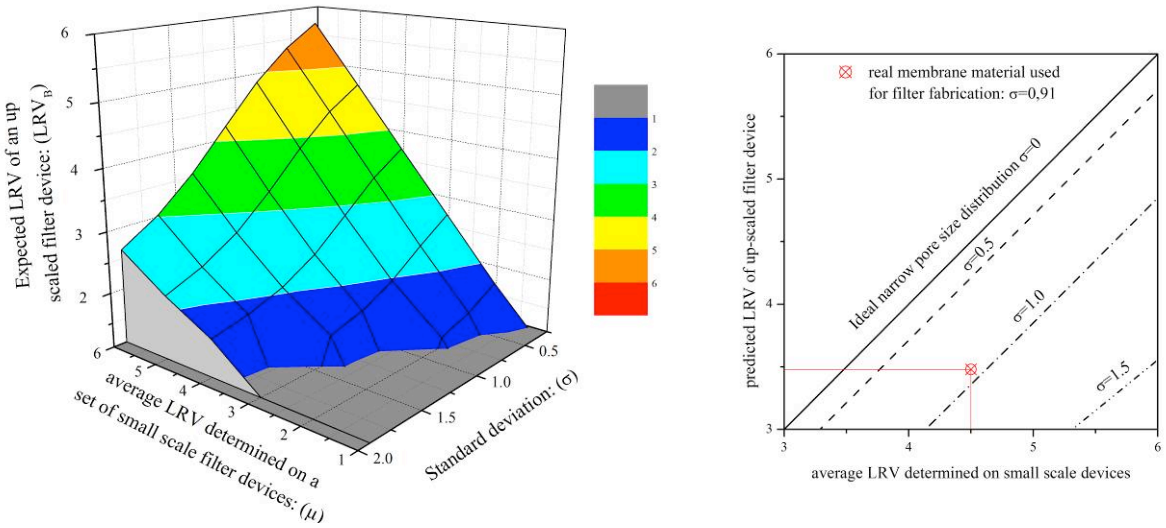

Figure 3.13: Impact of the average phage retention and membrane heterogeneity on the logarithmic reduction value of large scale filter devices (left). LRV-prediction of an up-scaled filtration device containing one layer of the experimentally considered membrane material: LRV_B= 3,4 (right)

The corresponding results are summarized in Table 3.2.

Table 3.2: Comparison of the LRV determined experimentally on a 0,2 m^2 large scale filter device with LRV calculated using the predicting tool.

LRV of an up-scaled filter device calculated theoretically		LRV determined experimentally on filter device with a 0.2 m^2 surface area (4 repeats)
Flow rate not considered	Flow rate considered	
3,64	3,46	3,7 ± 0,4

The results obtained experimentally are in accordance with the logarithmic reduction values determined using the model described above. Assuming that the assembled small and large scale devices did not contain any defects, the prediction tool appears to provide valuable approximation of LRV obtained after up-scaling. These results show once again the impact of membrane heterogeneity on the retention efficiency, but also that the contribution of the inhomogeneous flow distribution on virus breakthrough is minimal.

3.4.2 Influence of membrane layer configuration

A conceivable alternative to improve the retention efficiency of a virus filter is to increase the number of membrane layer contained in the device. An important feature of logarithms is that they reduce multiplication to addition and a filter device containing two superposed membrane layers may exhibit a two times higher retention compared to the corresponding monolayer configuration. Furthermore such a multilayer configuration would not require membrane material with tighter pores to permit higher retention and protein passage may not be affected. However, the resulting filter permeability will decrease due to increased flow resistance.

The use of small scale devices containing multiple membrane layers is not always adequate for precise up-scaling predictions, since such devices may exhibit LRV that exceed the detection limit. For that reason, the retention efficiency of a large scale multilayer filter device should be based on results obtained with monolayer small scale devices. Thus the model developed in the previous section may be suitable for multilayer prediction if the two following mathematically obvious hypothesis are confirmed experimentally: the additivity of LRV and the inversely proportional relationship between flow rate and number of layers.

Small scale devices containing 1, 2 and 3 layers of a membrane material with a targeted retention of 1-2 logs were assembled. Under such conditions, even the 3-layer-configuration should not provide LRV higher than 6. In order to ensure that the pressure applied on each membrane layer was similar for all filter devices, the filtrations experiments were performed at a constant operating pressure of 1, 2 and 3 bars respectively. LRV determinations were then determined according to the method described in previous section.

Figure 3.14 shows that the 3 different filter configurations all exhibit an equal LRV normalized to the number of membrane layers, confirming that LRVs are additive. As also expected, the resistance to the flow increased proportionally to the number of membrane layer, and equal flow rates were obtained with the 3 different device configurations when operated at proportionally increasing pressures.

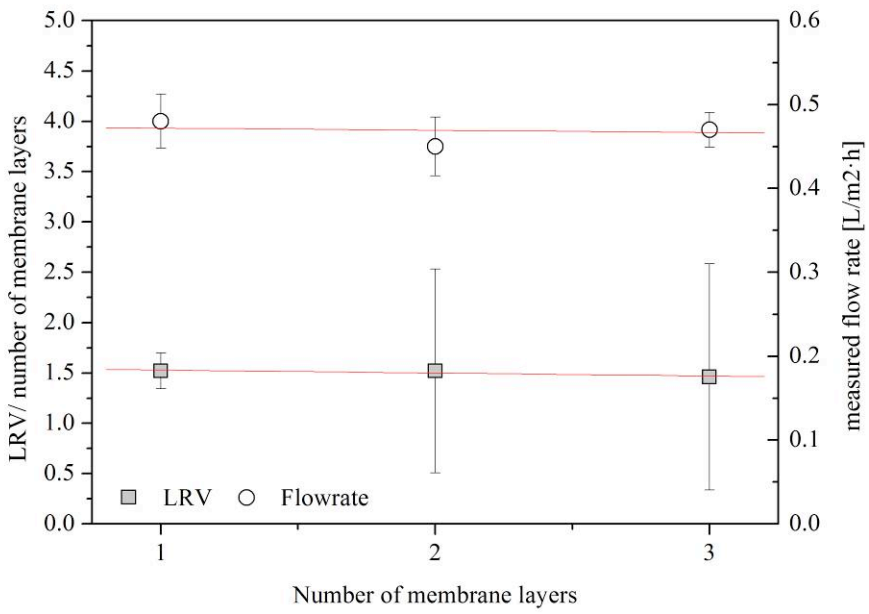

Figure 3.14: LRV and Flow rates measured on small scale devices containing 1, 2 and 3 layers of the same membrane material .Depending on the layer configuration, the operating pressure was set to 1, 2 and 3 bars respectively. (number of repeats=8)

Based on these confirmations, the developed prediction tool can be used to evaluate the retention capacity of an up-scaled multilayer filtration device. Since the convolution of two Gaussians, characterized by the parameters $[\mu_1;\sigma_1]$ and $[\mu_2;\sigma_2]$ is another Gaussian with the parameters $[\mu_3;\sigma_3]$ where:

$$\mu_3 = \mu_1 + \mu_2 \qquad \text{(Eq. 3.16)}$$

and

$$\sigma_3 = \sqrt{\sigma_1^2 + \sigma_2^2}\ , \qquad \text{(Eq. 3.17)}$$

Under the condition that similar membrane material is used in the multilayer filter device, P(n) is now described by:

$$P(n) = \frac{1}{\sigma\sqrt{2 \cdot k \cdot \pi}} \cdot e^{-\frac{(n-k\cdot\mu)^2}{2\cdot k\cdot\sigma^2}} \qquad \text{(Eq. 3.18)}$$

Where k corresponds to the number of membrane layers building the large scale device. μ and σ represent as before the statistical parameters determined experimentally on monolayer small scale devices.

Besides the observed improvement of the retention efficiency, Eq 3.17 and 3.16 also show that increasing the layer number amplifies the membrane heterogeneity. This phenomenon is illustrated in Figure 3.15, where the LRV distribution of a double and triple layer

configuration were simulated, based on the parameters determined experimentally in the previous section.

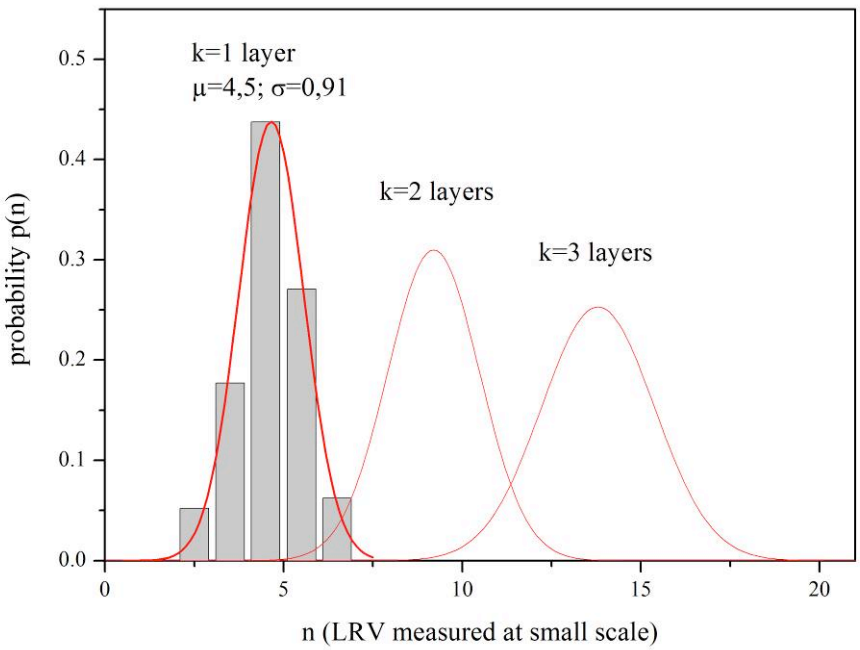

Figure 3.15: Simulated probability density function of LRV obtained with small scale devices containing 2 and 3 membrane layers. The used membrane material is characterized by the statistical parameters: μ=4,5 and σ=0,91

Considering the LRV additivity and the flow resistance proportionality regarding multilayer configurations, the experimentally determined J(n) can now be written as:

$$J_S(n) = \frac{0.0259}{k^2} \cdot n + \frac{0.596}{k} \qquad \text{(Eq. 3.19)}$$

As described in Eq. 3.19 and illustrated in Figure 3.16, the impact of the flow rate on phage retention is strongly reduced when the number of membrane layers k contained in the device increases. Therefore the use of multiple membrane layer contributes to homogenize the flow rate distribution in the device, whose impact on phage retention can be considered as negligible in large scale filter devices.

After replacement of both J(n) and P(n), Eq. 3.14 was used to predict the LRV of a large scale filter device, containing 2 membrane layers, at various μ and σ values. A 3-dimensional representation of this prediction is shown exemplarily in Figure 3.17. In the mean time, 0,2 m^2 large scale filter devices, containing 2 membrane layers were assembled. The same membrane material and assembly procedure as in section 3.4.1 was considered. As previously described,

the retention efficiency of the assembled large scale devices was assessed using PP7-bacteriophages as virus-like particles.

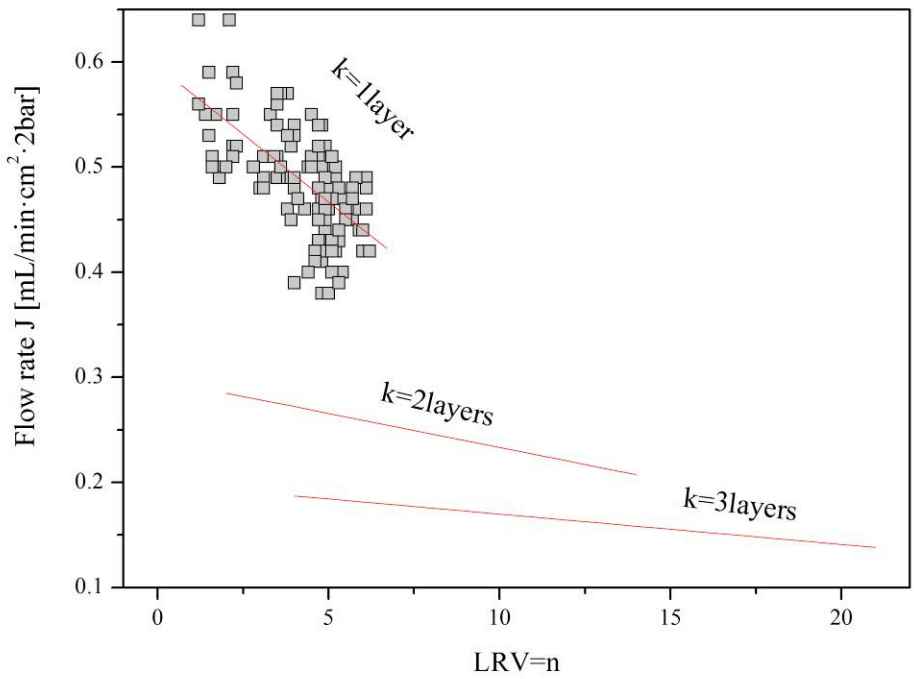

Figure 3.16: LRV-dependent filtration flow rate simulated on small scale devices containing 2 and 3 membrane layers.

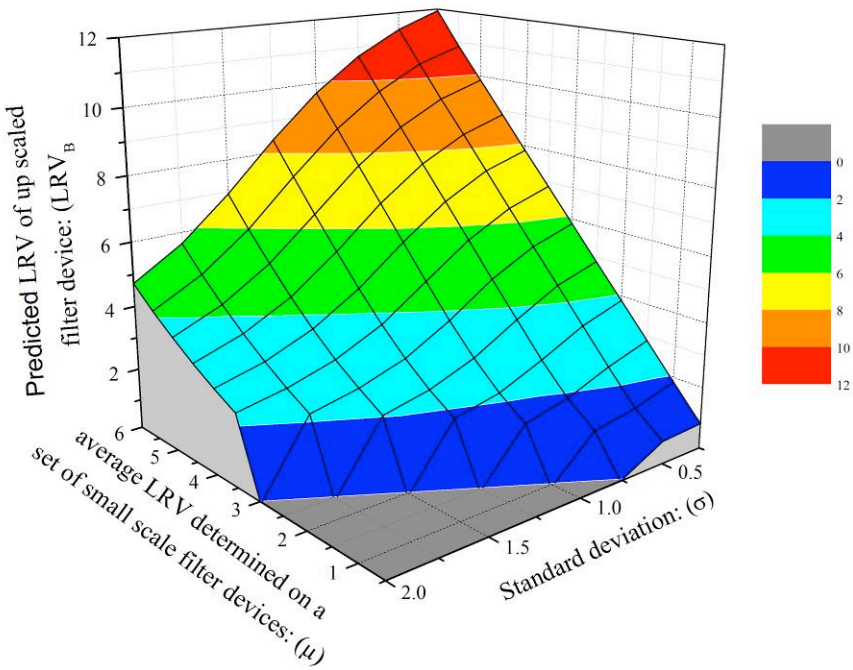

Figure 3.17: Impact of the average Phage retention and membrane heterogeneity on the logarithmic reduction value of large scale filter devices containing 2 membrane layers.

The experimentally determined LRV are summarized in Table.3.3 and compared with the predicted LRV.

Table.3.3: Comparison of the LRV determined experimentally on a 0,2 m^2 large scale filter device with the LRV calculated using the predicting tool. The number of membrane layers considered was 2

LRV of an up-scaled filter device calculated theoretically		LRV determined experimentally on filter device with a 0,2 m^2 surface area (4 repeats)
Flow rate not considered	Flow rate considered	
6,44	6,28	5,9 ± 0,3

Similar to results obtained in the previous section, where monolayer large scale devices were used, predicted LRVs are in accordance with predicted values when multilayer configurations are considered. Since the values determined experimentally lie close to the limit of detection inherent to the testing method, the LRV determined experimentally may have been underestimated.

3.5 Conclusion

In a first part, dominant mechanisms governing virus retention were identified. Using bacteriophage PP7 as a parvovirus-like-particle, the impact of the structure properties, the membrane orientation and the protein concentration in the spiked medium were analyzed. According to the results obtained within this part, a suitable virus retentive membrane should not exhibit a strong asymmetric structure due to pore size selectivity mechanisms and alteration of the flow distribution over the processing time. The side with the larger pores should be placed towards the feed solution, also referred to as skin down orientation, to provide higher LRV.

If the main goal of a spiking study is to evaluate the performance of new developed retentive materials, proteins should be absent from the feed solution, in order to avoid overestimating clearance values. In contrast, validation studies should be conducted at conditions that correspond to process scales and using the real process solution.

Generally, spiking studies are typically performed at scale down conditions due to logistic and economic limitations. However, successful up-scaling necessitates the availability of efficient prediction tools that are able to predict the performance of filter devices with larger surface area, taking into account membrane heterogeneity, retention properties and layer configuration measured on small scale devices.

The second part focused on the development of such a prediction tool, whose suitability was confirmed by comparison with experimental data. Consistent LRV predictions in large scale filtration devices were achieved using a set of data measured on small scale devices with a 400 times lower surface area. This was true for devices containing one single membrane layer as well as for configurations consisting of 2 superposed membrane layers. The results also illustrated the suitability of small-scale devices to evaluate the LRV of larger filtration devices. This is of great importance since manufacturing processes are typically validated based on downscale devices. Furthermore the valuable predictions obtained also argue for reliable device construction and for the absence of defects due to product related issues like pleating or sealing.

4 Characterization of dominant mechanisms governing membrane fouling

Besides the insurance of robust virus retention, an important feature required for a competitive virus filter is high filtration capacity. The membrane should be able to filter large amounts of process solution and ensure high product recovery.

One issue governing the performance of size exclusion based virus filtration is membrane fouling, a marked decrease of permeability as a function of permeated solution volume per membrane area, as was illustrated in the previous section.

It has been reported that membrane/solute interactions can significantly impact protein filterability [67, 68]. Adsorption of protein to the membrane surface due to hydrophobic or electrostatic interactions depends on the surface properties of both protein and membrane in a given solution environment. Electrostatic attraction/repulsion is less prominent at higher salt concentrations [69] or at pH-values near to the isoelectric point (PI) of the protein of interest [68, 70-74]. Additionally, hydrophobic interactions can also lead to adsorption of proteins on porous materials made of rather hydrophobic polymers like e.g. polysulfone (PS), polyethersulfone (PES) or polyvinyldifluoride (PVDF) [48].

Plasma derived therapeutics for intravenous administration, containing pooled immunoglobulin G (IgG) of over thousand of blood donors, are typical high plugging protein streams, whose filtration is often observed to be throughput limited. IgG consists of four polypeptide chains; two identical heavy chains and two identical light chains connected by disulfide bonds regions. Each chain consists of two different regions: the constant region and the variable region. The constant region is identical in all antibodies of the same isotype, and consequently in all antibodies contained in such therapeutic solutions. In contrast, the variable region exhibit a high degree of variability in order to interact with a large variety of antigens and confer passive immunity to deficient people which have decreased or abolished antibody production capabilities [8, 21]. However, the variability in the amino acid residues may diversify the electrical and hydrophobic properties of the IgG contained in the therapeutic mixture and, consequently, increase the number of interactions potentially leading to membrane fouling.

The main objective of this part is to determine how far adsorption due to electrostatic or hydrophobic interaction can impact the filtration performance of pooled IgGs. This involves the characterization of electrostatic and hydrophobic properties of both membrane and protein solution under a variety of operating conditions as well as the evaluation of their relative contribution to membrane fouling.

4.1 Electrostatic solute-membrane interactions

Many researchers have used the membrane surface charge as a correlating parameter to study fouling characteristics, with the greatest fouling typically observed under conditions where solute and membrane have opposite net charge [75, 76].

The pH of a solution has been found to be a major factor influencing protein adsorption to membrane filter [70]. Proteins have a net positive charge at pH-values below the isoelectric point (pI). Under these conditions and depending of the charge carried by the membrane, electrostatic attraction or repulsion can occur and lead to irreversible protein adsorption.

In order to be able to predict and consequently to prevent such mechanisms, it is necessary to determine the pI or pI-distribution of the concerned protein or protein mixture, respectively. The surface charge of the considered membrane also has to be characterized. This can be achieved by measurement of the zeta potential, which often is assumed to be an indirect, relative description of the membrane surface charge.

4.1.1 Isoelectric point distribution of pooled Immunoglobulins

2D-gelelectrophoresis was performed in order to determine the pI-distribution of the pooled IgG-preparation. 2D-gelelectrophoresis is an established technique that allows separation of proteins by isoelectric point in the first dimension and by mass in the second dimension. The obtained 2D-gelectrophoregram is shown in Figure 4.1.

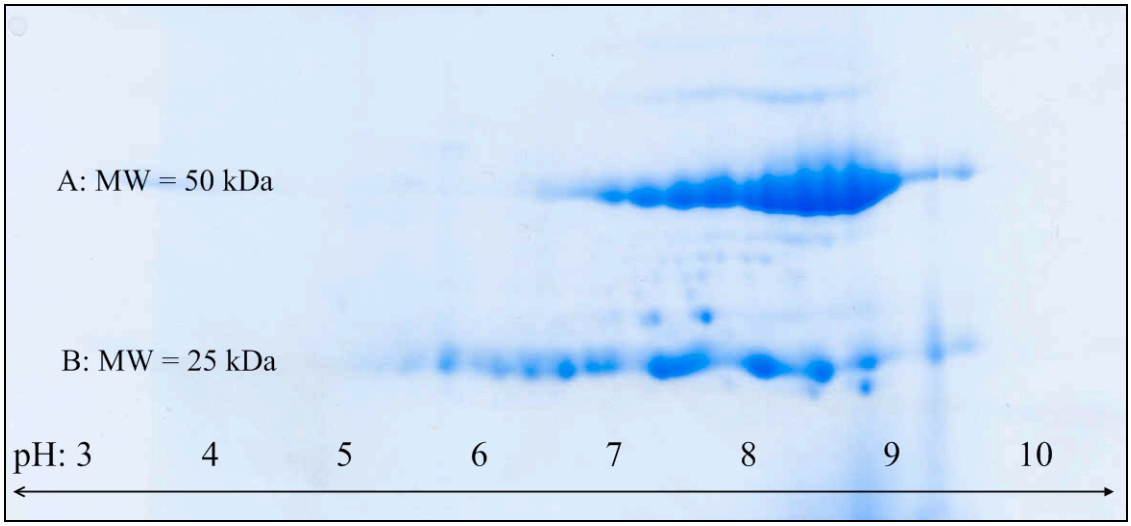

Figure 4.1: Image of 2D-gelelectrophoresis of pooled IgG isolated from blood plasma. (A) Heavy chain, (B) Light chain.

Figure 4.1 shows that the pI-ranges are 5-9.5 and 6.5-9.5 for the IgG-light chain and IgG-heavy chain respectively. The longer pI-distribution of the light chain compared to the heavy chain is due to the relative size of the IgG variable domain in comparison to the entire chain. Variations of the pI are mainly due to the amino acid composition in variable domains. The amino acid ratio between the variable region and the entire chain is approximately one fourth for the heavy chain and one half for the light chain. The high pI-diversity of the pooled IgG-preparation shows how changes in the amino acid sequence can confer a large variety of electrical properties to the protein mixture. The pI-ranges measured in this work are consistent to the pI-range determined by Bolton et al. in a polyclonal human IgG solution [29]. Even though isoelectric focusing was not performed with the protein in its native conformation, the average pI of pooled IgG is assumed to be close to 8.

4.1.2 Electrical properties of membrane surface

The zeta-potential is related to the charge functionality at the membrane-solution interface and also to the solution pH and electrolyte composition. At the boundary between solids and electrolyte solutions, the distribution of electrical charges differs from that in the bulk phase. A schematic of a typical ion distribution near a negatively-charged surface is shown in Figure 4.2. The charges on the solid surface are compensated by counter ions, forming an immobile layer (stern layer) and a diffuse double layer [77]. The surface of shear defines the region at which the fluid becomes mobile and is situated just beyond the outer Stern surface. The electrical potential at the surface of shear is defined as the zeta potential ζ and is typically

used to characterize the electrical properties at the solid surface. Zeta-potential measurements at different pH-values were performed in a flat sheet tangential module using an electrophoretic light scattering (ELS) based zeta-potential analyzer. The pH dependence of the ζ-potential was determined in 10^{-2} M KCl electrolyte solutions. The pH-value was varied in the interval of pH 2 to 7 by addition of 0,1 M HCl or KOH solution. Determination of the zeta-potential under alkaline conditions (pH>7) was not possible with the used apparatus.

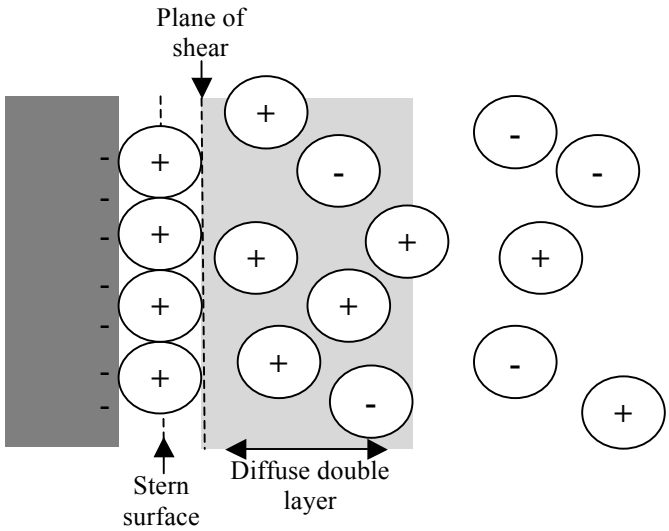

Figure 4.2: ion distribution near a negatively charged surface

Two different solid materials were tested. The PES based membrane material with a slight asymmetric morphology, analyzed in section 3.2 and the same material previously coated with pooled IgG. The coating process consisted in the overnight incubation of membrane material in a high concentrated (50g/L) IgG solution. Typically, this treatment leads to a shift of the pI of the membrane to the pI of the adsorbed protein [78, 79]. Here the membrane acts as a support material and allows indirectly the determination of the electrical properties of adsorbed proteins as a function of the pH value with the same experimental apparatus. A similar design of experiment was used by Nakamura et al. to estimate protein/membrane electrostatic interactions [79]. A more detailed description of the testing procedure is given in section 8.3.2

Figure 4.3 shows the ζ-potential as a function of pH-value. The virus retentive membrane exhibits negative ζ-potential values over the entire pH-range studied. The data suggest that the isoelectric point of the membrane lies close to pH=2. Very similar results were obtained from Susanto et al. [61] on PES based commercial UF-membranes having a MWCO of 100 kDa.
In the case of membrane coated with IgG, positive ζ-potential values were measured over the whole pH-range. These values are in accordance with the average pI of the IgG mixture

evaluated by 2D-gelelectrophoresis, since proteins have a positive net charge at pH-values below the pI. Lower absolute ζ-potential intensities were observed at pH-values close to the pI and the highest absolute ζ-potential intensities at strong acidic conditions (pH 2,2) where the proteins are almost fully protonated.

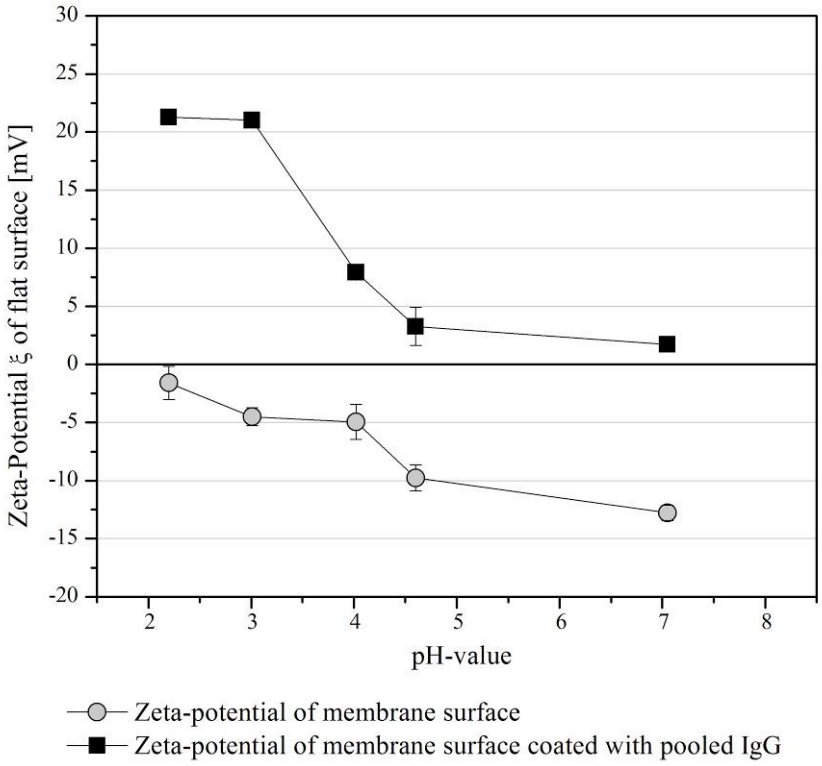

Figure 4.3: pH dependence of the zeta potential of a PES based virus retentive membrane and of pooled IgG adsorbed to the surface of the same membrane material. Number of repeats=3

Membrane and IgG have opposite charges over the entire measured range. Since greatest fouling is typically observed under conditions where the solute and membranes have opposite net charge [75, 76], electrostatic solute/membrane interactions may predominantly occur at pH-values below 8 and may be particularly marked at acidic pH-values. Further measurements of unspecific protein adsorption may confirm this hypothesis.

4.1.3 pH-dependent protein adsorption

Measurement of unspecific protein adsorption is routinely performed at SSB to characterize the protein binding capacity of new developed membrane materials but also for product release. Since determination of small amount of adsorbed protein is not possible by classical

measurement of the concentration decrease in the bulk, the method used here is derived from a protein determination method: the BCA-assay.

The method utilizes bicinchoninic acid (BCA) for the detection of Cu+ ions, which are formed after reduction of Cu^{2+} by proteins in an alkaline environment. A purple colored reaction product is formed by the chelation of two molecules of BCA with one cuprous ion (Cu+). Protein quantification is performed by measuring the absorbance at 562 nm. The procedure of the method used to assess the amount of proteins bound on the membrane surface is schematically described in Figure 4.4.

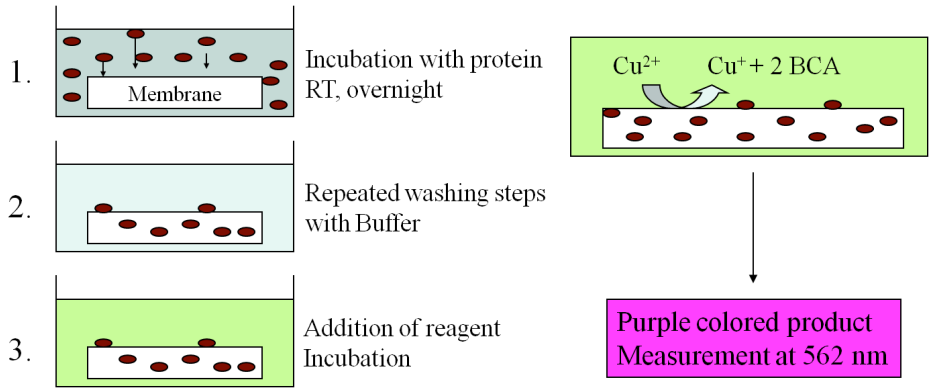

Figure 4.4: Schematic representation of the BCA-assay based procedure for the determination of unspecific protein adsorption

Membrane material is incubated more than 12 hours in a protein containing solution to ensure the diffusion of proteins into the fine porous structure. The method only determines the protein amount that is irreversibly bound to the membrane, since the washing steps used to remove unbound species lead to desorption of reversibly bound solutes. However, protein adsorption involves a change of conformation upon contact with the surface and is often described as irreversible in the literature [80-84].

In order to allow comparison of membrane materials exhibiting different morphologies, porosities and thicknesses, the amount of bound protein is normalized to the internal membrane surface area determined by BET measurements. A more detailed description of the experimental procedure is explained in section 8.4.3

PES-membrane disks were incubated overnight in buffered IgG solutions at different protein concentrations. Different buffers were used to allow the measurement at different pH-values.

Since the presence of salts can also affect the protein adsorption behavior, the ionic strength was set to a common value of 30 mM for all tested buffered IgG solutions. Figure 4.5 shows the obtained adsorption isotherms as a function of the pH-value.

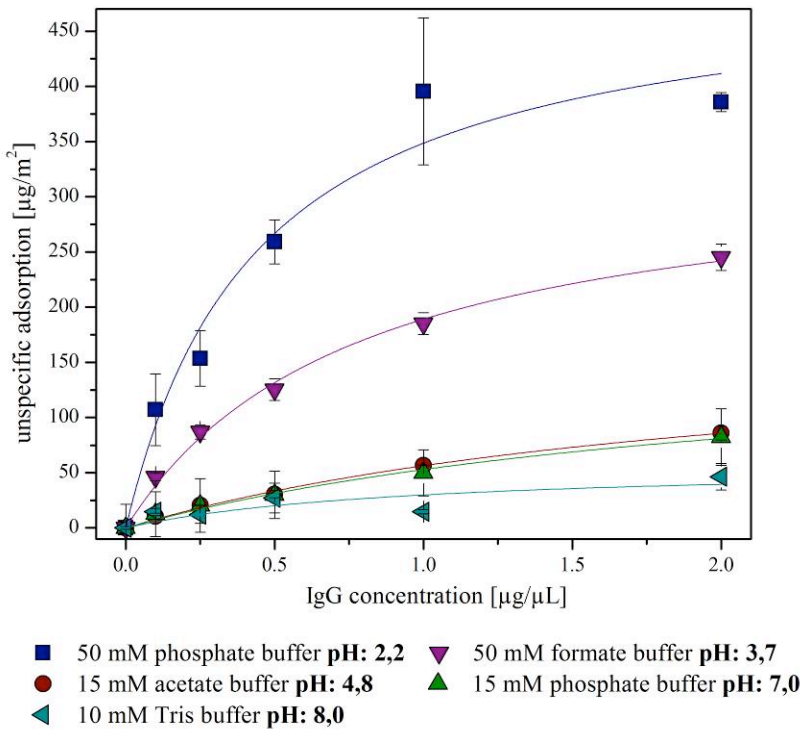

Figure 4.5: Adsorption isotherms of IgG to a PES based membrane under different pH-conditions. The ionic strength was equal in all tested buffers. Number of repeats: 3

The data were fitted using a monolayer Langmuir adsorption model, a simple non linear adsorption model. Eq. 4.1 describes the relationship between adsorbed and bulk concentration at steady state.

$$Q = Q_{max} \cdot \frac{k_l \cdot c}{1 + k_l \cdot c} \tag{4.1}$$

With Q the amount of protein adsorbed, Q_{max} the maximum amount of protein that can be adsorbed by building a monolayer, k_l the Langmuir constant that represents the solute/solid phase affinity and c the concentration of compound in the bulk.

It should be mentioned that the Langmuir model is extensively used in the literature to describe protein adsorption mechanisms [81, 82, 85]. The main assumptions of this model are:

- one molecule adsorbs to only one site and the number of sites is limited
- Molecules adsorb by building a monolayer

- Lateral interactions between molecules cannot occur
- The adsorption is irreversible.

Results obtained in Figure 4.5 confirm that adsorption of protein to the membrane surface is not a reversible process. The BCA based method used here involves a washing step post-adsorption that may desorb all reversibly bound molecules. One explanation proposed by Ramsden [81] for the irreversibility of the adsorption process is the denaturation of the molecule by its interactions with the surface. Paradoxically, despite the fact that the assumptions involved in Langmuir isotherms are seldom satisfied in the case of protein adsorption, it often provides fittings in good agreement with many systems [85, 86].

Higher adsorptions were obtained under strong acidic conditions. In contrast, low solute/membrane interactions were observed at pH-values closed to the pI of pooled IgG evaluated by 2D-gelelectropheris and confirmed by ζ-potential measurements. Figure 4.6 illustrates how the unspecific adsorption values obtained at an IgG concentration of 2 µg/µL correlate with the zeta potential intensities measured on membranes coated with IgG.

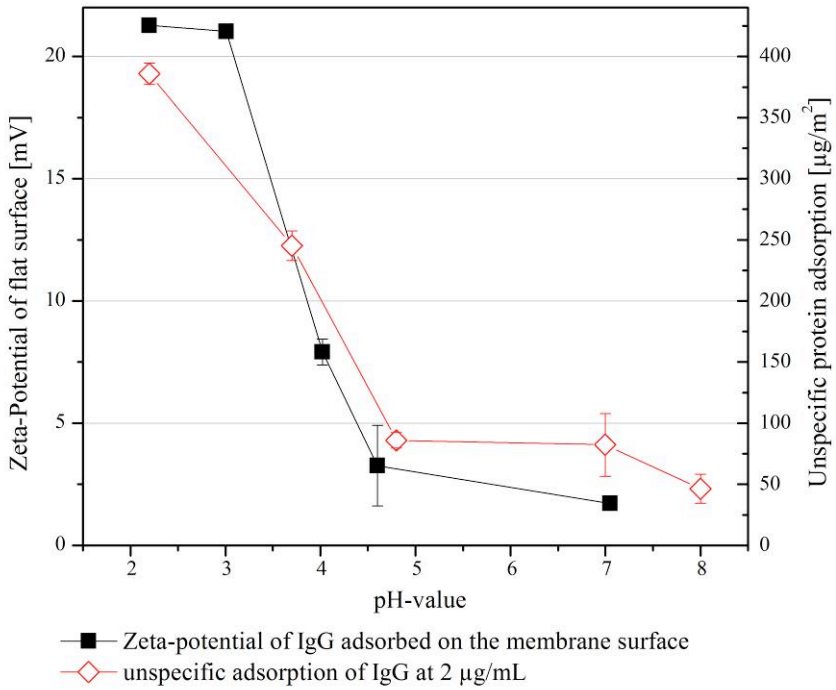

Figure 4.6: Correlation between unspecific adsorption and zeta-potential of adsorbed IgG under different pH conditions.

Strong electrostatic interactions are obtained when proteins are almost fully protonated. At pH values close to the average pI of the immunoglobulin mixture, these interactions are dramatically reduced. The valuable correlation obtained also points out that the intensity of

the negative zeta potential values, measured on the membrane surface without proteins, does not impact significantly the pH dependent adsorption of IgG, which appears to be mostly dominated by the protonation state of the considered proteins.

Additionaly, filtration experiments with IgG containing solutions were performed at different pH-values (see Figure 4.7). The same buffers as for the adsorption experiments were used. Stronger flow decay is observed at pH-values at which the protein protonation state is the highest and correlates with the unspecific adsorption values measured under similar conditions.

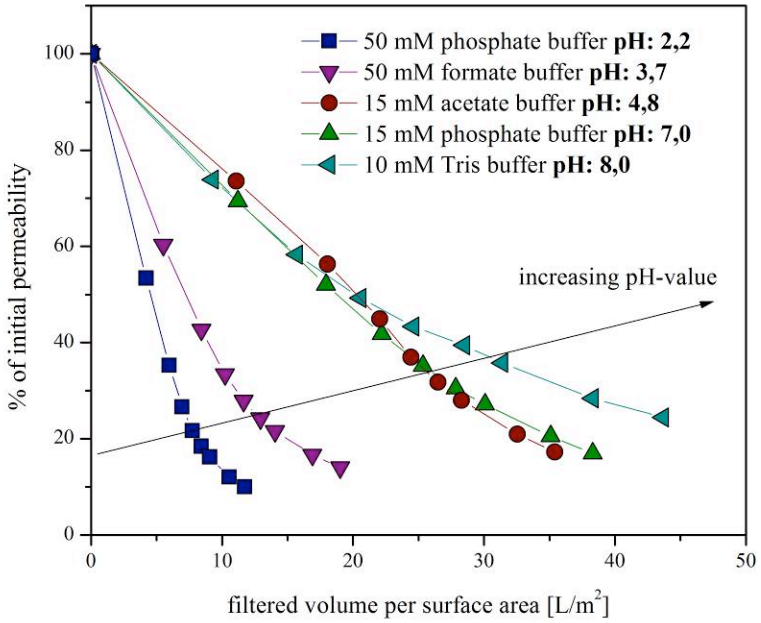

Figure 4.7: Influence of pH on flow decay during the filtration of 5g/L IgG-solutions. Filtration experiments were performed at a constant transmembrane pressure of 1 bar. All tested buffers were set to an equal ionic strength.

Within this study, the wide distribution of electrical properties of IgG from human plasma was demonstrated. The results suggest, that changes in the pH-value can dramatically impact the filtration performance of pooled IgG. Strong acidic conditions lead to a complete protonation of all proteins contained in the pool and consequently, enhance their irreversible binding onto the negatively charged membrane surface. However, such extreme pH conditions do not concern commercially pooled IgG for therapeutic purposes, which are typically stabilized in buffers at near-neutral pH-values. Under such conditions, adsorption due to electrostatic interactions is relatively low and may not be the dominant mechanism involved in membrane fouling.

4.2 Hydrophobic solute-membrane interactions

One can assume that adsorption driven by hydrophobic interactions dominates at pH-value near to the pI of the protein [69]. Variability in the amino acid composition does not only induce a wide pI-distribution but also may impact the hydrophobicity distribution of pooled IgG from human plasma. In order to evaluate the impact of hydrophobicity on the filtration performance of pooled IgG, the following strategy was proposed:

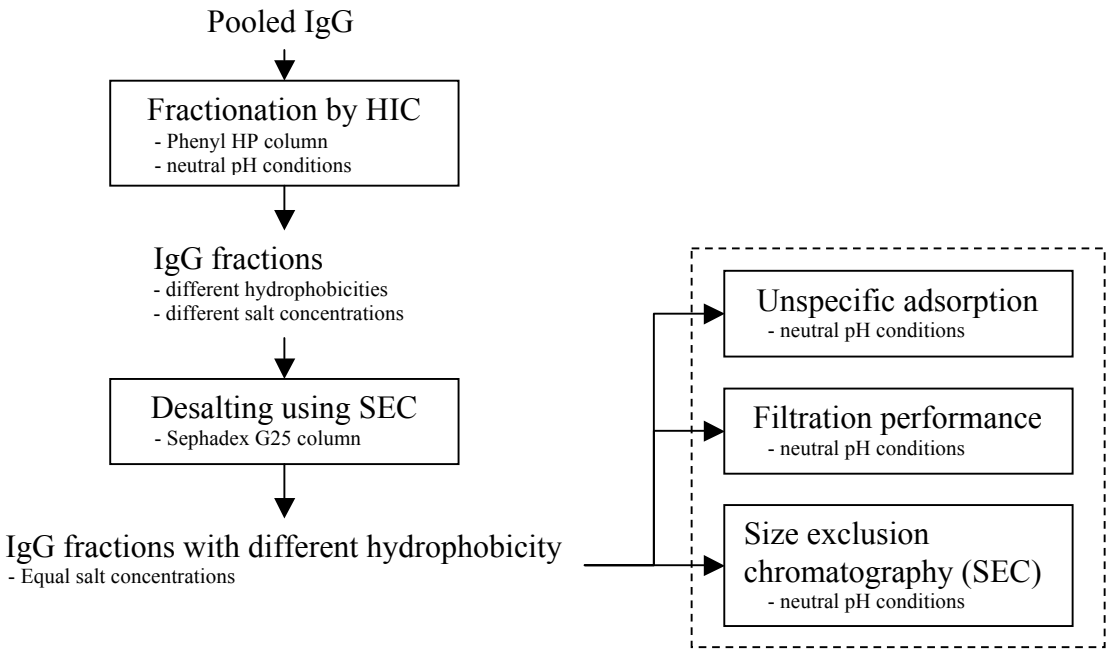

Figure 4.8: Fractionation strategy used to analyze solute/membrane hydrophobic interactions with pooled IgG.

The proposed strategy consists of the following steps:

- Fractionation of IgGs according to their hydrophobicity using Hydrophobic Interaction Chromatography (HIC). Since the separation is based on adsorptive mechanisms, the collected fractions should all exhibit a similar molecular size distribution.
- Desalting of the collected protein fractions in order to discriminate salt dependent adsorptive behavior.
- Determination of unspecific adsorption, filtration performance and molecular size distribution of IgG fractions generated by HIC.

4.2.1 Fractionation by Hydrophobic Interaction Chromatography (HIC)

Hydrophobic Interaction Chromatography (HIC) is a separation technique that uses hydrophobicity properties to separate proteins. In this type of chromatography, hydrophobic

groups such as phenyl, octyl or butyl are attached to the stationary column. The conditions for the separation are the opposite of those used for ion exchange chromatography. Initialy, a buffer with a high salt concentration is applied to the column. Non chaotropic salts like ammoniumsulfate compete with the hydratation layer at the protein surface and reduces its solvation. As a result, the hydrophobic sites of the protein become more exposed and adsorb to the hydrophobic medium. Bound proteins are eluted by gradually decreasing the salt concentration. More hydrophilic proteins will be eluted first while proteins with a strong hydrophobic character will need very low salt concentrations to desorb from the stationary phase.

In order to determine how far the variability in the amino acid composition can influence the hydrophobicity profile of pooled IgG isolated from human plasma, HIC was performed here at neutral pH-value. A stepwise elution using 3 different ammonium sulfate concentrations was performed and 3 different IgG peaks corresponding to 3 different degrees of hydrophobicity were collected (see Figure 4.9).

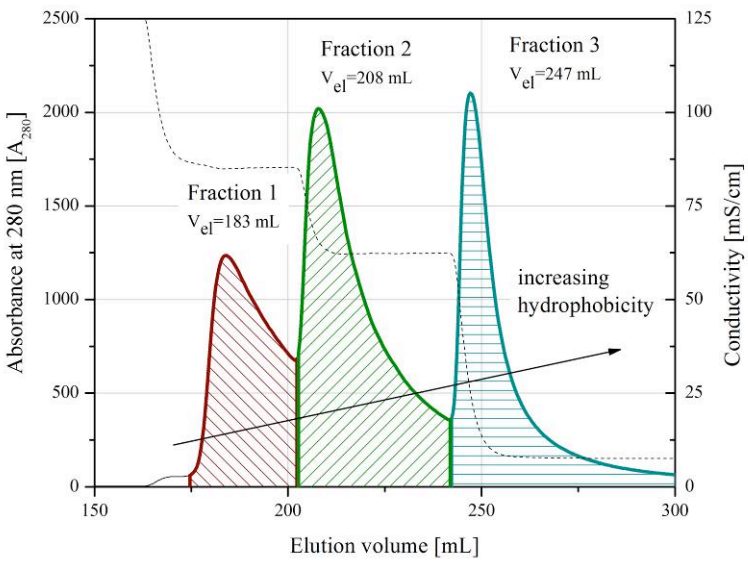

Figure 4.9: Fractionation of pooled IgG from human plasma by Hydrophobic Interaction Chromatography. Column: Phenyl HP (GE Healthcare); Flowrate: 3mL/min; Loading buffer: 1M $(NH_4)_2SO_4$, 50 mM phosphate buffer, pH: 7.0; Elution buffer: 50 mM phosphate buffer, pH: 7.0.

The proteins contained in the first and in the third fraction are respectively the most hydrophilic and the most hydrophobic components of the IgG mixture. The HIC chromatogram of the eluted IgG fractions in Figure 4.9 shows that polyclonal IgGs also exhibit a wide hydrophobicity distribution. It should be mentioned, that dissolution of protein

in ammoniumsulfate can, in some cases, lead to protein denaturation, potentially generating more hydrophobic molecules [87]. Furthermore, a similar separation profile may also be observed when the protein binding capacity of the column is exceeded. Thus, in order to ensure that the collected fractions effectively consisted of IgGs with different hydrophobicity that were present in the initial mixture, the HIC column was loaded with each protein fraction separately. The stepwise elution was repeated rigorously and, in every case, the different fractions/peaks were obtained with the identical elution volume.

Since high concentrations of non-chaotropic salts enhance the hydrophobic properties of proteins, the collected fractions were desalted using gel filtration (Sephadex G25) and set to a common concentration for further adsorption analysis and filtration experiments.

4.2.2 Correlation between hydrophobicity and unspecific protein adsorption

Measurement of the unspecific adsorption on virus retentive membranes was performed as described in section 8.3.1 with the different IgG fractions generated by HIC. The corresponding adsorption isotherms are shown in Figure 4.10.

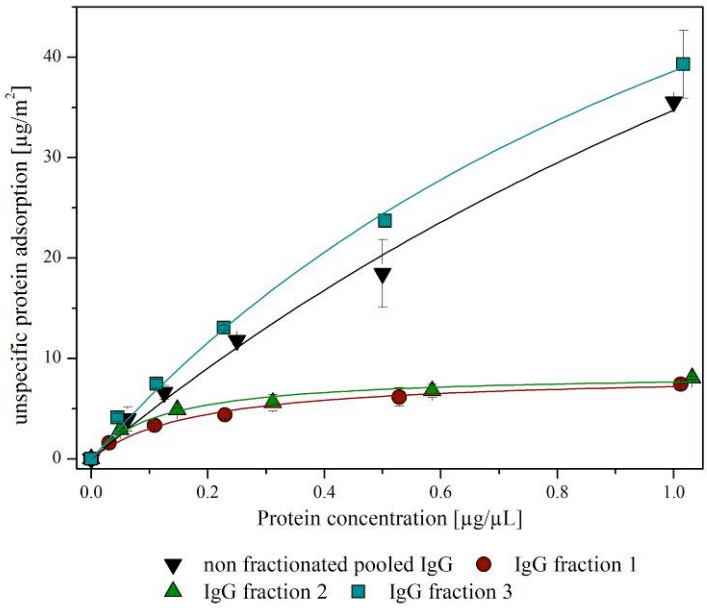

Figure 4.10: Adsorption isotherms of unfractionated IgG and IgG fractions generated by HIC to a PES based virus retentive membrane.

The obtained data clearly demonstrate the strong correlation between hydrophobicity of the fractions generated by HIC and the unspecific adsorption to the PES based virus retentive

membrane. The proteins contained in the most hydrophobic fraction (247 mL elution volume) were also the most adsorbing components of the protein mixture, while the two first collected fractions (183 and 208 mL elution volume), containing less hydrophobic molecules, did not exhibit strong interactions with the virus retentive membranes. The results also show how the most hydrophobic proteins contained in the IgG pool can strongly impact the adsorption behavior of the whole IgG mixture. According to the peak surface area ratios in Figure 4.9, the strong adsorbing IgGs represent less than one third of the complete eluted protein amount.

4.2.3 Filterability of immunoglobulin fractions

As a next step, filtration experiments with the collected IgG fractions were performed. All protein solutions were set to a common protein concentration of 1 g/L to allow comparison. The decrease of permeability as a function of the filtration volume is shown in Figure 4.11 for all tested protein solutions.

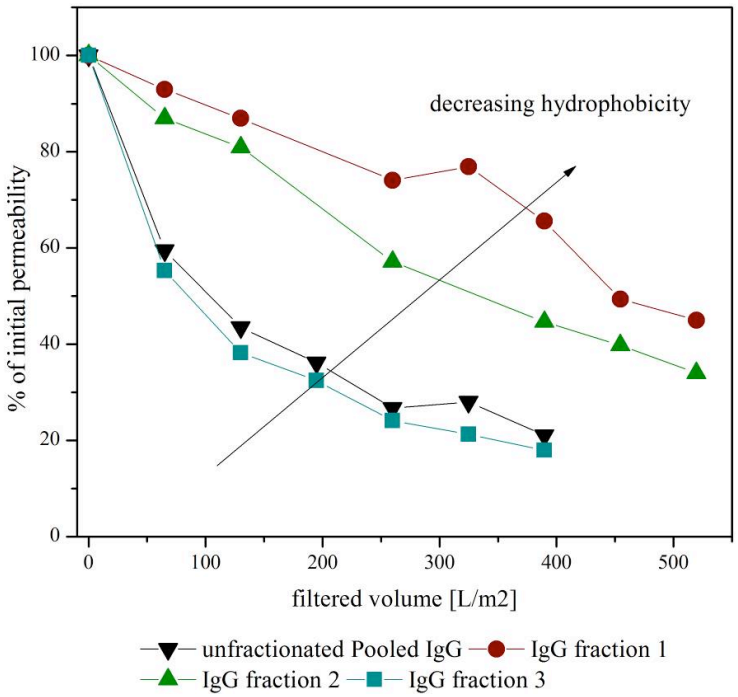

Figure 4.11: Filtration of different IgG fractions generated by HIC and of unfractionated pooled IgGs. The filtration experiments were performed at a constant transmembrane pressure of 1 bar. Protein concentration in all different fractions: 1 g/L

Similarly to the results obtained at different pH-values (see section 4.1.3), a consistent correlation between fouling propensity and degree of adsorption to the membrane could also

be observed within the following filtration experiments. Higher decrease of the permeability was obtained by filtering the high adsorbing proteins from the third IgG-fraction. In contrast a less marked decrease of the filtration flow rate was observed with the first protein fraction that contained the most hydrophilic IgGs. These results also illustrate how a small subset of molecules with a strong hydrophobic character can dominate the filterability of the whole pooled IgG mixture.

4.2.4 Molecular size of Immunoglobulin fractions

As already mentioned, the distribution of hydrophobicity observed on pooled IgG may be due to differences in the amino acid composition. Another conceivable possibility to explain hydrophobicity changes is the presence of different amount of protein aggregates in the IgG-fractions, which are often described as more hydrophobic than the corresponding monomeric molecule [88].

SEC-analysis was performed in order to determine the molecular size distribution of the proteins contained in the different fractions. As shown in Figure 4.12, very similar elution profiles were obtained for all protein containing fractions.

However, it should be mentioned that SEC is efficient in the separation of small aggregates of 2 or 3 monomers, but does not allow a precise detection and quantification of non-covalent aggregates that can be disrupted during the process [89-93]. Consequently it cannot be excluded that the obtained elution profiles do not correspond to the real aggregation state in the different solution.

The protein fractions do not contain notable levels of aggregate, reinforcing the hypothesis that adsorption and not size exclusion may be the main mechanism involved in this throughput limited filtration process. The more hydrophobic fraction may consist of denaturated IgG monomers or IgGs with more hydrophobic variable regions.

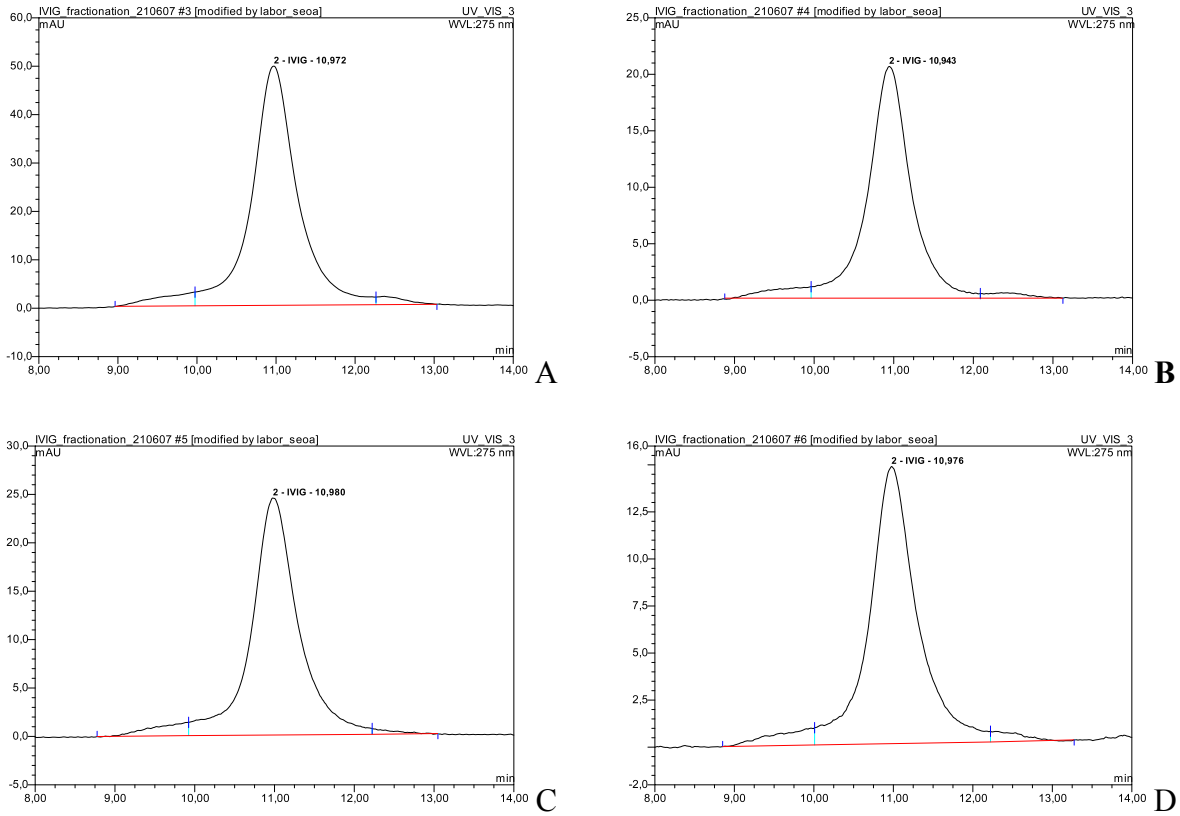

Figure 4.12: SEC-chromatograms of IgG fractions generated by HIC. A: unfractionated pooled IgG, B: first fraction, C: second fraction, D: third fraction. Column: PSS Proteema 300 Å, flowrate: 1 mL/min, elution buffer: 300 mM NaCl in 50 mM phosphate buffer pH 6.8, sample volume: 10 µL.

4.3 Adsorptive aspects of protein aggregation

Due to small size differences between viruses and therapeutic proteins, the performance of virus filtration often is sensitive to protein aggregates [16, 29, 39, 65, 94]. For this reason, virus filtration is typically performed with highly purified therapeutical solutions near the end of the manufacturing process. However, small amount of aggregates as dimers or trimers may be still present in the end formulated solution despite the resources involved in their removal. Wang et al have shown that hydrophobicity increases with the degree of aggregation [88]. Besides the obvious size exclusion based mechanism, adsorption due to increased hydrophobicity may also be involved in the entrapment of aggregates in the membrane structure.

In order to analyse the impact of adsorptive mechanisms in the retention of molecule aggregates, Bovine serum albumin (BSA) was used as a model protein due to its ability to form aggregates [95]. Theoretically, BSA-dimers or trimers should not be retained due to their

size. Due to the complexity to produce BSA solution with a definite amount of protein aggregates, SEC experiments of different commercially available lyophilized BSA-lots were performed to preselect an aggregate containing BSA.

Similarly to plasma isolated IgG, fractionation of the chosen BSA using HIC was performed as described above and the 3-step elution was repeated (see Figure 4.13).

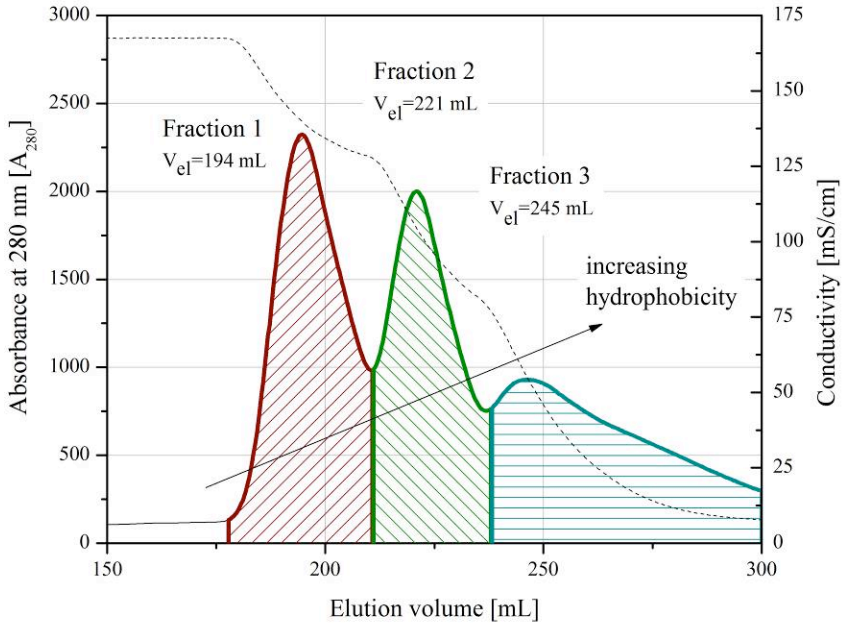

Figure 4.13: Fractionation of aggregates containing BSA by Hydrophobic Interaction Chromatography. Column: Phenyl HP (GE Healthcare); Flowrate: 3mL/min; Loading buffer: 1,5M $(NH_4)_2SO_4$, 50 mM phosphate buffer, pH: 7.0; Elution buffer: 50 mM phosphate buffer, pH: 7.0.

Three BSA fractions with increasing hydrophobicity (starting with fraction 1) were collected and used as samples for SDS-PAGE analysis under reducing and non reducing conditions. In the mean time, their adsorption behaviour to virus retentive membrane was tested as described in the previous section. The corresponding adsorption isotherms of the 3 fractions separated by HIC are shown in Figure 4.14.

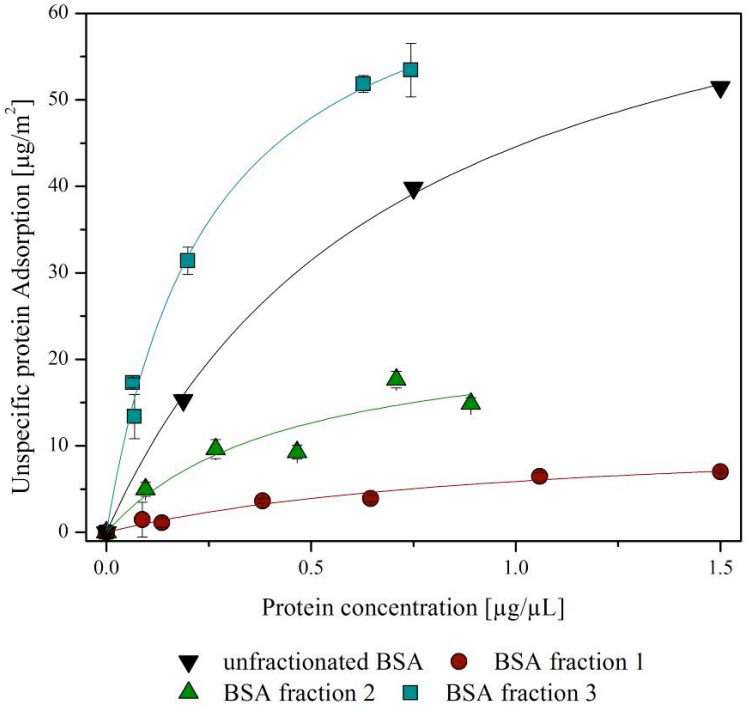

Figure 4.14: Adsorption isotherms of unfractionated BSA and BSA fractions generated by HIC on virus retentive membranes.

Here the three obtained fractions consisted of BSA fractions with different molecular size distribution. The SEC and SDS-PAGE analysis (Figure 4.15 and Figure 4.16) revealed that the hydrophobicity differences between the different fractions correlates with the amount of molecular aggregates in the fractions.

	Monomer rel. Area [%]	Dimer rel. Area [%]	Trimer* rel. Area [%]
Fraction 1	67.07	25.88	7.05
Fraction 2	42.47	35.78	21.75
Fraction 3	37.19	29.35	32.61

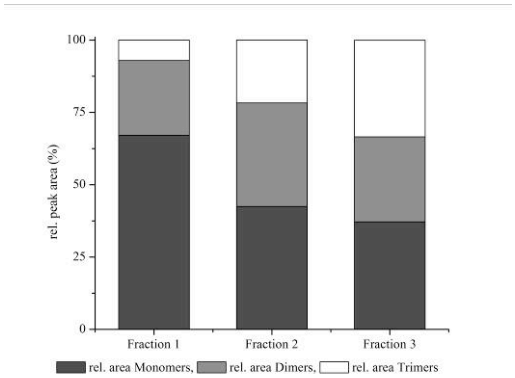

*: consists of trimers + larger protein aggregates.

Figure 4.15: Determination of relative amount of protein aggregates in BSA-fractions generated by HIC using SEC: Column: PSS Proteema 300Å, flowrate: 1 mL/min, elution buffer: 300 mM NaCl in 50 mM Phosphate buffer pH 6.8, sample volume: 10 µL.

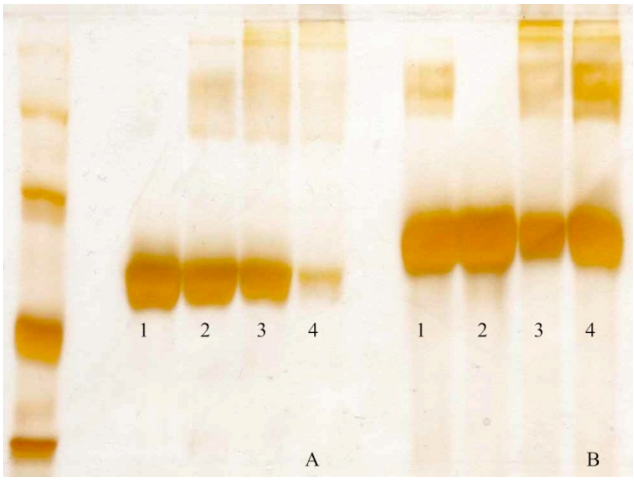

Figure 4.16: SDS-PAGE under reducing (A) and non reducing conditions (B) of different BSA-fractions obtained by HIC. 1: first fraction, 2: second fraction, 3: unfractionated BSA, 4: third fraction.

The most hydrophobic protein fraction was the fraction containing the highest level of protein aggregates. The results obtained strongly support the hypothesis of Wang et al. that the hydrophobicity of proteins increases with the degree of aggregation [88], i.e. a dimer is more hydrophobic than a monomer, a trimer more than a dimer, and so on.

Aggregate formation is frequently associated with changes in the protein conformation that can bring internal hydrophobic sites to become more exposed at the protein surface, resulting in higher hydrophobicity. Thus, the aggregate containing fraction was also strongly adsorbing on the membrane. It is often believed, that the entrapment of larger protein aggregates in the membrane matrix is only guided by size exclusion mechanisms [29, 96, 97]. The obtained results demonstrate how increased protein adsorption can be obtained in the presence of protein aggregates, suggesting that fouling is initiated by adsorptive mechanisms. Furthermore, the similar gel chromatograms obtained under reducing and non reducing conditions indicate that these aggregates may consist of covalently bound monomeric molecules that are not linked by disulfide bridges. Otherwise, only one band corresponding to monomeric molecules would have been observed under reducing conditions as the buffer contained both SDS and DTT, which separate, unfold and solubilise the different subunits/monomers of the protein complex/aggregate.

4.4 Conclusion

The data obtained within this study demonstrated how membrane fouling during virus filtration is mainly caused by irreversible adsorptive mechanisms. Such mechanisms are predominantly driven by electrostatic interactions when the considered protein is highly protonated. In the case of pooled IgG that exhibit an isoelectric point between approx. 5 and 9, strong adsorption to the negatively charged PES based membrane occurs when the pH-value in the surrounding environment is lower than 5. At pH-values close to neutral, and corresponding to the standard stabilization conditions for the majority of plasma derived therapeutics, unspecific adsorption is mainly driven by hydrophobic interactions.

A small subset of molecules with a strong hydrophobic character can dramatically affect the filterability of the whole solution. It can consist of protein aggregates like dimers or trimers but also of monomeric molecules exhibiting higher hydrophobicity.

In the case where foulants consist of impurities or aggregates that were not removed within previous purification steps, the use of a prefilter upstream of the virus filtration step is a conceivable alternative to attain higher throughput [29]. Furthermore it is known that product aggregates are potent inducers of immune responses to therapeutic protein products [98] and, consequently, the final presence of a minimal amount of protein aggregates in the product should be ensured. However, in the case of pooled IgG from human plasma, the foulants responsible for throughput limitations, are a part of the product and their removal may induce a loss in therapeutical activity.

For these reasons, reducing the hydrophobic interactions between the target protein and the membrane surface can prevent fouling without changing the therapeutical efficiency. In the first case it can be achieved by decreasing the salt concentration or changing the buffer composition. This alternative is not always accepted because it requires additional desalting operations and possible issues regarding the stabilization of the protein in the solution.

Another conceivable alternative is to optimize the surface properties of the considered membrane in order to reduce its hydrophobicity. The next part will focus on the development of a high capacity virus retentive membrane, exhibiting reduced interactions with high plugging streams, while ensuring high virus retention.

5 High capacity virus retentive membrane

Previously obtained data suggested, that unspecific adsorption due to hydrophobic interactions is mainly responsible for the throughput limitations observed while processing pooled IgG from human plasma.

Surface modification is a well established technology to prevent fouling in membrane related processes that are typically facing highly plugging solutions like natural organic matter in waste water treatment or complex culture media in sterile filtration. For these particular applications, many researchers reported the development of membranes exhibiting anti-fouling and low protein binding properties by coating the surface with hydrophilic polymers [58-62, 99]. Such low protein binding coating materials, sometimes referred to as hydrogels due to their swelling tendency, are the result of grafting reaction of hydrophilic polymers onto the membrane surface (see also section 2.2.2). One great advantage of this technology is, that hydrophobic PES based membrane materials can also be used as support matrix since the grafted hydrophilic layer acts as a barrier and provides a sterical shielding of the surface. Consequently, antifouling properties are combined with properties characterizing membranes made of rather hydrophobic polymers, which are: high mechanical and chemical resistance and high porosity [48, 61, 100].

As already mentioned in section 2.2.2, Electron beam initiated graft modification present many advantages compared to other excitation methods or chemical graft polymerization [49]. Two alternative approaches are distinguished. ‘Grafting-to’ is performed by coupling polymers to surfaces, while during ‘grafting-from’ monomers are polymerized using an initiation at the surface [48]. The potential advantages and limitations of both approaches have been already reported in section 2.2.2.

The main goal of this part was the development of a virus retentive membrane with high anti-fouling properties for highly plugging streams like e.g. pooled IgG from human plasma. Here E-beam initiated graft polymerization was used for the surface grafting of hydrophilic polymer onto the surface of PES based virus retentive membranes. The impact of the graft polymerization on solute/membrane interactions as well as on virus retention was analyzed within this study.

5.1 High throughput automated characterization of filtration capacity

An attractive approach to characterize normal flow filters and to determine the maximal filtration capacity is the V_{max} analysis [101]. Its determination is based on the pore constriction model [97, 101-104]. The membrane capacity V_{max} represents the maximum volume of fluid that will pass through the filter before it becomes completely plugged and the filtration data can be extrapolated to longer filtration times using the linearized form of the pore constriction model:

$$\frac{t}{V} = \frac{1}{Q_0} + \left(\frac{1}{V_{max}}\right)t \qquad \text{(Eq. 5.1)}$$

Where V is the total filtrate volume collected over time t and Q_0 is the initial volumetric filtrate flow rate. Then, V_{max} can be evaluated by plotting the time-to-volume-ratio t/V against the time t and then by taking the inverse of the slope (see Eq. 5.1). Flow decay data obtained over only a short filtration time suffice to determine the maximum filtration capacity after extrapolation. Consequently, this method is particularly appreciated in the case of tight virus filters, whose characterization is a time consuming process due to their low permeability.

However, the development of a new generation virus filter with optimized surface properties involves the testing of a large variety of materials grafted with various polymers at different concentrations, irradiation doses under a large variety of operating conditions. In order to rapidly identify the optimum modifications parameters and save resources, a large number of tests have to be conducted in parallel. This experimentation approach, often referred to as High Throughput Screening (HTS) has become more significant in the last decades with the improvement of robotics and the development of liquid handling devices and sensitive detectors.

Membrane permeability and V_{max}-value are the key parameters to characterize the filtration performance of new developments. Since their determination is particularly time consuming with moderately to high plugging solutions, a conceivable possibility to improve the testing throughput is the use of an automated manipulator system. Such a HTS system for the determination of filtration capacity was developed within this project and is shown in Figure 5.1.

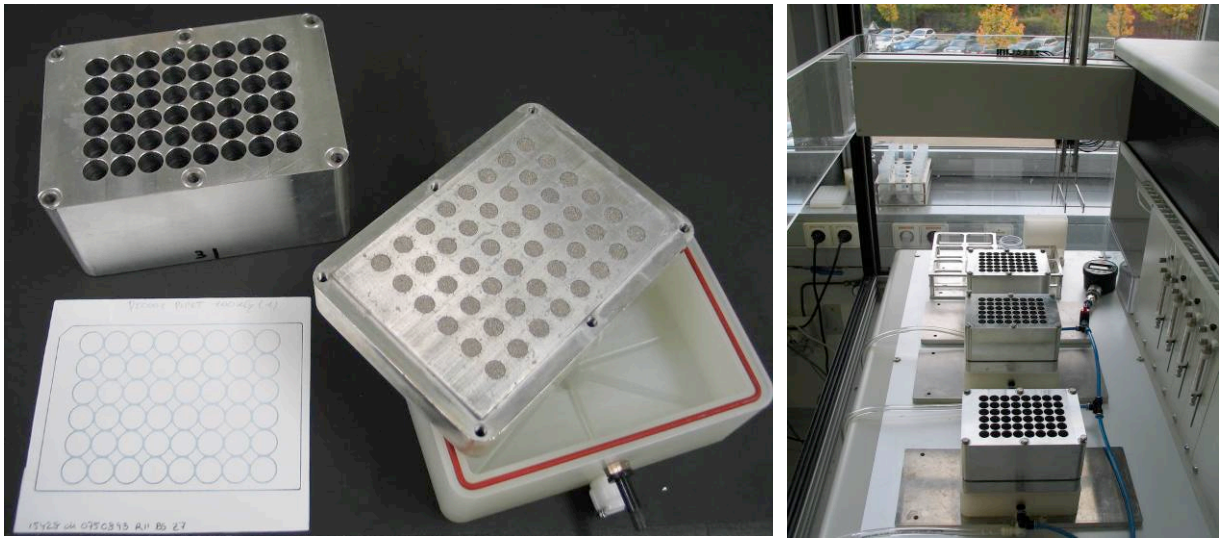

Figure 5.1: Image of a HTS filtration module allowing 48 filtrations in parallel. The corresponding preformed membrane in 6x8 format is shown on the bottom left corner of the picture (left). Automated manipulator system allowing the continuous determination of the retentate volume using the level detection feature of pipeting needles (right).

The automated manipulator system allows the simultaneous testing of 48 membrane disks having an effective surface area of 0.56 cm^2 in each filtration module. The system features four sampling needles with aspirating and dispensing functions carried by a robotic arm. Transmembrane pressure (TMP) is set by applying vacuum downstream to the membrane filter. The conductivity based level detection featured by the pipeting needles was used to determine the solution volume remaining in the wells. A schematic representation of the detection principle is shown in the appendices in Figure 8.1. The data obtained (volume and time) were collected and the permeability and V_{max}-value were calculated automatically.

The main advantage of the method is the high number of filtration experiments that can be conducted in parallel at a high degree of accuracy and reproducibility. The system can combine measurements with buffer and other media to assess respectively permeability and capacity in one run. Furthermore, only a small quantity of expensive IgG solution is needed for each filtration experiment (approx. 7 mL).

5.2 Electron-beam initiated graft modification

5.2.1 Screening of promising combination of mono and bifunctional vinyl compounds

As already described extensively, many patents and scientific articles reported successful graft polymerization reactions onto membrane surfaces using vinyl monomers and acrylate derivatives.

Radiation induced graft polymerization can be divided into different categories: mutual irradiation or preirradiation grafting. In the first case the membrane is impregnated with the monomer -and crosslinker- containing media and directly irradiated. In contrast preirradiation is performed before the impregnation to ensure that the graft polymerization only propagates from the surface [53] and prevent the formation of homopolymers. However, this way to operate necessitates a strict oxygen free environment, which is not always easy to implement at pilot scale.

Within this study, the mutual irradiation mode was used, due to its operational simplicity. Different combinations of monomers and crosslinkers were tested in a matrix form, and aqueous solutions containing a crosslinker and a monomer at respective concentration of 1% and 5% were prepared. This represents a crosslinker/monomer ratio of 1/5 and corresponds roughly to ratios typically used for graft polymerization as described in the literature. The different compounds were chosen according to the literature as well as the following prioritization: Pricing, availability and toxicity, which are determining for processes at industrial scale. Table 5.1 summarizes the different mono- and bifunctional compounds chosen for the modification screening.

Table 5.1: List of vinyl monomers and crosslinking agents used for modification screening

Monofunctional vinyl compounds		
2-Hydroxypropyl acrylate	HPA	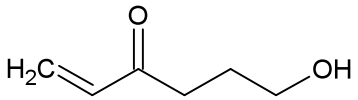
Ethylenglycol metacrylate	EGMA	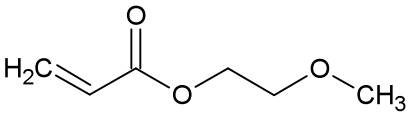
Poly(ethylenglycol metacrylate)	PEGMA	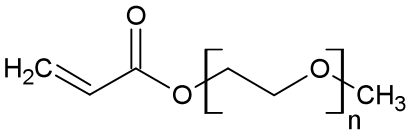
Bifunctional vinyl compounds		
3-acryloyloxy-2-hydroxypropyl methacrylate	AHM	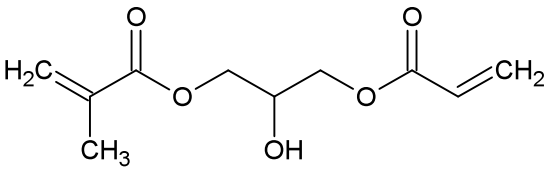
Tetraethylenglycol divinylether	TEGDVE	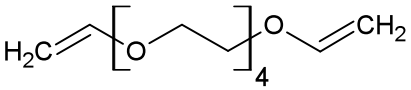
Tetraethylenglycol diacrylate	TEGDA	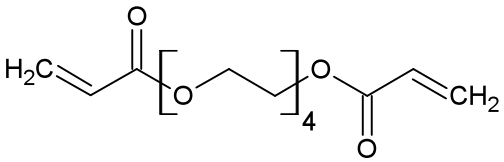

For screening purposes, membrane sheets were formed as a 6x8 arrangement, ready to adapt on the 48 supporting frits of the filtration module. The interstices between the disks were compressed to avoid liquid connections between the membrane disks and to allow targeted impregnation. Such a preformed membrane is shown in Figure 5.1. After impregnation, the membranes were then irradiated at 25 kGy to initiate the polymerization. The remaining monomer solution in the pores after irradiation was removed by 2 successive extractions in isopropanol and water. After drying, measurement of unspecific protein adsorption, permeability and capacity determinations were carried out using the HTS automated manipulator system described in section 5.1. The corresponding data is presented in Figure 5.2.

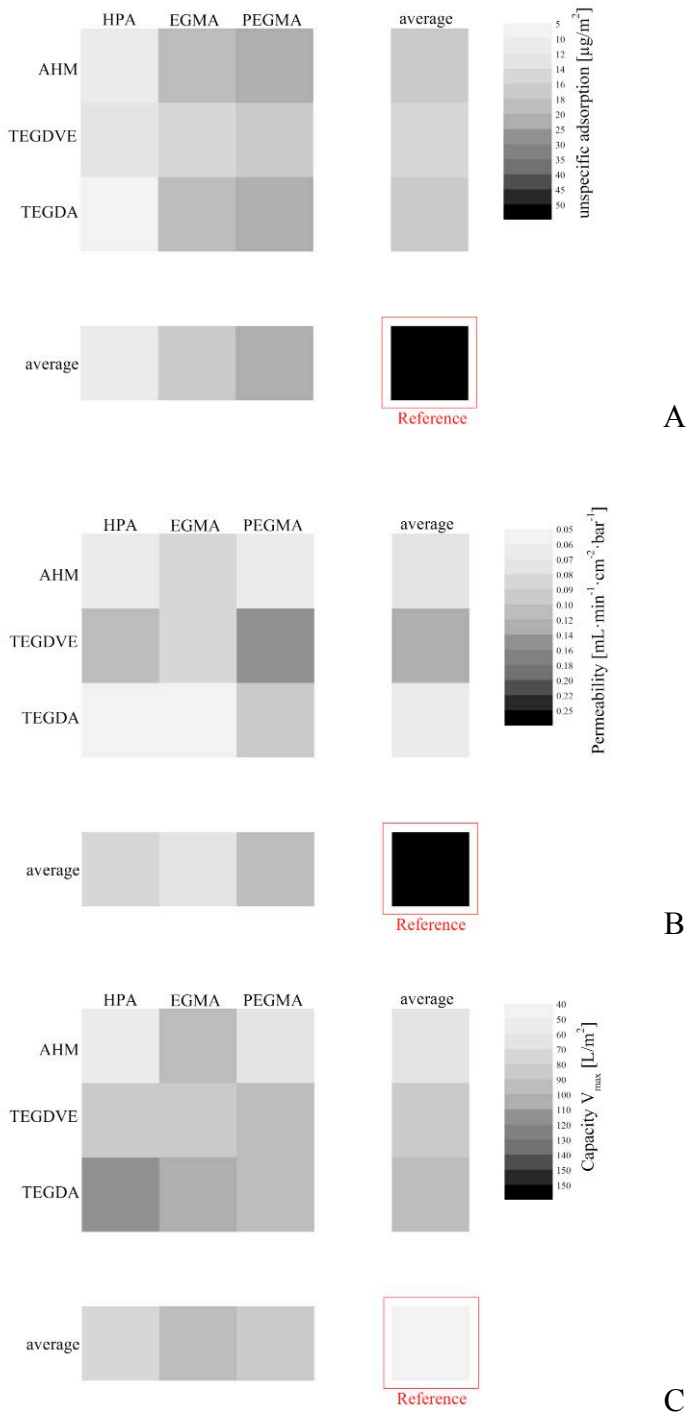

Figure 5.2: Screening of different monomer/crosslinker combinations. Total concentration: 6% in dionized water. Crosslinker/Monomer ratio 1/5. A: Measurement of unspecific protein adsorption was performed with an IgG concentration of 2g/L. B: Permeability was measured with 50 mM phosphate buffer pH: 7. C: Capacity was measured with a 5 g/L IgG-solution in 50 mM Phosphate buffer pH: 7. TMP=0,9 bars. Reference refers to unmodified PES-based membrane material. Number of repeats: 6

E-beam initiated graft polymerization resulted in significantly decreased adsorption values for all tested crosslinker/monomer combinations. The matrix representation pointed out some systematic trends. Lowest unspecific adsorptions were measured on membrane modified

using hydroxypropyl acrylate (HPA) as a monomer. In contrast, membrane modified with Polyethylenglycol metacrylate (PEGMA) exhibited the highest adsorption values with IgG. It appears that the size of the monomer used may impact the adsorption behavior on created surfaces. Similar UV initiated graft polymerization, performed by Taniguchi et al. on commercial PES based UF membrane, also demonstrated that small monomer molecules are more reactive and lead to higher degree of grafting [105]. Furthermore, the size of the molecule may also impact the network density of the formed protecting layer and lead to increased shielding properties.

No significant differences were observed between the 2 acrylate based crosslinker: 3-acryloyloxy-2-hydroxypropyl methacrylate (AHM) and tetraethylenglycol diacrylate (TEGDA). However, crosslinking using Tetraethylenglycol divinylether (TEGDVE) did not lead to similarly low adsorption values. The lowest unspecific protein adsorption was measured on membrane modified with the HPA/TEGDA combination.

Figure 5.2 also illustrated how graft polymerization can impact the membrane permeability. For all tested modified membranes lower permeability compared to the reference unmodified material were achieved. Strong correlations were observed between low unspecific adsorption and low permeability, which may describe the degree of pore constriction and the thickness of the formed layer. Membranes modified with the low MW monomers HPA and EGMA and the crosslinkers AHM and TEGDA were characterized by low permeability values. In contrast, the loss of permeability was less pronounced for membranes modified with TEGDVE as a crosslinker.

High filtration capacity should be theoretically attained by membranes exhibiting low unspecific protein adsorption and high permeability, which depends of the membrane structure. The use of TEGDVE as a crosslinker results in a moderated decrease of both unspecific adsorption and permeability. This leads to a higher overall filtration capacity in combination with all tested monomers. In the case of membranes using AHM as a crosslinker, the measured filtration capacity strictly correlated with the low membrane permeability and no significant improvement of the filtration performance with pooled IgG was observed.
However, in the case of TEGDA and particularly in the presence of HPA and EGMA as mono functional molecules, the capacity appeared to be principally determined by the protein binding characteristics of the membrane. The highest capacity was obtained using the

HPA/TEGDA based modification, which provides the membrane with very low adsorptive properties, but which also significantly increases the flow resistance in the membrane.

Despite of the low measured permeability, the HPA/TEGDA combination appears here to be the most promising modification system to attain higher filtration throughput. Due to reduced interactions with pooled IgG, higher capacity compared to the unmodified reference material was observed. Pore constriction due to the formation of a protective low adsorptive polymer layer on the membrane surface remains the most probable explanation for the observed decrease of permeability. It should be mentioned, that pore constriction also may provide the membrane with increased virus retentive properties, since these are mainly based on a size exclusion mechanism. For all these reasons, the HPA/TEGDA combination was chosen as a modification strategy. Next steps will focus on the optimum modification conditions, which include crosslinker/monomer ratio as well as irradiation dose, in order to determine the best compromise between flow and adsorptive characteristics.

5.2.2 Optimum crosslinker/monomer ratio in regard to unspecific adsorption

The previous section demonstrated, that graft polymerization using the mono-bifunctional vinyl monomer combination HPA/TEGDA leads to drastically increased filtration capacity with pooled IgG. The main goal of this part is to determine the optimum modification conditions regarding filtration performance. Using the HTS characterization system, different crosslinker/monomer ratios were used for modification at different irradiation doses. The influence of these parameters on permeability, unspecific protein adsorption and filtration capacity was analyzed. The total concentration of vinyl compound was kept at 6% (w/w) and the relative amounts of monomer and crosslinker were varied. The ratio R was calculated as follow:

$$R = \frac{C_{Crosslinker}}{C_{Monomer}} \tag{5.2}$$

So that R=0 describes a 6% concentrated solution without crosslinker and R=2 a solution that contains 2% monomer and 4% crosslinker. Figure 5.3 shows the influence of the crosslinker / monomer concentration ratio at different irradiation doses.

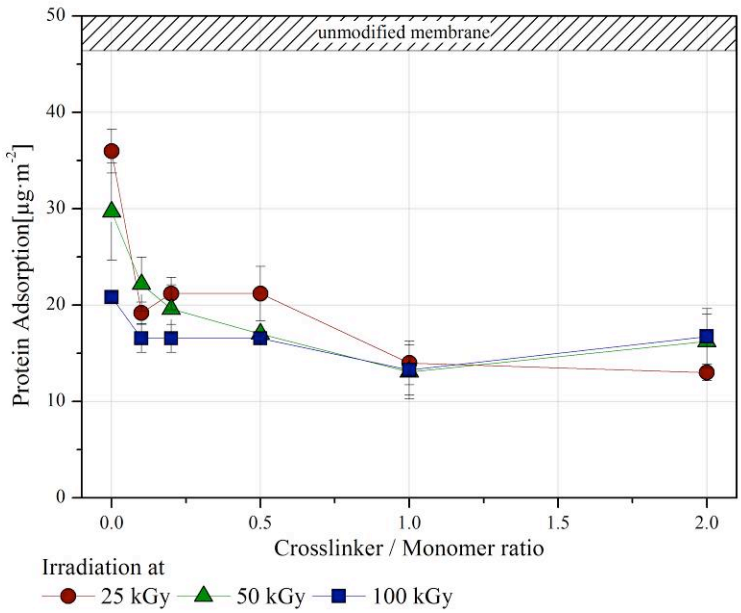

Figure 5.3: Influence of crosslinker / monomer ratio and irradiation dose on adsorptive properties of modified membranes. Number of repeats: 6

The data show, that the same minimal adsorption value was achieved at almost all tested concentration ratios. It can also be seen, that higher adsorption values were systematically obtained in the absence of crosslinker. This suggests, that polymerized chains alone cannot prevent solute/membrane interactions and necessitate a minimal amount of crosslinking agent to form a stable shielding network around the porous matrix. The data also demonstrates, that a relatively low irradiation dose is sufficient to initiate the grafting reaction and doses higher than 25 kGy appear not to further improve the membrane surface properties.

5.2.3 Impact of modification conditions on membrane filtration performance

Figure 5.4 illustrates how the modification conditions can impact membrane permeability. In contrast to adsorption values, which were not affected by a variation of dose, changes in permeability were obtained at increased irradiation doses. These differences are mainly due to the increase number of initiation sites at the membrane surface, since the polymerization period in a non-oxygen free environment may be short. It can be also seen, that increased crosslinker concentrations lead to an increase of the membrane flow resistance at all tested irradiation doses. Strong decrease of permeability were observed up to a crosslinker / monomer ratio of 0,5 (2% TEDGDA and 4% HPA). Further increase of the crosslinker concentration does not significantly impact the permeability, which asymptotically

approaches a minimum value. In that case, the amount of polymer grafted to the membrane surface appears to be limited by the size of the pores.

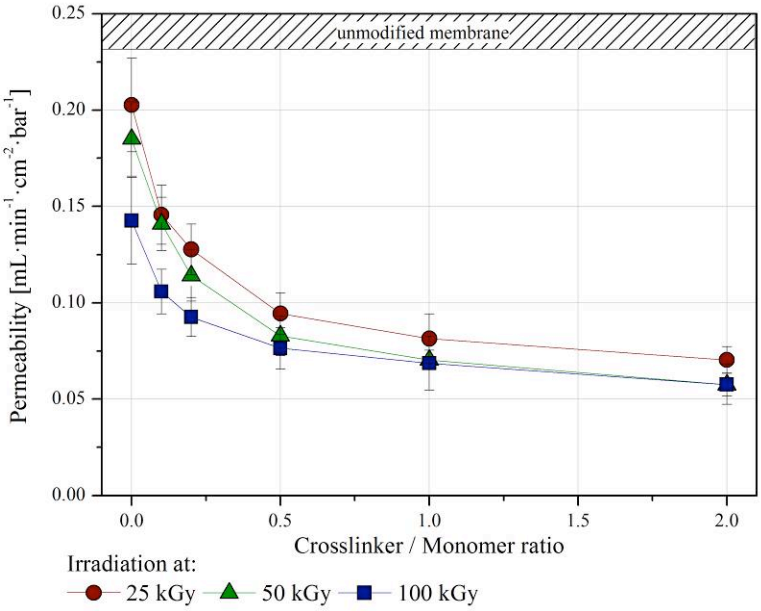

Figure 5.4: Influence of crosslinker / monomer ratio and irradiation dose on flow characteristics of modified membranes. Permeability measurements were performed using the HTS-characterization system at a constant TMP of 0,9 bar. Number of repeats: 6

Using the HTS characterization system, the filtration capacity of the different membrane material generated at different irradiation doses and crosslinker / monomer ratios was determined. The obtained data are summarized in Figure 5.5. The highest filtration capacity was obtained at an irradiation dose of 25 kGy and a crosslinker / monomer ratio of 0,2 (1% TEGDA and 5% HPA). A similar capacity profile and optimum TEGDA/HPA ratio was obtained at all tested irradiation doses. This suggests again, that the irradiation energy necessary to initiate the polymerization is relatively low, and that a further increase of the irradiation dose does not lead to significantly higher capacity values. It appears also that high filtration capacity is the result of an optimum balance between low unspecific adsorption and high permeability. As already mentioned, such conditions are attained with a crosslinker / monomer ratio of 0.2. Below this value, moderate decrease of permeability is achieved, but at the same time inefficient shielding of the membrane surface is attained. Above this value, the apparently efficient shielding of the membrane surface cannot compensate the strong loss of permeability, which mainly affects the resulting filtration capacity.

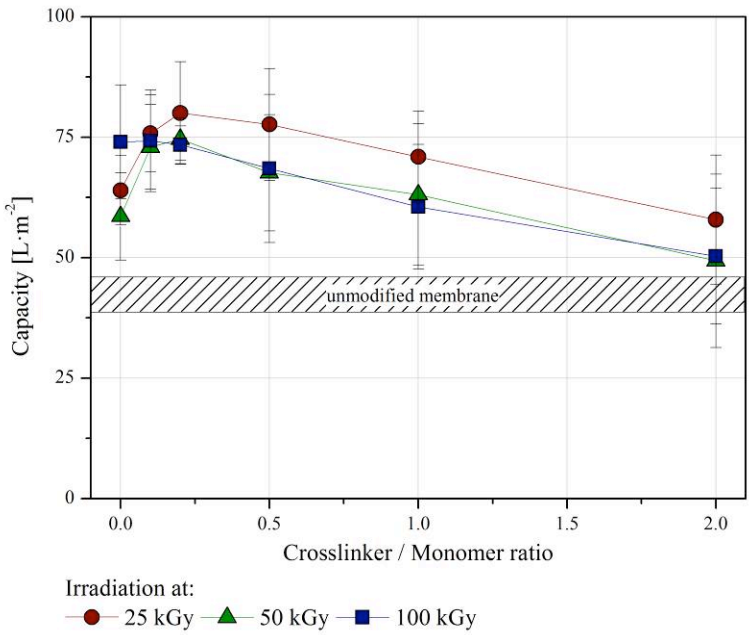

Figure 5.5: Influence of crosslinker / monomer ratio and irradiation dose on the filtration capacity of modified membranes. V_{max} determinations were performed using the HTS-characterization system at a constant TMP of 0,9 bar. Number of repeats: 6

Within these experiments, it was possible to find out which optimum conditions for modification were necessary to significantly improve the filter capacity with therapeutic solutions containing pooled IgGs. However, the mechanisms involved in the loss of permeability and shielding properties of the protecting layer grafted onto the membrane surface remain unclear. Next steps will focus on the elucidation of these mechanisms but also on the determination of the virus retentive properties of the new developed membrane material.

5.2.4 Structure and swelling properties of new developed porous material

In order to better understand the mechanisms involved in the loss of permeability, determination of the degree of grafting (DG) was performed as described in section 8.7.2 by weighing the amount of polymer bound to the membrane surface. The corresponding data obtained at an irradiation dose of 25 kGy are shown in Figure 5.6, together with specific membrane surface areas determined by BET measurements. Figure 5.4 pointed out that modified membranes still exhibit high permeability without crosslinker in the impregnation solution. However, high degree of grafting and low BET surface area were achieved compared to the reference material. This shows that the absence of crosslinker allows the grafting of an almost similar mass of polymer onto the membrane surface without providing

the membrane with high flow resistance. Higher crosslinker concentration does not result in significantly higher measured DG, but in a strong decrease of the water permeability up to 1/5 of the initial permeability when a crosslinker-to-monomer-ratio R=2 is considered. For this particular case, the DG value measured corresponds to a weight increase of approx. 3-4 %. This amount of grafted polymer appears to be underestimated, considering the corresponding loss of permeability. The formed three-dimensional crosslinked polymer network seems to act as a hydrogel, swelling upon contact with water and may explain the permeability behavior observed on membranes modified with crosslinker.

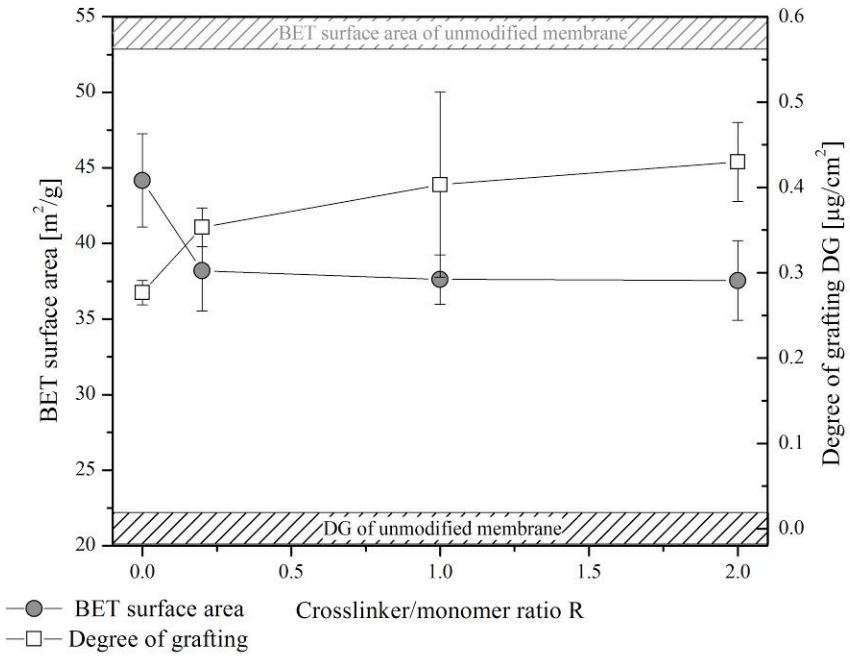

Figure 5.6: Influence of crosslinker / monomer concentration ratio on the degree of grafting and specific membrane surface area. DG was measured by weighing the membrane before and after modification. The unspecific membrane surface area was assessed by BET measurements. Irradiation dose: 25 kGy.

In order to confirm the assumption that the layer formed on the membrane surface consists of a hydrogel swelling upon contact with water, permeability measurements with air were performed and the air-to-water permeability ratio was determined.

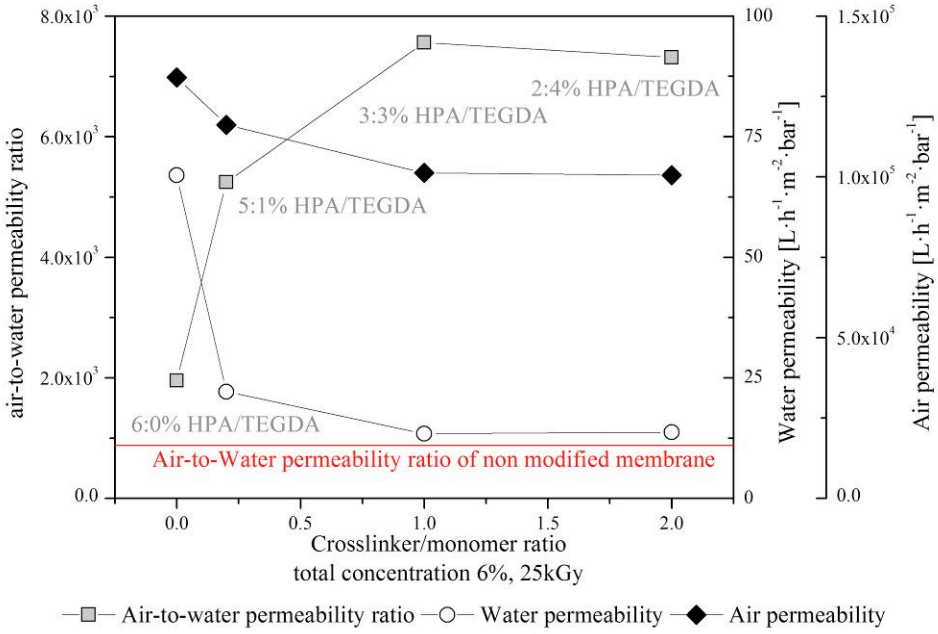

Figure 5.7: Influence of crosslinker / monomer ratio on the swelling properties of modified membranes. Air and water permeability were measured respectively at 10 mbar and 1 bar.

Figure 5.7 demonstrates the influence of the crosslinking agent on the swelling properties of modified membranes. The decrease of air permeability corresponds to the decrease of porosity occurring during graft polymerization. One assumes, that the grafted polymer does not swell with water, a proportional decrease of the water permeability should be measured and a similar air-to-water permeability ratio would be expected for all tested membrane materials. However, the data show, that the increase of the concentration of TEGDA in the solution dramatically affects the water permeability, but does not lead to a proportional decrease of the air permeability. The resulting air-to-water permeability ratio, corresponding to the hydrogel swelling ability, also increases with the addition of crosslinker up to a crosslinker/monomer ratio R=1. Above this value, a further increase of the crosslinker/monomer ratio does not result in a further increase of the hydrogel swelling ability. As already explained, the amount of polymer grafted onto the membrane surface may be sterically limited by the size of the pores.

To sum up, a low protein binding membrane was generated by electron beam initiated graft polymerization. Using a system comprising a mono- and a bifunctional acrylate derivative, efficient graft polymerization onto the membrane surface was achieved and a membrane exhibiting higher filtration capacity due to lower unspecific protein adsorption was developed.

The crosslinked polymer network formed acts as a hydrogel, swelling upon contact with water, which provides an efficient shielding of the hydrophobic membrane surface and prevents possible interactions with solutes. However, the formed swelling layer also negatively impacts the membrane permeability, being less than a third of its initial value after modification. Since membrane permeability is often associated with pore size and porosity, the size exclusion based retentive properties of the new generated material may also differ from the non-modified reference material. Furthermore, section 3.2 reported that virus retention also might be affected by adsorptive mechanisms. In this case, the low protein binding properties of the modified membrane may have disadvantageous effects on virus retention. Eventually, the improvement of the membrane capacity only can be evaluated at comparable virus retentive properties. For this reason, the next part will focus on the optimization of the structure of the basis membrane before modification and on the evaluation of the virus retentive properties of the newly developed membrane material.

5.3 Trade-off between filtration capacity and retention

Membrane material exhibiting improved filtration capacity with pooled IgG was developed in the previous section. The fabrication of such low protein binding porous material consists of two main production steps:

- The casting of a membrane with adequate structure properties, or in other terms, with a slight asymmetric structure (see section 3.2).
- The optimization of the membrane surface properties using electron beam initiated surface graft modification under the conditions described in the previous section.

E-beam initiated graft polymerization leads to the formation of a hydrogel onto the membrane surface with fouling resistant properties but may also alter the pore size distribution. Section 3.3 already pointed out the trade-off relationship between filtration capacity and virus retention. Wider pores typically lead to a significant gain in filtration capacity, but may also dramatically affect the retentive properties of the membrane. For this reason, it is essential to determine how far the modification associated pore narrowing as well as the reduction of membrane-to-protein interactions can impact virus retention.

In order to obtain the optimal compromise between filtration capacity and virus retention, different membrane material, exhibiting incrementally increasing pore sizes, were casted. The production of material, exhibiting various pore sizes but similar morphology, is empirically achieved by changing the casting conditions.

This reference material was then modified under the conditions determined in the previous section: the membranes were impregnated in a monomer solution containing respectively 5 % HPA and 1 % TEGDA and irradiated at 25 kGy. After 2 successive extractions in isopropanol and water, the membranes were dried at 100 °C for 30 min. Permeability, filtration capacity and LRV of the produced material were then determined.

Figure 5.8 shows the performance characteristics of the casted membrane material before and after graft modification. As already discussed, graft modification with the above mentioned parameters results in a dramatic decrease of permeability, which was observed here for all tested membrane material. The most pronounced loss of permeability was measured on membrane exhibiting the tighter pores (1/5 of initial permeability value). This result is expected, since equal amount of grafted polymer will result in different degree of pore narrowing, depending of the pore diameter of the initial material.

In the case of non modified casted material, also referred to as reference material, permeability increase does not result in a proportional increase of the filtration capacity. This is especially true for permeability values ranging from 0,2 to 0,35 $mL \cdot min^{-1} \cdot cm^{-2} \cdot bar^{-1}$, where no capacity improvement was measured. This data suggests that the filtration capacity of the reference membrane material is dominated by adsorptive mechanisms. Wider pores do not lead to higher protein passage due to high membrane/solute interactions.

In contrast, in the case of modified membranes, the improvement of the filtration capacity proportionally correlates with the increase of permeability and, consequently, with the enlargement of the pores. Here, the filtration capacity appears to be less affected by adsorptive mechanisms. Due to efficient shielding of the membrane surface, unspecific protein adsorption is significantly reduced and filtration capacity is predominated by size exclusion mechanisms. These results also illustrate how small permeability differences can have dramatic consequences regarding protein passage and filtration capacity.

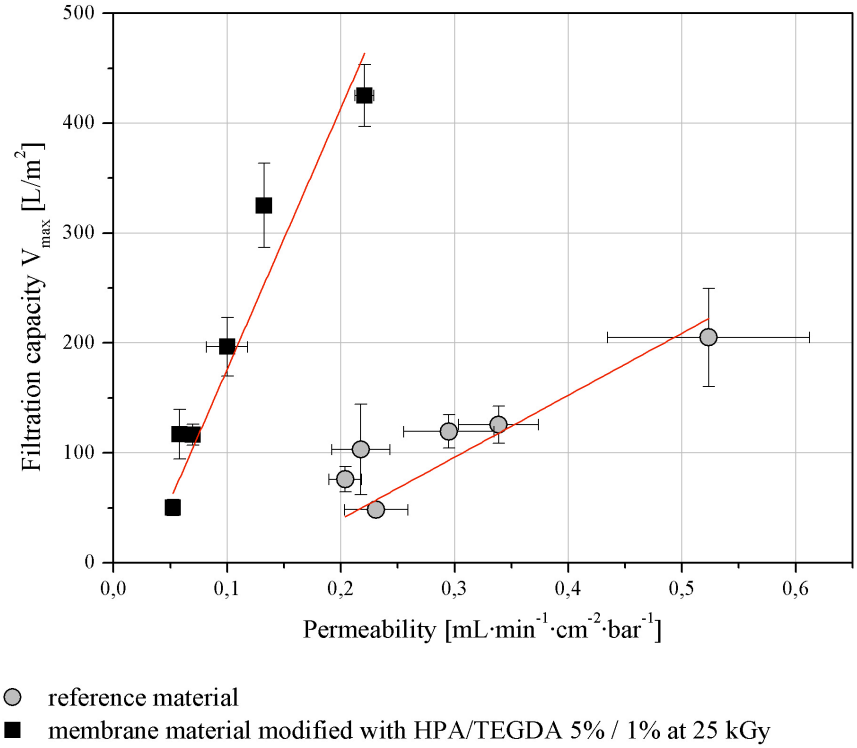

Figure 5.8: Filtration capacity Vs Permeability for various membrane materials exhibiting different pore sizes but similar morphology. Both parameters were measured before and after the modification process using the automated HTS-characterization system at a TMP of 0,9 bars. Number of repeats: 6

The virus retentive capacity of the different membrane materials was also assessed before and after graft modification using the bacteriophage based determination method described in section 3.1. The V_{max} value was then plotted against the corresponding LRV, in order to highlight the trade-off relationship between filtration capacity and bacteriophage retention (see Figure 5.9).

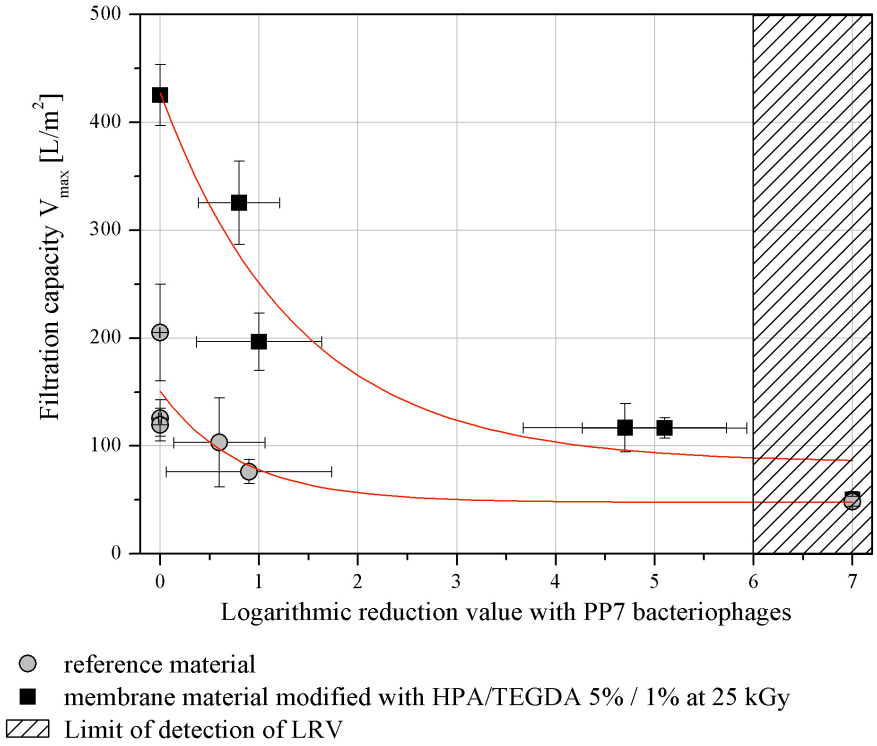

Figure 5.9: Trade-off between filtration capacity and bacteriophage retention before and after graft polymerization. Number of repeats: 6

The data shows, as expected, that the graft modification of a given reference material leads to an increase of its LRV value. For the two reference membranes that were exhibiting LRV > 0, the retention efficiency was improved approx. by a factor 5 after modification.

The data also illustrates, how moderate LRV decreases can lead to considerable capacity improvements. The chosen graphical representation also allows the direct comparison of V_{max}-values at equal LRV. Within the LRV range considered here, e-beam initiated graft polymerization results in an increase by a factor 2,5-3 of the filtration capacity compared to the reference material. No differences between both materials as regards capacity could be observed at a LRV above the limit of detection and the obtained values may be then underestimated.

5.4 Applicability of the development

Previous sections reported the development of a new high capacity membrane material for virus filtration. The development as well as the evaluation of the capacity of this new material was achieved using a buffered model solution containing 5g/L polyclonal antibodies. Since

fouling also depends on the physicochemical properties of the contained solutes in a given environment, the filtration performance may vary with different process solutions. In this part, the following different process antibody solutions, reflecting different process stages and therapeutic applications, were obtained from proprietary sources and tested using the HTS-characterization system on modified and unmodified membrane material:

- A highly purified therapeutic solution (before final formulation) containing a highly concentrated monoclonal antibody (20 g/L mAb) in PBS-buffer obtained by cell cultivation.
- A process intermediate bulk obtained after successive protein A and IEX chromatography and containing polyclonal antibodies (pAb) isolated from human plasma. Protein concentration is 8 g/L in 10 mM acetate buffer pH: 5,0.
- A formulated therapeutic solution for intravenous administration containing 10 g/L polyclonal antibodies (pAb) from human plasma stabilized in 10 mM acetate buffer pH: 4,8.

The corresponding V_{max}-values and filtration curves are shown in Table 5.2 and Figure 5.10 respectively. To better illustrate the performance particularities between both membrane materials, buffer filtration curves were added in order to better compare the two membrane's filtration behavior.

Table 5.2: Comparison of filtration capacity obtained with two different membrane materials for various real process solutions. Both membranes have a LRV of 5 with PP7-bacteriophages. Filtration experiments were performed using the HTS-characterization system at a constant TMP of 0,9 bar.

Process solution	Filtration capacity V_{max} [L/m^2]	
	Untreated membrane	Modified membrane
mAb 8 g/L in PBS-buffer pH: 6,2 (purified antibody)	778 ± 130	801 ± 264
pAb 8 g/L in acetate buffer pH: 5 (process intermediate)	70 ± 12	170 ± 20
pAb 10 g/L in acetate buffer pH: 4,8 (final product formulation)	79 ± 13	193 ± 17

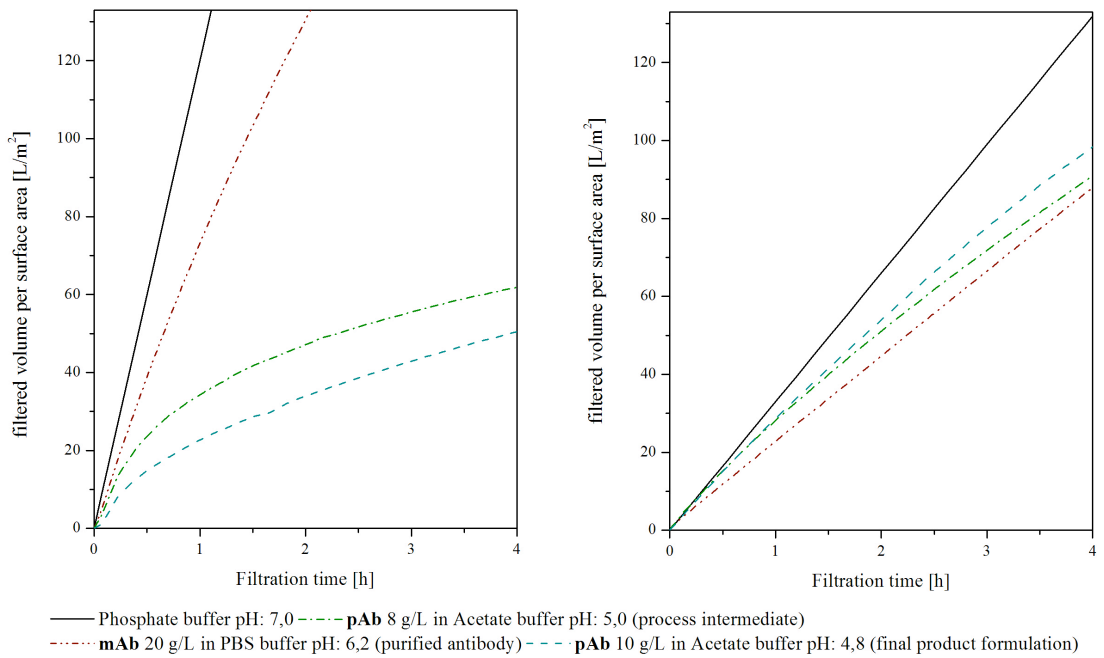

Figure 5.10: Filtration performance of new development (right) compared to unmodified virus retentive membrane (left) with different real process antibody solutions. Both membranes have a LRV of 5 with PP7-bacteriophages. Filtration experiments were performed using the HTS-characterization system at a constant TMP of 0,9 bar.

As already mentioned, the swelling ability of the modified membrane leads to increased flow resistance within the fine porous structure and to decreased permeability with buffer compared to the untreated material. This property explains the different flow behavior obtained with buffer alone. The mAb-containing solution appears to foul the untreated membrane moderately. In contrast to polyclonal IgG from human plasma, this biotech-derived product does not contain proteins with a strong hydrophobic character that preferably binds to the membrane surface. Furthermore, since the measured pI of this protein is close to 7, the chosen stabilizing PBS-buffer (pH: 6,2) should not induce strong electrostatic interactions with the membrane surface (see section 4.1). In contrast, strong decay of the permeate flow was obtained with both solutions containing similar concentrations of polyclonal immunoglobulins and the obtained results illustrate again the high fouling propensity of solution containing pooled IgG from human plasma. With these two solutions, complete membrane plugging was almost achieved after 4 hours of filtration through the untreated membrane material.

Using the modified material, a more linear increase of the permeate volume as a function of time was obtained for all tested process solutions. This results in overall higher measured V_{max}-values. With the mAb-containing solution, no decrease of the permeate flux was observed at all and the extrapolation method used to estimate the V_{max}-value has led to high standard deviation values. Minimum flow decay must be observable during the filtration process to allow the extrapolation based V_{max}-determination to provide reliable results. Nevertheless, these results pointed out the low suitability of modified membranes for moderately plugging therapeutic solution due to unfavorable low permeability. However, for applications where the surface properties are more determining than the flow characteristics, higher filtration capacities are achieved. This is especially true for both process solutions containing pooled IgGs, where the use of the newly developed membrane resulted in increased filtration capacity by a factor of approx. 2,5 compared to the non-modified material. The obtained filtration curves also illustrate the low product- or solution-dependent properties of the new developed membrane material. These results also confirmed the suitability of the IgG-containing model solution used during the screening phase, since a similar improvement of the capacity was obtained with real process solutions containing pooled IgGs.

5.5 Conclusion

Within this part a high capacity membrane for size exclusion based virus removal was developed. Using an electron beam and an innovative high throughput characterization system, graft polymerization and characterization of different combinations of acrylate derivatives were performed respectively at different concentrations and irradiation doses. Modification experiments revealed, that an irradiation dose of 25 kGy is enough to achieve maximal grafting densities under the experimental conditions and mutual irradiation approach chosen here. Graft polymerization on PES-based membrane using the mono-functional vinyl-compound 2-hydroxypropyl acrylate (HPA) and the bi-functional vinyl-compound tetraethylenglycol diacrylate (TEGDA) at a concentration ratio of 5% / 1% resulted in a decrease of the unspecific protein adsorption and permeability due to the formation of a swelling hydrogel. The grafted hydrogel provides the modified membrane with fouling resistant properties and reduced membrane-to-solute interactions due to efficient shielding of the hydrophobic membrane surface. With the tested IgG containing model solution, an increased filtration capacity by a factor of 2,5 compared to the non-treated material was achieved at equal virus-retentive properties.

The suitability of the developed material was also evaluated with solutions originating from different manufacturing processes and stages. It appears that the developed membrane material is especially suitable for high plugging therapeutic solutions containing polyclonal antibodies like e.g. pooled IgG from human plasma. However, as regards capacity, the developed membrane remains unable to compete with unmodified, high permeable membranes when moderately plugging solution, such as biotech-derived solutions containing monoclonal antibodies, are used.

6 General conclusion and outlook

The main objective of this PhD thesis was the development of a high capacity membrane for size exclusion based virus removal. The membrane had to feature high retentive properties against small non-enveloped viruses and high filtration capacity for high plugging therapeutic solutions e.g. pooled immunoglobulin from human plasma.

To achieve this goal, new insights about mechanisms governing virus filtration were provided. Particularly, the considerable impact of the membrane structure on virus retention was demonstrated. The obtained data illustrated the low suitability of membranes exhibiting strong asymmetric structures for virus removal. It has been shown, that these structures are especially susceptible for virus breakthrough when flow decay and fouling occur. “Worst case” testing conditions are used for the evaluation of virus filters. However, these conditions are often met in current processes in the presence of proteins. In the light of these results, it appears that “worst case” testing conditions have to be clarified and defined for every filter device, especially within evaluation studies, when the viral safety of a determined process operation unit is validated.

Virus clearance by size-exclusion based filtration is often assumed to be robust and media and/or protein independent. It was shown within this study, that the fouling-driven decrease of the permeate rate during the filtration process may also influence the clearance efficiency. Consequently, different retention characteristics may be obtained with solutions containing molecules exhibiting different fouling propensity, or with solutions having different salt and additive composition, since it may influence the hydrophobic or electrostatic properties of the contained solute. Therefore, evaluation of virus retention should be performed with the real process solution.

The work realized in this PhD-thesis also demonstrated that virus filtration is a scalable technology. Using a prediction tool, which considers relevant factors such as membrane heterogeneity or layer configuration, it was possible to estimate the LRV obtained at a larger scale. These results also indicated the reliability of device manufacturing at SSB. Generally, since the presence of defects can have dramatic consequences leading to virus breakthrough, it is essential to consider the use of multiple layer configurations as an additional security. Furthermore, the trade-off relationship existing between virus retention and filtration capacity

shows that the use of a combination of two membrane layers will provide higher capacity than a single membrane exhibiting similar retention.

Retention testing with real parvoviruses could not be performed within this work. It was evaluated here using bacterial viruses having the same diameter as the smallest pathogen parvovirus B19. Since the separation is based on size exclusion it is highly probable that the high capacity membrane developed here also exhibits similar retention against such viruses. Similarly to therapeutic protein, adsorption of viruses due to electrostatic or hydrophobic interaction also probably occurs during the filtration. This phenomenon may lead to overestimated LRV and may also differ between viruses having the same size but different surface properties. Furthermore, interaction between immunoglobulins and viruses due to antigen recognition may also be particularly pronounced for therapeutic solution containing pooled IgG and lead to unexpected higher retention values. Future works could focus on the elucidation of such phenomena. The composition of the buffer used for retention testing may also have a great impact on the obtained results due to changes in the protonation state and surface hydrophobicity of the considered virus but also of its infectivity. As a consequence, developing membrane materials able to prevent protein-membrane interactions is probably the most appropriate approach to ensure that molecular sieving is the dominant mechanism involved in virus retention and to guarantee the clearance of a large variety of viruses.

An important preliminary work for the design of a virus retentive membrane with adequate surface properties was also the elucidation of the mechanisms governing membrane fouling. In the case of therapeutics solution containing pooled immunoglobulin from human plasma, fouling is mainly due to adsorptive mechanisms. Electrostatic interactions with negatively charged membranes occur at pH-value below 4,8, where all proteins contained in the mixture are highly protonated. At higher pH-values adsorption is dominated by hydrophobic interactions. The results showed that pooled IgGs exhibit a wide hydrophobicity distribution and contain hydrophilic proteins but also species with a stronger hydrophobic character. Based on these observations, it appeared that removing a part of the product by using for example an adsorptive prefilter prior to the virus filtration step may lead to capacity increase. However it would also have a negative impact on the therapeutic activity by removing an active part of the product.

In order to attain higher filtration capacity and to ensure that high product recovery is achieved, membrane modification was carried out using electron beam initiated graft polymerization. A low protein binding membrane exhibiting an approximately 2,5-3 times higher capacity than the reference membrane material at equal retention was developed within this work. The developed membrane consists of a PES-based matrix coated with a swelling hydrogel. The formed hydrogel provides the membrane with low protein binding properties due to efficient shielding of the hydrophobic matrix surface. One important feature of this new development is its ability to filter with similar productivity a large variety of different process solution, originating from different processes and purification stages. This feature provides a clear benefit regarding capacity as well as up-scaling ability.

However, due to insufficient permeation rate, the membrane developed in this work is clearly restricted to plugging streams, e.g. in the plasma fractionation industry and does not appear as appropriate for biotech-derived therapeutics, which usually lead to less fouling. For this reason, the next challenge is the optimization of the flow characteristics of such low protein binding membranes.

First, particular attention should be paid on the optimization of the basis material for modification. Higher permeability can be achieved with more asymmetric membrane structure. Modification of such asymmetric structures would combine low adsorption properties with high flow rate. In this case, modification of the membrane surface may also reduce fouling and gradual pore plugging phenomena that are mainly responsible for virus breakthrough. Another conceivable alternative to increase the permeation rate is the increase of the membrane surface area contained in the considered device. This can be achieved by optimizing the membrane pleating strategy but also by using hollow fibers, whose high surface-to-volume ratio allows high packing densities.

Besides the optimization of the membrane structure, higher permeability can be also attained by optimizing the modification process. A better control of the polymerization reaction and of the hydrogel thickness may also allow the fabrication of more permeable membranes. Alternative “grafting from” approaches such as pre-irradiation or peroxidation involve the creation of free radicals at the membrane surface only and may also prevent the formation of homopolymers, which increase the flow resistance in the membrane. Additionally, it could also reduce the amount of extractable compounds that may contaminate the filtrate. In

contrast to the pre-irradiation approach that requires a strict oxygen free environment, the peroxide-based grafting method may be easier to implement with the pilot scale e-beam available at SSB. In this case the membrane would be subjected to radiation in the presence of oxygen to form stable hydroxy peroxides. These would be then decomposed to form the free radicals necessary to initiate the reaction.

In conclusion, virus filtration performance mainly depends on three interacting properties, which are retention, capacity and permeability. Asymmetric membranes with small pores typically exhibit high retention and permeability but low capacity. As a consequence, high membrane surface area is required to allow the filtration of a large solution volume in a minimum processing time. In contrast, membranes with larger pores will allow high permeability and capacity but low retention. The membrane developed in this work features high retention and high capacity for high plugging protein solutions but low permeability. Consequently, it has a great potential for the plasma fractionation industry since the low added value on the product makes the saved filter resources more valuable than the time lost in filtration.

7 References

1. Burnouf, T. and M. Radosevich, *Nanofiltration of plasma-derived biopharmaceutical products.* Haemophilia, 2003. **9**(1): p. 24-37.
2. Willkommen, H., *Blood product safety and public health authorities.* Anasthesiologie Intensivmedizin Notfallmedizin Schmerztherapie, 1999. **34**(8): p. 497-500.
3. Bos, O.J., et al., *Virus validation of pH 4-treated human immunoglobulin products produced by the Cohn fractionation process.* Biologicals, 1998. **26**(4): p. 267-76.
4. Kempf, C., et al., *Virus inactivation during production of intravenous immunoglobulin.* Transfusion, 1991. **31**(5): p. 423-7.
5. Jornitz, M.W. and T.H. Meltzer, *Filtration and Purification in the biopharmaceutical Industry, Second Edition*. Drugs and the pharmaceutical sciences. Vol. 174. 2008, New York: Informa Healthcare.
6. Omar, A. and C. Kempf, *Removal of neutralized model parvoviruses and enteroviruses in human IgG solutions by nanofiltration.* Transfusion, 2002. **42**(8): p. 1005-10.
7. Terpstra, F.G., et al., *Viral safety of Nanogam, a new 15 nm-filtered liquid immunoglobulin product.* Vox Sang, 2006. **90**(1): p. 21-32.
8. Buchacher, A. and G. Iberer, *Purification of intravenous immunoglobulin G from human plasma - aspects of yield and virus safety.* Biotechnol. j., 2006. **1**: p. 148-163.
9. Schneider, B., et al., *Contamination of coagulation factor concentrates with human parvovirus B19 genotype 1 and 2.* Thrombosis and Haemostasis, 2004. **92**(4): p. 838-845.
10. Blumel, J., et al., *Parvovirus B19 transmission by heat-treated clotting factor concentrates.* Transfusion, 2002. **42**(11): p. 1473-1481.
11. Nubling, C.M., H. Willkommen, and J. Lower, *Hepatitis-C Transmission Associated with Intravenous Immunoglobulins.* Lancet, 1995. **345**(8958): p. 1174-1174.
12. Chudy, M., et al., *A new cluster of hepatitis A infection in hemophiliacs traced to a contaminated plasma pool.* Journal of Medical Virology, 1999. **57**(2): p. 91-99.
13. Santagostino, E., et al., *Transmission of parvovirus B19 by coagulation factor concentrates exposed to 100 degrees C heat after lyophilization.* Transfusion, 1997. **37**(5): p. 517-522.
14. Scheiblauer, H., et al., *Prevalence of hepatitis C virus in plasma pools and the effectiveness of cold ethanol fractionation.* Clinical Therapeutics, 1996. **18**: p. 59-70.

15. Wu, C.G., et al., *Parvovirus B19 transmission by a high-purity factor VIII concentrate.* Transfusion, 2005. **45**(6): p. 1003-1010.
16. Bolton, G., et al., *Normal-flow virus filtration: detection and assessment of the endpoint in bioprocessing.* Biotechnol. Appl. Biochem., 2005. **42**: p. 133-142.
17. Hamalainen, E., H. Suomela, and P. Ukkonen, *Virus inactivation during intravenous immunoglobulin production.* Vox Sang, 1992. **63**(1): p. 6-11.
18. Syedain, Z.H., D.M. Bohonak, and A.L. Zydney, *Protein Fouling of Virus Filtration Membranes: Effects of Membrane Orientation and Operating Conditions.* Biotechnol. Prog., 2006. **22**: p. 1163-1169.
19. Yokoyama, T., et al., *Removal of small non-enveloped viruses by nanofiltration.* Vox Sanguinis, 2004. **86**: p. 225-229.
20. Brough, H., et al., *Performance of a novel viresolve NFR virus filter.* Biotechnology Progress, 2002. **18**(4): p. 782-795.
21. Tran, H., et al., *Functional integrity of intravenous immunoglobulin following irradiation with a virucidal dose of gamma radiation.* Biologicals, 2004. **32**(2): p. 94-104.
22. Teschner, W., et al., *A new liquid, intravenous immunoglobulin product (IGIV 10%) highly purified by a state-of-the-art process.* Vox Sanguinis, 2006. **92**(1): p. 42-55.
23. Valdes, R., et al., *Chromatographic removal combined with heat, acid and chaotropic inactivation of four model viruses.* J Biotechnol, 2002. **96**(3): p. 251-8.
24. Aranha, H., *Viral Clearance Strategies for Biopharmaceutical safety: Part 1: general considerations.* Biopharm International, 2001a. **14**(5): p. 42-54.
25. Ray, S. and K. Tarrach, *Virus Clearance Strategy Using a Three-Tier Orthogonal Technology Platform.* Biopharm International, 2008. **Oct**: p. 50-58.
26. Blumel, J., et al., *Inactivation of parvovirus B19 during pasteurization of human serum albumin.* Transfusion, 2002. **42**(8): p. 1011-8.
27. Kaufmann, B., A.A. Simpson, and M.G. Rossmann, *The structure of human parvovirus B19.* Proc Natl Acad Sci U S A, 2004. **101**(32): p. 11628-33.
28. Boschetti, N., et al., *Different susceptibility of B19 virus and mice minute virus to low pH treatment.* Transfusion, 2004. **44**(7): p. 1079-86.
29. Bolton, G.R., S. Spector, and D. Lacasse, *Increasing the capacity of parvovirus-retentive membranes: performance of the Viresolve Prefilter.* Biotechnol Appl Biochem, 2006. **43**(Pt 1): p. 55-63.

30. Hongo-Hirasaki, T., et al., *Removal of small viruses (parvovirus) from IgG solution by virus removal filter Planova 20N.* Journal of Membrane Science, 2006. **278**: p. 3-9.

31. Kreil, T.R., et al., *Removal of small nonenveloped viruses by antibody-enhanced nanofiltration during the manufacture of plasma derivatives.* Transfusion, 2006. **46**: p. 1143-1151.

32. Zhang, M., et al., *A novel, Q-PCR based approach to measuring endogenous retroviral clearance by capture protein A chromatography.* Biotechnol Bioeng, 2009. **102**(5): p. 1438-47.

33. Aranha-Creado, H. and H. Brandwein, *Application of bacteriophages as surrogates for mammalian viruses: A case for use in filter validation based on precedents and current practices in medical and environmental virology.* Pda Journal of Pharmaceutical Science and Technology, 1999. **53**(2): p. 75-82.

34. Lute, S., et al., *Characterization of coliphage PR772 and evaluation of its use for virus filter performance testing.* Applied and Environmental Microbiology, 2004. **70**(8): p. 4864-4871.

35. Oshima, K.H., et al., *The Removal of Phages T1 and Pp7, and Poliovirus from Fluids with Hollow-Fiber Ultrafilters with Molecular-Weight Cutoffs of 50000, 13000, and 6000.* Canadian Journal of Microbiology, 1995. **41**(4-5): p. 316-322.

36. Clem, A.L., et al., *Virus detection and identification using random multiplex (RT)-PCR with 3 '-locked random primers.* Virology Journal, 2007. **4**: p. -.

37. van Reis, R. and A. Zydney, *Bioprocess membrane technology (vol 297, pg 16, 2007).* Journal of Membrane Science, 2007. **302**(1-2): p. 271-271.

38. Tarrach, K., et al., *The effect of flux decay on a 20-nm nanofilter for virus retention.* Biopharm International, 2007: p. 15-18.

39. Parrella, J., Y. Wu, and D.W. Kahn, *RUNspike, a Complementary Virus Filter Spiking Method: A Solution to the Problem of Reduced Throughput Due to the Addition of the Virus Spike.* PDA J Pharm Sci and Tech, 2009. **63**: p. 547-558.

40. Mulder, M., *Basic Principles of Membrane Technology*. 1991, Dordrecht: Kluwer Academic Publishers.

41. Kim, Y.D., et al., *A new modeling of asymmetric membrane formation in rapid mass transfer system.* Journal of Membrane Science, 2001. **190**(1): p. 69-77.

42. Young, T.H., Y.H. Huang, and L.Y. Chen, *Effect of solvent evaporation on the formation of asymmetric and symmetric membranes with crystallizable EVAL polymer.* Journal of Membrane Science, 2000. **164**(1-2): p. 111-120.

43. Buonomenna, M.G., et al., *Poly(vinylidene fluoride) membranes by phase inversion: the role the casting and coagulation conditions play in their morphology, crystalline structure and properties.* European Polymer Journal, 2007. **43**(4): p. 1557-1572.

44. Kim, S.R., K.H. Lee, and M.S. Jhon, *The effect of ZnCl2 on the formation of polysulfone membrane.* Journal of Membrane Science, 1996. **119**(1): p. 59-64.

45. Lin, D.J., et al., *Effect of salt additive on the formation of microporous poly(vinylidene fluoride) membranes by phase inversion from LiClO4/water/DMF/PVDF system.* Polymer, 2003. **44**(2): p. 413-422.

46. Wang, D.L., K. Li, and W.K. Teo, *Porous PVDF asymmetric hollow fiber membranes prepared with the use of small molecular additives.* Journal of Membrane Science, 2000. **178**(1-2): p. 13-23.

47. Reuvers, A.J., J.W.A. Vandenberg, and C.A. Smolders, *Formation of Membranes by Means of Immersion Precipitation .1. A Model to Describe Mass-Transfer during Immersion Precipitation.* Journal of Membrane Science, 1987. **34**(1): p. 45-65.

48. Ulbricht, M., *Advanced functional polymer membranes.* Polymer, 2006. **47**(7): p. 2217-2262.

49. Uyama, Y., K. Kato, and Y. Ikada, *Surface modification of polymers by grafting.* Grafting/Characterization Techniques/Kinetic Modeling, 1998. **137**: p. 1-39.

50. Yamagishi, H., J.V. Crivello, and G. Belfort, *Development of a Novel Photochemical Technique for Modifying Poly(Arylsulfone) Ultrafiltration Membranes.* Journal of Membrane Science, 1995. **105**(3): p. 237-247.

51. Kroll, S., et al., *Heterogeneous surface modification of hollow fiber membranes for use in micro-reactor systems.* Journal of Membrane Science, 2007. **299**(1-2): p. 181-189.

52. Wirsen, A. and A.C. Albertsson, *Graft-Polymerization of Acrylamide onto Lldpe Film by Electron-Beam Preirradiation in Air or Argon .1. Influence of Dose, Grafting Temperature, and Monomer Concentration.* Journal of Polymer Science Part a-Polymer Chemistry, 1995. **33**(12): p. 2039-2047.

53. Xi, Z.Y., et al., *Modification of polytetrafluoroethylene porous membranes by electron beam initiated surface grafting of binary monomers.* Journal of Membrane Science, 2009. **339**(1-2): p. 33-38.

54. Ulbricht, M. and G. Belfort, *Surface modification of ultrafiltration membranes by low temperature plasma .2. Graft polymerization onto polyacrylonitrile and polysulfone.* Journal of Membrane Science, 1996. **111**(2): p. 193-215.

55. Ulbricht, M., et al., *Photo-induced graft polymerization surface modifications for the preparation of hydrophilic and low-protein-adsorbing ultrafiltration membranes.* Journal of Membrane Science, 1996. **115**(1): p. 31-47.

56. Thom, V.H., et al., *Optimizing cell-surface interactions by photografting of poly(ethylene glycol).* Langmuir, 2000. **16**(6): p. 2756-2765.

57. Liu, Z.M., et al., *Surface modification of polypropylene microfiltration membranes by the immobilization of poly (N-vinyl-2-pyrrolidone): a facile plasma approach.* Journal of Membrane Science, 2005. **249**(1-2): p. 21-31.

58. Ju, H., et al., *Preparation and characterization of crosslinked poly(ethylene glycol) diacrylate hydrogels as fouling-resistant membrane coating materials.* Journal of Membrane Science, 2009. **330**(1-2): p. 180-188.

59. Kang, G.D., et al., *Preparation and characterization of crosslinked poly(ethylene glycol) diacrylate membranes with excellent antifouling and solvent-resistant properties.* Journal of Membrane Science, 2008. **318**(1-2): p. 227-232.

60. Sagle, A.C., et al., *PEG-based hydrogel membrane coatings.* Polymer, 2009. **50**(3): p. 756-766.

61. Susanto, H. and M. Ulbricht, *Photografted thin polymer hydrogel layers on PES ultrafiltration membranes: Characterization, stability, and influence on separation performance.* Langmuir, 2007. **23**(14): p. 7818-7830.

62. Susanto, H. and M. Ulbricht, *High-performance thin-layer membranes for ultrafiltration hydrogel composite of natural organic matter.* Water Research, 2008. **42**(10-11): p. 2827-2835.

63. Bhattacharya, A. and B.N. Misra, *Grafting: a versatile means to modify polymers - Techniques, factors and applications.* Progress in Polymer Science, 2004. **29**(8): p. 767-814.

64. Smith, T.J., et al., *Crosslinking kinetics of methyl and ethyl (alpha-hydroxymethyl)acrylates: effect of crosslinker type and functionality.* Polymer, 2003. **44**(20): p. 6211-6216.

65. Korneyeva, M. and S. Rosenthal, *Virus removal by nanofiltration.* Methods Mol Biol, 2005. **308**: p. 221-31.

66. Yigzaw, Y., et al., *Exploitation of the adsorptive properties of depth filters for host cell protein removal during monoclonal antibody purification.* Biotechnology Progress, 2006. **22**(1): p. 288-296.

67. Boyd, R.F. and A.L. Zydney, *Analysis of protein fouling during ultrafiltration using a two-layer membrane model.* Biotechnology and Bioengineering, 1998. **59**(4): p. 451-460.

68. Nakamura, K. and K. Matsumoto, *Protein adsorption properties on a microfiltration membrane: A comparison between static and dynamic adsorption methods.* Journal of Membrane Science, 2006. **285**(1-2): p. 126-136.

69. Li, S.J., J. Hu, and B.L. Liu, *A study on the adsorption behavior of protein onto functional microspheres.* Journal of Chemical Technology and Biotechnology, 2005. **80**(5): p. 531-536.

70. Shields, P.A. and S.R. Farrah, *Influence of Salts on Electrostatic Interactions between Poliovirus and Membrane Filters.* Applied and Environmental Microbiology, 1983. **45**(2): p. 526-531.

71. Palacio, L., et al., *Contact angles and external protein adsorption onto UF membranes.* Journal of Membrane Science, 1999. **152**(2): p. 189-201.

72. Nystrom, M., et al., *Fractionation of model proteins using their physiochemical properties.* Colloids and Surfaces a-Physicochemical and Engineering Aspects, 1998. **138**(2-3): p. 185-205.

73. Ehsani, N. and M. Nyström, *Fractionation of BSA and myoglobin with modified and unmodified ultrafiltration membranes.* Bioseparation, 1995. **5**: p. 1-10.

74. Saksena, S. and A.L. Zydney, *Effect of Solution pH and Ionic-Strength on the Separation of Albumin from Immunoglobulins (IgG) by Selective Filtration.* Biotechnology and Bioengineering, 1994. **43**(10): p. 960-968.

75. Lawrence, N.D., et al., *The use of streaming potential measurements to study the fouling and cleaning of ultrafiltration membranes.* Separation and Purification Technology, 2006. **48**(2): p. 106-112.

76. Le Bolay, N. and A. Ricard, *Streaming potential in membrane processes: Microfiltration of egg proteins.* Journal of colloid and interface science, 1995. **170**: p. 154-160.

77. Jacobasch, H.J., G. Bauböck, and J. Schurz, *Problems and results of zeta-potential measurements on fibers.* Colloid and Polymer Science, 1985. **263**: p. 3-24.

78. Causserand, C., M. Nyström, and P. Aimar, *Study of streaming potentials of clean and fouled ultrafiltration membranes.* Journal of Membrane Science, 1994. **88**(2): p. 211-222.

79. Nakamura, K. and K. Matsumoto, *Properties of protein adsorption onto pore surface during microfiltration: Effects of solution environment and membrane hydrophobicity.* Journal of Membrane Science, 2006. **280**(1): p. 363-374.

80. Fang, F., J. Satulovsky, and I. Szleifer, *Kinetics of protein adsorption and desorption on surfaces with grafted polymers.* Biophysical Journal, 2005. **89**(3): p. 1516-1533.

81. Ramsden, J.J., *Puzzles and Paradoxes in Protein Adsorption.* Chemical Society Reviews, 1995. **24**(1): p. 73-78.

82. Calonder, C. and P.R. Van Tassel, *Kinetic regimes of protein adsorption.* Langmuir, 2001. **17**(14): p. 4392-4395.

83. Satulovsky, J., M.A. Carignano, and I. Szleifer, *Kinetic and thermodynamic control of protein adsorption.* Proceedings of the National Academy of Sciences of the United States of America, 2000. **97**(16): p. 9037-9041.

84. Fang, F. and I. Szleifer, *Kinetics and thermodynamics of protein adsorption: A generalized molecular theoretical approach.* Biophysical Journal, 2001. **80**(6): p. 2568-2589.

85. Norde, W., *Adsorption of Proteins from Solution at the Solid-Liquid Interface.* Advances in Colloid and Interface Science, 1986. **25**(4): p. 267-340.

86. Barbe, S., *Fluid Dynamics in Sartobind Membrane Adsorber Systems*, in *Naturwissenschaftliche Fakultät*. 2009, Leibniz University: Hannover. p. 139.

87. McCue, J.T., et al., *Modeling of protein monomer/aggregate purification and separation using hydrophobic interaction chromatography.* Bioprocess and Biosystems Engineering, 2008. **31**(3): p. 261-275.

88. Wang, L. and R. Ghosh, *Fractionation of monoclonal antibody aggregates using membrane chromatography.* Journal of Membrane Science, 2008. **318**(1-2): p. 311-316.

89. Cromwell, M.E., E. Hilario, and F. Jacobson, *Protein aggregation and bioprocessing.* AAPS J, 2006. **8**(3): p. E572-9.

90. Philo, J.S., *A critical review of methods for size characterization of non-particulate protein aggregates.* Curr. Pharm. Biotechnol. , 2009. **10**: p. 359-372.

91. Demeule, B., et al., *Characterization of protein aggregation: the case of a therapeutic immunoglobulin.* Biochim Biophys Acta, 2007. **1774**(1): p. 146-153.

92. Gabrielson, J.P., et al., *Quantitation of aggregate levels in a recombinant humanized monoclonal antibody formulation by size-exclusion chromatography, asymmetrical*

flow field flow fractionation, and sedimentation velocity. J Pharm Sci, 2007. **96**(2): p. 268-79.

93. Liu, J., J.D. Andya, and S.J. Shire, *A critical review of analytical ultracentrifugation and field flow fractionation methods for measuring protein aggregation.* AAPS J, 2006. **8**(3): p. E580-9.
94. Kern, G. and M. Krishnan, *Virus Removal by Filtration: Points to consider.* Biopharm International, October 2006. **19**(RP1031EN00).
95. Zydney, A. and S.T. Kelly, *Mechanisms for BSA fouling during microfiltration.* Journal of Membrane Science, 1995. **107**(1-2): p. 115-127.
96. Duclos-Orsello, C., W.Y. Li, and C.C. Ho, *A three mechanism model to describe fouling of microfiltration membranes.* Journal of Membrane Science, 2006. **280**(1-2): p. 856-866.
97. Zydney, A. and C.C. Ho, *Effect of membrane morphology on the initial rate of protein fouling during microfiltration.* Journal of Membrane Science, 1999. **155**: p. 261-275.
98. Rosenberg, A.S., *Effects of protein aggregates: an immunologic perspective.* AAPS J, 2006. **8**(3): p. E501-7.
99. Akizawa, T., et al., *Efficiency and Biocompatibility of a Polyethylene Glycol Grafted Cellulosic Membrane During Hemodialysis*. 1989, Transactions of the American Society for Artificial Internal Organs. p. 333-335.
100. Staude, B. and L. Breitbach, *Polysulfones and Their Derivatives - Materials for Membranes for Different Separation Operations.* Journal of Applied Polymer Science, 1991. **43**(3): p. 559-566.
101. Zydney, A.L. and C.C. Ho, *Scale-up of microfiltration systems: fouling phenomena and Vmax analysis.* Desalination, 2002. **146**: p. 75-81.
102. Bowen, W.R., J.I. Calvo, and A. Hernandez, *Steps of membrane blocking in flux decline during protein microfiltration.* Journal of Membrane Science, 1995. **101**: p. 153-165.
103. Loh, S., et al., *Interplay among membrane properties, protein properties and operating conditions on protein fouling during normal-flow microfiltration.* Journal of Membrane Science, 2009. **332**: p. 93-103.
104. Zeman, L.J. and A.L. Zydney, *Microfiltration and Ultrafiltration: Principles and Applications*. 1996, New York: Marcel Dekker, Inc.

105. Taniguchi, M. and G. Belfort, *Low protein fouling synthetic membranes by UV-assisted surface grafting modification: varying monomer type.* Journal of Membrane Science, 2004. **231**(1-2): p. 147-157.

8 Appendices

8.1 List of abbreviation

Abbreviation	Name
AHM	3-acryloyloxy-2-hydroxypropyl methacrylate
BCA	Bicinchoninic acid
DG	Degree of grafting
DTT	Dithitreitol
e-beam	Electron beam
EGMA	Ethylenglycol metacrylate
ELS	electrophoretic light scattering
HBV	Hepatitis B virus
HCV	Hepatitis C virus
HF	Hollow fiber
HIV	Human immunodeficiency virus
HIC	Hydrophobic interaction chromatography
HPA	2-Hydroxypropyl acrylate
HTLV	Human T-lymphotropic virus
HTS	High throughput screening
IgG	Immunoglobulin G
LRV	Logarithmic reduction value
mAb	Monoclonal antibody
MBAA	N,N-methylene bisacrylamide
MF	Microfiltration
MWCO	Molecular weight cut-off
NFF	Normal flow filtration
pAb	Polyclonal antibody
PEG	Poly(ethylene glycol)
PEGMA	Poly(ethylene glycol) methacrylate
PES	Polyethersulfone
pfu	Plaque forming unit
pI	Isolelectric point
PPV	Porcine Parvovirus

Abbreviation	Name
PS	Polysulfone
PVDF	Polyvinylidenfluoride
PVP	Polyvinylpirrolidone
RT-PCR	Real-time polymerase chain reaction
S&D	Solvent and detergent
SDS	Sodium dodecylsulfate
ss-RNA	Single-strain ribonucleic acid
SSB	Sartorius Stedim Biotech
TEGDA	Tetraethylenglycol diacrylate
TEGDVE	Tetraethylenglycol divinylether
TFF	Tangential flow filtration
TMP	Transmembrane pressure
UF	Ultrafiltration
UV-C	Shortwave ultraviolet

8.2 Materials

8.2.1 Equipments

Equipment	manufacturer
Zinsser LISSY automated manipulator Software: Zinsser WinLissy	Zinsser Analytic GmbH, Germany
Synergy 2 multi-mode plate reader Software: Gen5 Data Analysis	BioTek, Winooski USA
Densometer Gurley 4150	Inspiratech 2000 Ltd, United Kingdom
Laboratory Electro-Beam Accelerator 400	Electron Crosslinking AB, Germany
Gemini V surface analyzer	Micromeritics, Norcross, USA
VacPrep 061 degasser	Micromeritics, Norcross, USA
Zeta Potential analyzer (Delsa™ Nano)	Beckman Coulter, Fullerton, USA
PTA-Line Bendtsen P62400	PTI Paper testing Instruments, Germany
Electron beam equipment EC-LAB 400	Crosslinking AB, Sweden
Chromatography system: Äkta explorer	GE Healthcare, Pittsburg, USA
HiPrep™ 26/10 Desalting Column prepacked with Sephadex G25	GE Healthcare, Pittsburg, USA

Equipment	manufacturer
16/10 HiLoad Phenyl-sepharose HP	GE Healthcare, Pittsburg, USA
PDA 100 Detector for HPLC	Dionex, USA
ASI 100 Automated Injector for HPLC	Dionex, USA
STH 585 column oven for HPLC	Dionex, USA
P580 Pump for HPLC	Dionex, USA
SEC column Proteema 300Å	PSS Polymer Standards Service, Germany
Stainless steel 5L pressure tank	Sartorius-Stedim Biotech, Göttingen, Germany
Stainless steel filter holder 200 mL	Sartorius-Stedim Biotech, Göttingen, Germany
Precision balance CPA	Sartorius Mechatronics, Göttingen, Germany

8.2.2 Membranes

All membranes used in this work were provided by Sartorius-Stedim Biotech (Göttingen, Germany)

- Prefiltration of IgG containing media: Sartopore 2, 0.1 µm
- Sterile filtration of bacteriophage containing solution: Sartopore 2, 0.2 µm

8.2.3 Chemicals & culture media

Chemicals	manufacturer
KH_2PO_4	Sigma Aldrich, St. Louis, USA
2-mercaptoethanol	Acros Organics, Geel, Belgium
Acetone	Sigma Aldrich, St. Louis, USA
Trichloroacetic acid TCA	Sigma Aldrich, St. Louis, USA
3-(3-Cholamidopropyl)dimethylammonio-1-propanesulfonate CHAPS	Sigma Aldrich, St. Louis, USA
Dithiotreitol DTT	Sigma Aldrich, St. Louis, USA
Bromophenol blue	Sigma Aldrich, St. Louis, USA
Sodium dodecylsulfate SDS	Sigma Aldrich, St. Louis, USA
Coomassie brilliant blue	Serva, Heidelberg, Germany
Duracryl SDS PAGE gel	Genomics solutions, Ann Arbor, USA
Laemmli sample buffer	Bio-Rad, Hercules, USA
Tris/glycine/SDS buffer	Fisher Scientific, Waltham, USA

Chemicals	manufacturer
Silver staining	Pierce Biotechnology, Rockford, U.S.A
Tris/HCl gels 12% acrylamide	Bio-Rad, Hercules, USA
Iodoacetamide	Sigma Aldrich, St. Louis, USA
K_2HPO_4	Sigma Aldrich, St. Louis, USA
Protein solution. Pooled human Immunoglobulins (IgGs) (Cytoglobin® 5% against Cytomegalovirus)	Bayer AG, Wien, Austria
3-Hydroxypropylacrylate (HPA)	Sigma Aldrich, St. Louis, USA
Tetraethylenglycol divinylether (TEGDVE)	Sigma Aldrich, St. Louis, USA
3-acryloyloxy-2-hydroxypropyl methacrylate (AHM)	Sigma Aldrich, St. Louis, USA
Poly(ethylenglycol metacrylate) (PEGMA)	Sigma Aldrich, St. Louis, USA
Ethylenglycol metacrylate (EGDA)	Sigma Aldrich, St. Louis, USA
Tetraethylenglycol diacrylate (TEGDA)	Sigma Aldrich, St. Louis, USA
Bicinchoninic acid assay BCA™ Protein Assay	Fisher Scientific, Waltham, USA
2-Propanol	Sigma Aldrich, St. Louis, USA
Nutrient broth agar (BD213000)	BD diagnostics, New Jersey USA
Nutrient broth (BD 234000)	BD diagnostics, New Jersey USA

8.2.4 Bacteriophage and bacterial strains

Name	Strain
Pseudomonas aeruginosa	1C Fa. ATCC 15692-B2
Pseudomonas aeruginosa Bacteriophage PP7	Fa. ATCC 15692-B2

8.3 Characterization of membrane surface properties

8.3.1 Measurement of unspecific protein adsorption

A dilution serie of the collected samples was performed. A microtiter plate was used to allow parallel measurement. Each well contained one membrane disk and was filled with 200 µL of each protein dilution. After overnight incubation with agitation, the membrane was washed 3 times with buffer and BCA reagent (BCA™ Protein Assay, Pierce) was added to each well. After the colorimetric reaction, the absorption at 582 nm in each well was measured (Synergy

2 multi-mode plate reader, Biotek). The adsorbed protein concentration on each membrane disc was calculated from a linearly regressed IgG calibration curve. Then, the determined adsorption was normalized with the membrane surface area, determined by BET-measurements and plotted against the protein concentration in the remaining solution.

8.3.2 Measurement of zeta-potential

Zeta-potential of flat surfaces were measured with a zeta potential analyzer (Delsa™ Nano, Beckman-Coulter) using electrophoretic light scattering. Zeta potential measurements of the outer membrane surface were performed at 25°C with ultrapure water (Arium, Sartorius-Stedim Biotech) buffered with 10 mM KCl. Membrane isoelectric points measurements were performed from pH 2.2 to pH 7.0 by adding small quantities of HCl with a titrator. Each measurement was repeated three times to ensure reproducibility.

8.4 Characterization of membrane structure properties

8.4.1 Air and liquid permeability

<u>Measurement of liquid permeability in standard stainless steel filter holder</u>

10m mM phosphate buffer pH: 7,2 was used to perform the measurement. The filtration device (Minisart) was connected to the stainless steel filter holder (Sartorius-Stedim Biotech), which was then filled with the solution to be tested. The filtration tube was hermetically closed and connected to a stainless steel pressurized tank (Sartorius-Stedim Biotech). After setting the pressure, the valve above the cylinder was opened and the filtration started. The increase of the collected filtrate as a function of time was measured by weighing (precision balance CPA).

<u>Measurement of liquid permeability in automated characterization system</u>

An automated manipulator system (Zinsser Lissy) was used for V_{max} and permeability measurements. The measurement principle is illustrated in Figure 8.1. The liquid detection feature of the pipetting needles was used to measure the volume decrease in the wells as a function of time. Membrane sheets were preformed in a 6x8 well arrangement in order to easily adapt to the supporting frits of the filtration unit. The filtration unit consists of three different parts as was shown in Figure 5.1: The collecting part in which the filtered liquid is collected; the supporting part, which consist of an 6x8 arrangement of supporting frit on which the membrane is laid; the reservoir part, which contains the solution to be filtered.

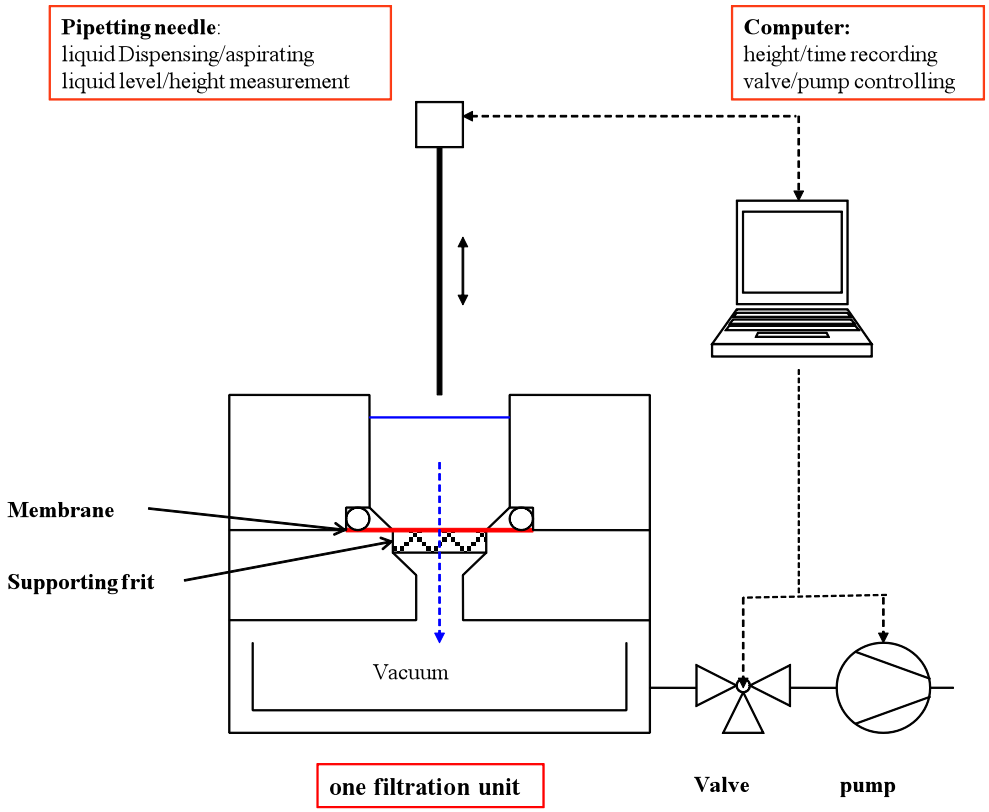

Figure 8.1: Schematic representation of the liquid level detection in filtration experiments.

The membrane sheet was wet with dionized water and placed on the supporting part of the filtration unit. The different solutions were filled into the corresponding bottles and the measurement was started. The automated manipulator system was programmed to fill the different well with the solution to be tested. 4 mL and 7 mL were used to allow a precise measurement of membrane permeability and filtration capacity respectively. A controlled vaccum (negative pressure of 0,9 bar) was applied in the collecting part of the filtration unit and the measurement was automatically started. A data set with 5 values (Volume/Time) within 30 minutes was obtained and the slope of the linear regression was used to calculate the permeability J ($mL \cdot min^{-1} \cdot cm^{-2} \cdot bar^{-1}$) as described in Eq. 8.1.

$$J = \frac{slope}{A \cdot P} \qquad \text{(Eq. 8.1)}$$

with A the filtration surface area in cm^2

and P: the operating pressure in bar

Measurement of air permeability

Membrane disks having a diameter of 70 mm were cut and tested using a air permeability testing instrument (PTA-Line Bendtsen P62400) at a pressure of 10 mbar. After the measurement the same membrane disk was used for liquid permeability testing as described above.

8.4.2 Electron microscopy

SEM imaging was performed using FEI Quanta 200F FEG-SEM scanning electron microscope (FEI, Hilsboro, Oregon, USA).

Membrane samples were washed with deionised water and dried for 30 min at 30°C. Perpendicular and tangential cuts were performed using a freezing microtome (Leica CM30505 cryostat and Leica CE/CN knife holder, Leica Microsystems Nussloch GmbH).

For investigations using ETD detector, sputter coating (K550 Sputter Coater, Emitech Ltd.) was performed with gold (approx. 150 Angstroms thin layer) at 35 mA during 3 min under vacuum (0.01 mbar).

8.4.3 BET surface area

Membrane internal surface area was measured using the Gemini V BET surface analyzer (Micromeritics, USA).

Measurement principle

The system uses physical adsorption and capillary condensation principles to obtain information about the surface area and porosity of a solid material. A sample contained in an evacuated sample tube is cooled to cryogenic temperature, then is exposed to analysis gas at a series of precisely controlled pressures. With each incremental pressure increase, the number of gas molecules adsorbed on the surface increases. The equilibrated pressure (P) is compared to the saturation pressure (Po) and their relative pressure ratio (P/Po) is recorded along with the quantity of gas adsorbed by the sample at each equilibrated pressure. As adsorption proceeds, the thickness of the adsorbed film increases. Any micropores in the surface are filled first, then the free surface becomes completely covered, and finally the larger pores are filled by capillary condensation. The process may continue to the point of bulk condensation

of the analysis gas. Then, the desorption process may begin in which pressure systematically is reduced resulting in liberation of the adsorbed molecules. As with the adsorption process, the changing quantity of gas on the solid surface at each decreasing equilibrium pressure is quantified. These two sets of data describe the adsorption and desorption isotherms. Analysis of the shape of the isotherms yields information about the surface and internal pore characteristics of the material. The schematic of the BET surface analyzer is shown in Figure 8.2

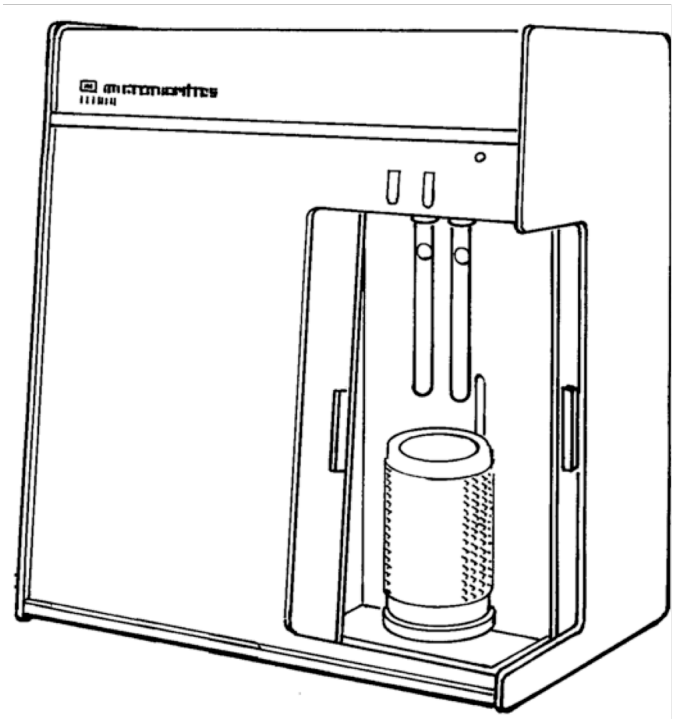

Figure 8.2: schematic of the Gemini BET surface analyzer

Procedure

Membrane samples (15 cm^2) disks were cut in approx. 2 mm stripes and placed into the sample tube. Moisture was removed from the tube by using the Vacprep 061 degasser (Micromeritics, USA) operating 2 hours at 120°C under vacuum. After weighing the dried sample, the tube was connected to the analyzer and liquid nitrogen was filled into the dewar. Then the analysis was started.

8.5 Determination of the filtration performance:

8.5.1 Determination of virus retention with bacteriophage PP7

For this experiment the *Pseudomonas aeruginosa Bacteriophage PP7* (Fa. ATCC 15692-B2) was chosen due to its size similarity with small non-enveloped viruses. A bacteriophage

solution with a start concentration higher than $1 \cdot 10^7$ pfu/mL in 50 mM phosphate buffer pH: 7.0 was sterile filtered (Sartopore 2, 0.2 µm, Sartorius-Stedim Biotech, Germany) and 50 mL of the prepared solution was then filtered using virus retentive filters as described in section 8.4.1 at a positive transmembrane pressure (TMP) of 1 bar. 100 µL of the obtained filtrate was mixed with 900 µL of nutrient broth (BD 234000, BD diagnostics) and the obtained solution was then used for the next 1:10 dilution step. 300 µL of a bacterial preculture (*Pseudomonas aeruginosa* 1C Fa. ATCC 15692-B2) with an optical density of 2 were diluted in 30 mL of nutrient broth. Then 150 µL of this diluted bacterial culture were added to 150 µL of each bacteriophage dilution and mixed thoroughly. After 10 min incubation at room temperature, 2.5 mL of nutrient broth agar (BD 213000, BD diagnostics) were added to the mixture and overlaid on the surface of a solid nutrient agar plate. After 18-24h incubation at 37°C the plaques on the plate were counted. The virus log reduction value (LRV) was calculated using the following equation:

$$LRV = \log_{10}\left(\frac{C_0}{C_f}\right) \qquad \text{Eq. 8.2}$$

Where C_0 and C_f represent the concentration of bacteriophage in the feed medium and in the filtrate respectively.

8.5.2 Filtration capacity

Measurement of the filtration capacity was performed at constant pressure with the standard filter holder (Sartorius-Stedim Biotech, Göttingen, Germany) or with the high throughput automated measurement system (Lissy, Zinsser, germany) as described in section 8.4.1.
The filtration capacity V_{max} was determined using the linearized form of the pore constriction model:

$$\frac{t}{V} = \frac{1}{Q_0} + \left(\frac{1}{V_{max}}\right)t \qquad \text{(Eq. 8.3)}$$

Where V is the total filtrate volume (in liters) collected over time t and Q_0 is the initial volumetric filtrate flow rate. V_{max} was evaluated by plotting the time-to-volume-ratio t/V against the time t and then by taking the inverse of the slope (see Eq. 8.4).
V_{max} in L/m^2 was then calculated as follow:

$$V_{max} = \frac{Slope}{A} \qquad \text{(Eq. 8.4)}$$

with A: the filtration surface area in m^2

8.6 Physico-chemical properties of therapeutic protein solutions

8.6.1 Protein fractionation by hydrophobic interaction chromatography (HIC)

The protein solutions were diluted in a 1 M $(NH_4)_2SO_4$, 50 mM phosphate-buffer and 80 mL of the sample with a final concentration of 5g/L were loaded on a phenyl HIC-column (16/10 Hiload Phenyl-sepharose HP, GE Healthcare). The used chromatography system was an Äkta (GE lifescience) explorer system. The protein fractions were eluted stepwise by different ammonium sulfat concentrations. The collected fractions were desalted (Sephadex G25, GE Healthcare) and concentrated by ultrafiltration (Vivaspin 20, Sartorius-Stedim Biotech). The obtained desalted fractions were adjusted to a common concentration of 2g/L by measurement of the extinction at 280 nm and addition of 50 mM phosphate buffer and used as samples for measurement of the unspecific protein adsoprtion, filtration experiments, SDS-PAGE and SEC-analysis.

8.6.2 Size exclusion chromatography (SEC)

SEC was performed by loading 100 µL of the protein samples to the column (PSS Proteema 300Å) with a diol guard column. The separation was operated under isocratic conditions with a flowrate of 1mL/min and an elution buffer of 300mM NaCl in 50mM phosphate buffer pH 6.8. The different protein populations were detected by measuring the absorbance at 280 nm.

8.6.3 2D-gelelectrophoresis

The IgG-solution was precipitated by adding 3 volumes of chilled (-20°C) 13.3% TCA/0.093% 2-mercaptoethanol in acetone, followed by incubation overnight at -20°C. Samples were centrifuged at 5 000 × g at -20°C and pellets were resuspended in chilled (-20°C) acetone, containing 0.07% 2-mercaptoethanol. Samples were spun again at 5 000 × g at -20°C. All acetone was removed by drying at 30°C. The pellets were then redissolved at 30°C in CHAPS buffer (7 M urea, 2 M thiourea, 2% CHAPS, 2% ampholytes 3–10, 65 mM DTT, 0.1% bromophenol blue) to a concentration of 2.5 mg/ml. 400 µL (1 mg) of this solution were loaded onto an 18 cm immobilized pH 3–10 nonlinear gradient strip (GE Healthcare) and passively rehydrated for 16 hours. The strips were then focused to 100,000 Vh (Genomic Solutions Investigator), equilibrated in 10 ml equilibration buffer I (6 M urea, 375 mM Tris/HCl pH 7.4, 2% SDS, 2% glycerol, 2% DTT), followed by 10 ml equilibration buffer II

(6 M urea, 375 mM Tris/HCl pH 7.4, 2% SDS, 2% glycerol, 2% iodoacetamide), and applied to an 8–18% gradient Duracryl SDS PAGE gel (Genomic Solutions). The gels were stained with Coomassie brilliant blue.

8.6.4 SDS-PAGE

SDS/PAGE was used to characterize molecular-size distributions. Samples were diluted in Laemmli sample buffer (Bio-Rad), with or without the addition of 5% (v/v) DTT (2-mercaptoethanol; Acros Organics, Geel, Belgium). Samples with DTT were incubated for 10 min at 95°C in order to reduce disulphide bonds. After this denaturation step, the samples and a proteinmarker were loaded on Tris/HCl-containing gels with a 12% (w/v) acrylamide concentration (Bio-Rad Laboratories). The gels were electrophoresed in Tris/glycine/SDS buffer (Fisher Scientific) and stained by silver staining (Pierce Biotechnology, Rockford, IL, U.S.A.).

8.7 Electron beam initiated surface modification

8.7.1 Graft modification with vinyl monomers

<u>Sample preparation</u>

Membrane sheets (100x200 mm) were impregnated in the monomer solution for 1 minute at room temperature. After impregnation, the membrane was placed between two layers of 30 µm thin PE-film and pressed to remove the excess monomer solution. The superposed sandwich configuration was then placed into the drawer of the laboratory electron beam (EC-LAB400, Crosslinking AB).

For screening experiments, membrane sheets were formed as a 6x8 arrangement, ready to adapt on the 48 supporting frits of the filtration module. The automated manipulator system (Lissy Zinsser) was used to pipet 11 µL of the different monomer solutions on each preformed disk of the membrane sheet. The membrane was then placed into 2 layers of PE film to prevent evaporation and then into the drawer of the laboratory electron beam (see Figure 8.3).

Figure 8.3: Laboratory electron beam equipment EC-LAB 400

Irradiation of sample

A high voltage of 190 keV was set on the e-beam equipment to ensure the complete penetration of electrons along the whole membrane thickness. After placing the membrane in the irradiation drawer/chamber, the forming process was started. During the forming process, high voltage controlled discharges are used to clean the electron accelerator. Dust particles, oil residue, hydrocarbons or other contamination inside the accelerator head can be burned off and / or pumped out through the vacuum system during forming. The accelerator is forming at approx. 8 kV above the high voltage set point value and needs at least 5 minutes at the forming voltage before the accelerator is formed. After the forming process the irradiation dose was entered in the control panel and the beam operation was started.

Extraction of the samples

After the irradiation process, the membrane samples were removed and placed inside an extraction bath with isopropanol to remove the remaining monomer solution. After 30 min agitation, the solvent was removed and replaced by dionized water and agitated again 30 min. After the extraction process the membranes were dried 30 min at 100 °C.

8.7.2 Degree of grafting

Degree of grafting was determined by weighing the dried membrane before and after the modification process. Typically, this experiment was performed parallel to BET-

measurements, where samples have to be weighted and dried. Similarly to BET-measurements, membrane samples disks (15 cm^2) were cut in approx. 2 mm stripes and placed into a previously dried and weighted sample tube. Moisture was removed from the tube by using the Vacprep 061 degasser (Micromeritics, USA) operating 2 hours at 120°C under vacuum. Degree of grafting DG in $\mu g/cm^2$ was calculated as described in Eq. 8.5.

$$DG = \frac{m_f - m_i}{A} \qquad \text{(Eq. 8.5)}$$

with m_i and m_f: the sample mass in µg before and after the modification respectively
and A: the sample surface area.

8.7.3 Membrane swelling

Membrane swelling was characterized by using the ratio between air and water permeability as described in section 8.4.1.

8.8 CV

Persönliche Daten

Name:	Louis Villain
Adresse:	Lindener Marktplatz 12
	30449 Hannover
Telefon:	+49 (0) 170 5226166
Geburtsdatum und Ort:	11.11.1980 in Laxou (Frankreich)
Staatsangehörigkeit:	französisch
Familienstand:	Ledig

Studium

Juni 1998	Bacalauréat général (Abitur), Fachrichtung Naturwissenschaft (Bac S – scientifique), Lycée Jacques Callot in Vandoeuvre (Frankreich)
Sept. 1998 - Juni. 1999	Studium an dem „Ecole Européenne en Genie des Materiaux (E.E.I.G.M)“, in Nancy (Frankreich)
Sept. 1999 – Juli 2001	Diplôme Universitaire de Technologie Génie Biologique (DUT), Institut Universitaire de Technologie (IUT) Brabois, Université Henri Poincaré, Nancy (Frankreich)
März-Juli 2001	DUT-Abschlussarbeit „Etablissement d'un manuel HACCP“, Fa. HAXAIRE, Lapoutroie (Frankreich)
Sept. 2001 – August 2004	Diplomstudium (FH) an der Fachhochschule Lippe und Höxter, Fachbereich „Lebensmitteltechnologie“, Schwerpunkt „Biotechnologie“
März 2004 - August 2004	Diplomarbeit „Selektive Extraktion von 2S-Protein aus Paranuss“ unter der Leitung von Prof. Dr. Danneel, zentrales Chemie-Labor der FH Lippe und Höxter, Lemgo
Sept. 2004 – Nov. 2006	Masterstudium in Life Science an der Leibniz Universität Hannover

April 2006 – Nov. 2006	Masterarbeit „Optimierung und Überwachung der Produktion His-getagter Proteine im Mikrohohlfasersystem“ unter der Leitung von Prof. Dr. Scheper, Institut für technische Chemie (TCI), Leibniz Universität, Hannover
Seit Januar 2007	Externe Promotion im F&E Bereich der Firma Sartorius-Stedim Biotech GmbH in Göttingen. Thema: „Entwicklung eines hochkapazitiven Membranfilters für die Virusabreicherung“ unter der Leitung von Prof. Dr. Scheper, Institut für technische Chemie (TCI), Leibniz Universität, Hannover

Berufliche Erfahrung

Sept. 2002 – Juli 2004	Wissenschaftliche Hilfskraft und Betreuung des Sensorik Praktikums unter der Leitung von Dipl. Ing. Schwarze, Zentrales Chemie-Labor der FH Lippe und Höxter, Lemgo
Januar 2007 – Nov. 2009	PhD-Student im Bereich „Forschung und Entwicklung / Fällbad“ der Firma Sartorius-Stedim Biotech GmbH, Göttingen
Since Dec. 2009	Wissenschaftlicher Mitrabeiter im Bereich „Forschung und Entwicklung / Membranemodifizierung“der Firma Sartorius-Stedim Biotech GmbH, Göttingen

EDV-Kenntnisse

MS-Office, Originlab Pro

Sprachkenntnisse

Verhandlungssichere Deutsch- und Englischkenntnisse

Französisch als Muttersprache

8.9 List of publications

Scientific articles:

Villain, L., L. Meyer, et al. (2008). "Development of a novel membrane aerated hollow-fiber microbioreactor." Biotechnol Prog 24(2): 367-371.

Oral presentations

Villain, L., "Hydrophobic Interactions between IVIG-fractions and virus retentive membranes". Sept. 2007, Network Young Membrains, Thessaloniki, Greece

Villain, L., Thom, V., Masselin, I. and T. Scheper. "Virus retentive filtration of polyclonal Immunoglobulins: dominant filtration mechanisms and strategies to prevent fouling". Oct. 2008, Bioperspectives, Hanover, Germany

Villain, L., "Development of a high capacity membrane for size exclusion based virus removal". Sept. 2009, Network Young Membrains 2009, Montpellier, France

Villain, L., Rico Perez, V, Dathe, J. E., Börger, M., Masselin, I., Thom, V. and T. Scheper. "Viral clearance using size exclusion based membrane filtration: Dominant filtration mechanisms and strategies to attain higher throughput". Sept. 2009, Euromembrane, Montpellier, France

Posters:

Villain, L., Thom, V "High capacity membrane for size exclusion based virus removal". March 2010, Dechema Infotag Membrantechnik, Frankfurt am Main, Germany

Ray, S., Villain, L., Masselin, I., Thom, V., Tarrach, K. and U. Gottschalk. "Experimental evidence supporting implementation of orthogonal virus clearance platform 'Early-on' in biomanufacturing". June 2008, Recovery of Biological Products XIII, Quebec City, Canada.

Schmidt, A., Kroll, S., Meyer, L., Villain, L., Beutel, S. And T. Scheper. “Hollow fiber micro-bioreactors – all-rounder in biotechnological processses“. Sept. 2008, International Congress on Biocatalysis, Hamburg, Germany.